

DETECTING QUEUE LENGTH ON URBAN ARTERIALS USING FLOATING
CAR DATA (FCD)

A THESIS SUBMITTED TO
THE GRADUATE SCHOOL OF NATURAL AND APPLIED SCIENCES
OF
MIDDLE EAST TECHNICAL UNIVERSITY

BY

ORUÇ ALTINTAŞI

IN PARTIAL FULFILLMENT OF THE REQUIREMENTS
FOR
THE DEGREE OF DOCTOR OF PHILOSOPHY
IN
CIVIL ENGINEERING

NOVEMBER 2018

Approval of the thesis:

**DETECTING QUEUE LENGTH ON URBAN ARTERIALS USING
FLOATING CAR DATA (FCD)**

submitted by **ORUÇ ALTINTAŞI** in partial fulfillment of the requirements for the degree of **Doctor of Philosophy in Civil Engineering Department, Middle East Technical University** by,

Prof. Dr. Halil Kalıpçılar
Dean, Graduate School of **Natural and Applied Sciences**

Prof. Dr. İsmail Özgür Yaman
Head of Department, **Civil Engineering**

Assoc. Prof. Dr. Hediye Tüydeş Yaman
Supervisor, **Civil Engineering, METU**

Prof. Dr. Kağan Tuncay
Co-Supervisor, **Civil Engineering, METU**

Examining Committee Members:

Prof. Dr. Murat Güler
Civil Engineering, METU

Assoc. Prof. Dr. Hediye Tüydeş Yaman
Civil Engineering, METU

Prof. Dr. Halim Ceylan
Civil Engineering, Pamukkale University

Assist. Prof. Dr. Hande Işık Öztürk
Civil Engineering, METU

Assist. Prof. Dr. Murat Özen
Civil Engineering, Mersin University

Date: 15.11.2018

I hereby declare that all information in this document has been obtained and presented in accordance with academic rules and ethical conduct. I also declare that, as required by these rules and conduct, I have fully cited and referenced all material and results that are not original to this work.

Name, Surname: Oruç Altıntaşı

Signature:

ABSTRACT

DETECTING QUEUE LENGTH ON URBAN ARTERIALS USING FLOATING CAR DATA (FCD)

Altıntaşı, Oruç

Doctor of Philosophy, Civil Engineering

Supervisor: Assoc. Prof. Dr. Hediye Tüydeş Yaman

Co-Supervisor: Prof. Dr. Kağan Tuncay

November 2018, 149 pages

Accurate estimation of queue lengths whether in the approach of a signalized intersection or near a bottleneck location along an uninterrupted urban arterial is essential for better traffic management. This requires reliable traffic data, which is traditionally obtained from loop detectors, video cameras, etc. More recently, Floating Car Data (FCD) is being increasingly used as an alternative traffic data source due to its lower cost and high coverage area. Commercially available FCD is obtained from GPS equipped vehicles moving in the traffic and can provide speed or travel time data for many segments for even 1-min intervals in real-time. The main focus of this thesis is to develop a mathematical model to estimate queue length (QL) in both signalized intersections and uninterrupted arterials using FCD. The model is mainly based on determination of speed threshold value for QL estimation. Speed field, generated from FCD using 4-node quadratic interpolation technique, was used to generate imaginary vehicle trajectory data and provided iso-speed contours in FCD. The model performance was first tested in VISSIM environment by creating a hypothetical approach leg of a signalized intersection. Later, model performance was evaluated in two study corridors (an uninterrupted urban arterial and a signalized intersection) located in Ankara. For the signalized case, selection of speed threshold of 20 km/h

provided promising estimation results with a root mean square error (RMSE) of 23.21 m and a mean absolute percentage error (MAPE) of 7.68%. For the uninterrupted corridor, selection of speed threshold as 42 km/h provided the maximum QL profile over time.

Keywords: Floating Car Data (FCD), Queue length estimation, FCD quality, Signalized intersection, Uninterrupted urban arterial

ÖZ

HAREKETLİ ARAÇ VERİSİ (FCD) KULLANARAK KENTSEL ARTERLERDE KUYRUK UZUNLUĞU TESPİTİ

Altıntaşı, Oruç
Doktora, İnşaat Mühendisliği
Tez Danışmanı: Doç. Dr. Hediye Tüydeş Yaman
Ortak Tez Danışmanı: Prof. Dr. Kağan Tuncay

Kasım 2018, 149 sayfa

Kuyruk uzunluğunun sinyalize kavşak yaklaşım kolunda veya kesintisiz kentsel arterdeki dar boğaz yakınlarında doğru tahmin edilmesi iyi bir trafik koridor yönetimi için önemlidir. Kuyruk boyunun doğru tahmini güvenilir trafik verisinin olmasını gerektirir ki bu trafik verisi geleneksel olarak döngü detektörlerinden, video kamera vb. verilerden elde edilmektedir. Düşük maliyeti ve geniş ağ alanı sebebiyle, Hareketli Araç Verisi (FCD) son zamanlarda alternatif veri kaynağı olarak daha fazla kullanılmaktadır. Trafikte hareket eden GPS donanımlı araçlardan elde edilen FCD, gerçek zamanlı olarak 1 dakikalık aralıklarla bile birçok segment için hız veya seyahat süresi verilerini sağlamaktadır. Bu tezin ana konusu, FCD verisi kullanarak hem sinyalize kavşakta hem de kesintisiz kentsel arterde kuyruk uzunluğunu tahmin etmek için matematiksel bir model geliştirmektir. Geliştirilen model temel olarak kuyruk uzunluğu tahmini için eşik hız değerinin belirlenmesine dayanmaktadır. 4-düğüm noktalı sonlu eleman interpolasyonu tekniği kullanılarak FCD'den elde edilen hız alan verisi, sanal araç takip verisini oluşturmak ve FCD'de eş-hız eğrilerini elde etmek için kullanılmıştır. Modelin performansı öncelikle VISSIM benzetim ortamında oluşturulan bir sinyalize kavşağın yaklaşım kolunda test edilmiştir. Sonrasında, modelin performansı Ankara ili içerisinde bulunan iki koridorda (kesintisiz kentsel

arter ve sinyalize kavşak) değerlendirilmiştir. Sinyalize kavşak için, eşik hız değeri 20 km/sa olduğunda, önerilen modelle gözlemlenen kuyruk boyu ile tahmin edilen kuyruk boyunun ortalama karesel hatanın karekökü (RMSE) değeri 23.21 m ve ortalama mutlak yüzde hata (MAPE) değeri 7.68% olarak hesaplanmıştır. Kesintisiz akımın olduğu kentsel arterde ise eşik hız değeri 42 km/sa olarak seçildiğinde, kuyruk boyunun zaman içerisindeki değişim profili elde edilmiştir.

Anahtar Kelimeler: Hareketli Araç Verisi (FCD), Kuyruk boyu tahmini, FCD kalitesi, Sinyalize kavşak, Kesintisiz kentsel arter

To Harun Altıntaşı

ACKNOWLEDGMENTS

Firstly, I would like to express my sincere gratitude to my supervisor Assoc. Prof. Dr. Hediye Tüydeş Yaman for her enormous encouragement, endless patience, stimulating guidance and continuous support of my Ph.D study. Her guidance helped me in all the time of my research and I am feeling very lucky to study with her not only for her excellent scientific knowledge but also for her hearty attempts during my life in general. I also would like to express my sincere gratitude to my co-advisor Prof. Dr. Kağan Tuncay for his support, motivation, insightful comments and encouragement throughout my study. Whenever I have experienced a difficulty, his guiding and manner of approaching of a problem always relieved me.

I would to extend my thanks to the rest of my thesis committee: Prof. Dr. Halim Ceylan not only for his guidance in academia but also for his valuable experiences in life he shared and Asst. Prof. Dr. Hande Işık Öztürk for her valuable comments. I also thank to Prof. Dr. Murat Güler and Asst. Dr. Murat Özen for their insightful comments.

I thank my fellow colleagues; Vesile Hatun Akansel, Ayhan Öner Yücel, Başak Varlı, Ege Cem Saltık, Pınar Karataş Sevinen, Beyhan İpekyüz and Gülçin Dalkıç for their friendship.

I would also offer my special thanks to ISSD company, especially thanks to Şule Yücel, Metin Barış and Fulya Özsan for their helps during my academic study and allowing to use FCD database.

My wife have supported me during this dissertation. I greatly appreciate her patience, supports and love in me. Last but not the least, I would like to thank to my family: my parents, brother for supporting me spiritually throughout writing this thesis.

TABLE OF CONTENTS

ABSTRACT	v
ÖZ	vii
ACKNOWLEDGMENTS	x
TABLE OF CONTENTS	xi
LIST OF TABLES	xiv
LIST OF FIGURES	xvi
LIST OF SYMBOLS	xxi
CHAPTERS	
1. INTRODUCTION	1
1.1. Research Objective	2
1.2. Scope of the Study	3
1.3. Structure of the Thesis	4
2. LITERATURE REVIEW	5
2.1. FCD Studies	5
2.1.1. Traffic State Estimation	6
2.1.2. Traffic Flow Estimation	8
2.1.3. FCD Quality Evaluation	9
2.1.4. Penetration Rate for FCD Quality	12
2.2. Traffic Flow Modeling	14
2.2.1. Traffic Fundamental Diagram	14
2.2.2. Queue Definitions for Interrupted and Uninterrupted Traffic Flows	16
2.2.3. Traffic Flow at Signalized Intersections	19

2.2.4. Shockwaves in Signalized Intersections.....	22
2.3. Queue Length Estimation Studies.....	24
2.3.1. Queue Length Estimation with Loop Detector.....	25
2.3.2. Queue Length Estimation with Probe Vehicle Data	28
2.3.3. Queue Length Estimation by Fusing Loop Detector with Probe Vehicle Data	31
3. FCD STRUCTURE AND QUALITY	35
3.1. FCD Structure	35
3.2. Study Corridor 1.....	38
3.2.1. Ground Truth Data	39
3.3. Study Corridor 2.....	41
3.3.1. GT Data for Muhsin Yazıcıoğlu Street	42
3.4. FCD Quality in Turkey	44
3.4.1. Descriptive Evaluations.....	44
3.4.2. Speed Estimation Performance	46
3.4.3. LOS Estimation Performance.....	52
3.4.4. FCD Performance for Urban Corridor Monitoring	53
3.5. Evaluation of Current FCD Penetration Rate	57
3.6. Potential use of FCD for Monitoring Urban Traffic in Ankara	59
4. METHODOLOGY FOR DETECTING QUEUE LENGTH USING FCD	61
4.1. Speed Field Estimation from FCD.....	63
4.2. Selection of Speed Threshold for Queue Length Estimation.....	65
5. QUEUE LENGTH ESTIMATION WITH FCD IN VISSIM ENVIRONMENT	67

5.1. Signalized Intersection in VISSIM Environment.....	67
5.1.1. Determination of Optimum Speed Threshold.....	70
5.1.2. Performance Evaluation.....	72
5.2. VISSIM Scenarios	73
5.2.1. Undersaturated Condition	74
5.2.2. Mixed Condition	79
5.2.3. Generalized Relation.....	89
5.3. Estimating Queue Length with Different Penetration Rates	90
5.3.1. Queue Length Estimation Results.....	91
6. QUEUE LENGTH ESTIMATION WITH COMMERCIAL FCD	95
6.1. Queue Length Estimation at Signalized Intersection	95
6.2. Queue Length Estimation on Dumlupinar Boulevard	105
6.3. Generalization of Queue Length Estimation for Study Corridor	111
7. CONCLUSIONS AND FURTHER RECOMMENDATIONS	115
7.1. General Overview and Conclusions	115
7.2. Recommendations for Future Studies	118
REFERENCES.....	121
APPENDICES	
A. STATIC INFORMATION TABLE OF FCD SEGMENTS.....	131
B. METHODOLOGY FOR GT VERSUS FCD EVALUATION.....	135
C. ESTIMATION OF QUALITY OF FCD UNDER VARYING PENETRATION RATES	139
CURRICULUM VITAE.....	147

LIST OF TABLES

TABLES

Table 2.1. Studies comparing FCD with different traffic data sources on Freeways.	11
Table 2.2. Studies comparing FCD with different traffic data sources on urban arterials.	12
Table 2.3. Loop detector location and related parameters for urban signalized intersections (FHWA, 2006).	26
Table 3.1. Static information of sample road segments located in the Dumlupınar Blvd. Corridor.	37
Table 3.2. Sample dynamic attributes for the “676111” road segment.	38
Table 3.3. Traffic analysis results of the Approach 1 and 2.	43
Table 3.4. FCD speed performance based on $MAPE_u$, $RMSE_u$ and R^2 measures.	48
Table 3.5. $MAPE_u$ and $RMSE_u$ distribution in HCM-based LOS speed intervals (2-day analysis).	51
Table 3.6. Comparison of GT- and FCD-based LOS estimations for Segment 57 (2-day analysis).	53
Table 3.7. Estimated level of FCD penetration, $\tilde{\delta}_{FCD}$, from speed data for different analysis periods (Oct. 25, 2016).	58
Table 5.1. Traffic conditions and corresponding input parameters for simulation based queue length estimation.	73
Table 5.2. ν_{opt} and corresponding $MAPE_q$ and $RMSE_q$ values for different λ values for C1.	77
Table 5.3. ν_{opt} and corresponding $MAPE_q$ and $RMSE_q$ values for different λ values for C2 and C3.	86
Table 5.4. ν_{opt} and corresponding $MAPE_q$ and $RMSE_q$ values for different λ values.	90

Table 5.5. Performance evaluation and v_{opt} values under different penetration rate of FCD.....	92
Table 6.1. $MAPE_Q$ and $RMSE_Q$ of estimated queue lengths for different v_{opt} values for Approach 1.....	98
Table 6.2. $MAPE_Q$ and $RMSE_Q$ of estimated queue lengths for different v_{opt} values for Approach 2.....	103
Table A.1. Static information of the FCD road segments on Dumlupınar Blvd.....	131
Table A.1. Static information of the FCD road segments on Dumlupınar Blvd (continued).....	132
Table A.1. Static information of the FCD road segments on Dumlupınar Blvd (continued).....	133
Table A.2. Static information of the FCD road segments on Muhsin Yazıcıoğlu Street.....	134
Table B.1. Average speed intervals and corresponding LOS values for urban roads based on HCM (2010).....	137
Table C.1. δ and corresponding δ_q values for different time periods of the day of October 25, 2016.....	140

LIST OF FIGURES

FIGURES

Figure 2.1. Floating Car Data (FCD) based studies.....	6
Figure 2.2. Shockwave speeds in fundamental diagram (Liu et al., 2011).....	15
Figure 2.3. Space time diagram including vehicle trajectories for several signal cycles on a signalized approach (HCM, 2010).	16
Figure 2.4. Space time diagram including vehicle trajectories for oversaturated road segments for uninterrupted flows (HCM, 2010).....	17
Figure 2.5. Flow-density relation for FFS of 75 mi/h (HCM, 2010).....	18
Figure 2.6. Generalized shape of speed-flow curve for uninterrupted flows (Hall et al., 1992).	19
Figure 2.7. Saturation flow rate and lost time for a signalized intersection (HCM, 2010).	21
Figure 2.8. Shockwave speeds for a signalized intersection (Liu et al., 2009).	24
Figure 2.9. Shockwave speeds and break points at an intersection (Liu et al., 2009).	26
Figure 2.10. a) Detector occupancy time, b) time gap data for a one cycle (Liu et al., 2009).	27
Figure 2.11. Representation of scenarios a) Case 1 and Case 2, b) Case 3 for Cai et al., (2014) study.	33
Figure 3.1. a) Location of two study corridors in Ankara (Be-mobile, 2018); bi-directional location of some of the FCD segments in b) Dumlupınar Boulevard, c) Muhsin Yazıcıoğlu Street.	36
Figure 3.2. a) Locations of Study Corridor 1 of 3.6 km length b) with 40 FCD segments in the eastern part, c) 42 FCD segments in the western part d) with a close look-up on the control Segment 57 with GT data.	39
Figure 3.3. Traffic counting results of two counting days.....	40
Figure 3.4. Study Corridor 2 located between 2 signalized intersections of length 327 m covered in 8 FCD segments.....	41

Figure 3.5. Lane based as well as average observed queue lengths for Approach 1 and 2.....	43
Figure 3.6. Speed profile of the \bar{u}_{FCD}^t and \bar{u}_i as well as u_{\max}^t and u_{\min}^t for the two weekdays between 07:30-16:00.	45
Figure 3.7. Fundamental diagram and LOS threshold limits of GT data.....	46
Figure 3.8. Fundamental diagram and LOS threshold limits of GT data and FCD speeds.	46
Figure 3.9. Speed estimations using a) raw FCD speeds, \bar{u}_{FCD}^t , b) filtered FCD speeds, \bar{u}_{FCD*}^t , for the whole study period.	49
Figure 3.10. Speed estimations using a) raw FCD speeds, b) filtered FCD speeds for the AM peak.....	50
Figure 3.11. LOS estimations for the study corridor using a) raw FCD speeds, b) transformed FCD speeds, c) transformed filtered FCD speeds for the day of October 21.....	54
Figure 3.12. LOS estimations for the study corridor using a) raw FCD speeds, b) transformed FCD speeds, c) transformed filtered FCD speeds for the day of October 25.....	55
Figure 3.13. Comparison of LOS estimations for Segment 57 for a) October 21, b) October 25 data.	56
Figure 3.14. Dominant traffic states (more than 50% probability) for October month.	57
Figure 4.1. Framework for queue length estimation from FCD.	62
Figure 4.2. a) Imaginary vehicle trajectory data generation, b) thematic speed map for the study corridor 1.	64
Figure 5.1. Framework for simulation-based queue length estimation from FCD.	68
Figure 5.2. Vehicle trajectory data with Joined/Leaved Queue Data Set in VISSIM.	69
Figure 5.3. FCD speed and imaginary vehicle trajectory data generation.	69
Figure 5.4. Thematic speed maps with iso-speed contours.....	70

Figure 5.5. Iso-speed contour with Joined/Leaved Queue Dataset for error calculation.	72
Figure 5.6. Comparison of the queue lengths obtained from vehicle trajectory data and speed thematic map for FCD with a) 60 sec b) 30 sec, c) 15 sec epoch times for C1.	75
Figure 5.7. Iso-speed contours for a) 60 sec, b) 30 sec and c) 15 sec epoch times with observed queue lengths obtained from vehicle trajectory data for C1.	76
Figure 5.8. Derivation of $SSE_{e,z}$ and v_z function for v_{opt} determination for C1.	77
Figure 5.9. Comparison of the cycle based estimated queue lengths with observed ones for C1.	78
Figure 5.10. Comparison of the queue lengths obtained from vehicle trajectory data and speed thematic map for FCD with a) 60 sec b) 30 sec, c) 15 sec epoch times for C2.....	81
Figure 5.11. Iso-speed contours for a) 60 sec, b) 30 sec and c)15 sec epoch times with observed queue lengths obtained from vehicle trajectory data for C2.	82
Figure 5.12. Comparison of the queue lengths obtained from vehicle trajectory data and speed thematic map for FCD with a) 60 sec b) 30 sec, c) 15 sec epoch times for C3.....	83
Figure 5.13. Iso-speed contours for a) 60 sec, b) 30 sec and c)15 sec epoch times with observed queue lengths obtained from vehicle trajectory data for C3.	84
Figure 5.14. Derivation of $SSE_{e,z}$ and v_z function for v_{opt} determination for C2.	85
Figure 5.15. Derivation of $SSE_{e,z}$ and v_z function for v_{opt} determination for C3.	85
Figure 5.16. Comparison of the cycle based estimated queue lengths with observed ones for C2.....	87
Figure 5.17. Comparison of the cycle based estimated queue lengths with observed ones for C3.....	88
Figure 5.18. Derivation of $SSE_{e,z}$ and v_z function for v_{opt} determination for the test network.	90

Figure 5.19. Queue length estimation result with different FCD vehicle penetration rate for simulation-based archival data.	93
Figure 5.20. Queue length estimation result with different FCD vehicle penetration rate for short term archival data.	94
Figure 6.1. a) Observed queue lengths with thematic speed map, b) observed average queue lengths with iso-speed contours for Approach 1.	97
Figure 6.2. Thematic speed map of Approach 1 with a) $v_{QL} = 15$ km/h, b) $v_{QL} = 20$ km/h.	99
Figure 6.3. Thematic speed map of Approach 1 with a) $v_{QL} = 25$ km/h, b) $v_{QL} = 30$ km/h.	100
Figure 6.4. a) Observed queue lengths with thematic speed map, b) observed average queue lengths with iso-speed contours for Approach 2.	102
Figure 6.5. Thematic speed map of Approach 2 with a) $v_{QL} = 15$ km/h, b) $v_{QL} = 20$ km/h, c) $v_{QL} = 25$ km/h, and d) $v_{QL} = 30$ km/h.	104
Figure 6.6. Thematic speed map obtained from commercial FCD speed data with a) $v_{QL} = 27$ km/h, b) $v_{QL} = 42$ km/h for queue length estimation on October 21, 2017. .	106
Figure 6.7. Estimated queue lengths for two different v_{QL} values for Dumlupinar Blvd. on a) October 21, 2017, b) October 25, 2017.....	107
Figure 6.8. Thematic speed map obtained from commercial FCD speed data with a) $v_{QL} = 27$ km/h, b) $v_{QL} = 42$ km/h for queue length estimation on October 25, 2017.	108
Figure 6.9. Thematic speed map of a) Segments 56, 57 and 58, b) lane 1, c) lane 2, d) lane 3, e) comparison of lane-based queued vehicles with imaginary queued vehicle for different v_{QL}	110
Figure 6.10. Generalized queue length profile obtained from different speed thresholds for Approach 1 and 2.....	113
Figure C.1. Monte Carlo simulation approach to derive quality-penetration rate relation for FCD speed.....	140

Figure C.2. Variation of Speed R^2 performance of Monte Carlo simulation by penetration rate.....	141
Figure C.3. Variation of $MAPE_u$ and $RMSE_u$ performance for Monte Carlo Simulations.....	142
Figure C.4. Variations of $MAPE_u$ and $RMSE_u$ measures as a function of penetration rates for whole analysis period.....	143
Figure C.5. Variations of $MAPE_u$ and $RMSE_u$ measures as a function of penetration rates for AM peak.....	144
Figure C.6. Variations of $MAPE_u$ and $RMSE_u$ measures as a function of penetration rates for off-peak period.....	145

LIST OF SYMBOLS

T	: analysis time period
K	: set of Monte Carlo simulation runs
q^t	: minute-based flow at time t , $t \in T$ (GT)
u_i^t	: spot speed of a vehicle i observed in minute t , $t \in T$ (GT)
u_{\max}^t	: maximum spot speed observed at time t , $t \in T$ (GT)
u_{\min}^t	: minimum spot speed observed at time t , $t \in T$ (GT)
\bar{u}^t	: space mean speed at time t , $t \in T$ (GT)
\bar{u}_{tr}^t	: space mean speed at time t , $t \in T$ truncated at the speed limit (GT)
\bar{u}_{FCD}^t	: average speed from commercial FCD at time t , $t \in T$
\bar{u}_{FCD*}^t	: filtered average speed from commercial FCD at time t , $t \in T$
\tilde{u}_{FCD}^t	: simulated FCD speed obtained from Monte Carlo Simulation at time t , $t \in T$
δ	: penetration rate in Monte Carlo simulation in GT speed data
δ_q	: calculated penetration rate based on GT flow data
$\tilde{\delta}_{FCD}$: estimated commercial FCD penetration rate (%)
δ_{FCD}	: Simulated FCD penetration rate from VISSIM simulation (%)
LOS^t	: Level of Service estimated from Ground Truth at time t , $t \in T$
LOS_{FCD}^t	: Level of Service estimated from commercial FCD at time t , $t \in T$
$MAPE_u$: mean absolute percent error (MAPE) between GT and FCD speeds
$MAPE_{u,k}^\delta$: $MAPE_u$ in k^{th} Monte Carlo simulation, $k \in K$, for penetration rate δ
$MAPE_{u,\max}^\delta$: maximum $MAPE_u$ in K simulations for penetration rate δ
$MAPE_{u,\min}^\delta$: minimum $MAPE_u$ in K simulations for penetration rate δ
\overline{MAPE}_u^δ	: average of $MAPE_u$ values in K simulations for penetration rate δ
$RMSE_u$: root mean square error between GT and FCD speeds
$RMSE_{u,k}^\delta$: $RMSE_u$ in k^{th} simulation, $k \in K$, for penetration rate δ
$RMSE_{u,\max}^\delta$: maximum $RMSE_u$ in K simulations, for penetration rate δ
$RMSE_{u,\min}^\delta$: minimum $RMSE_u$ in K simulations for penetration rate δ

- \overline{RMSE}_u^δ : average of $RMSE_u$ in K simulations for penetration rate δ
 S : set of all segments in the network
 λ : epoch time for FCD speed updates
 $u_s^{t,\lambda}$: average FCD speed of segment s ($s \in S$) at time interval t ($t \in T$) for epoch time = λ
 N_m : interpolation function for corner m ($m=1,2,3,4$)
 $U(x,t)$: estimated speed value for an imaginary vehicle at position x and time t
 v_z : speed threshold value for drawing an iso-speed contour
 v_{opt} : optimum speed threshold for representing queue length
 v_{QL} : speed threshold for an iso-speed contour representing queue length
 Q_n : observed queue length for signal cycle $n, n \in N$
 \hat{Q}_n : estimated queue length obtained from FCD speed for signal cycle $n, n \in N$

CHAPTER 1

INTRODUCTION

Signalized intersections are designed to follow a stop-and-go traffic management, which inherently causes queue formations. However, oversaturation at these intersections make them more susceptible for longer travel times and delays, if signal timings are not properly designed. For delay minimization, queue length (QL) of an approach is one of the main parameters (Tiaprasert et al., 2015). Typical methods for QL (which is also called maximum queue length) include either a cumulative traffic input-output model or a shockwave based model (Li et al., 2013). The former requires the determination of the cumulative arrival and departure flows continuously at intersections that cannot be always practical in real cases (Cai et al., 2014). The most common technique is implementation of Lighthill-Whitham-Richard (LWR) shockwave model, which uses the principles of conservation of vehicles and a traffic fundamental diagram that relates the flow-density relation (Cetin, 2012). To measure the arrival traffic flow rate, signal control systems traditionally utilize fixed-point sensors (i.e. inductive loop detectors) to estimate QLs and arrange the signal timings to minimize them (Bagheri et al., 2015). However, cost of installation and operation of these sensors is economically challenging for urban arterials with complex network and queue formation structures which requires data collection at many locations.

QL estimation for uninterrupted flows such as, freeways, multilane highways or major urban arterials is also essential for better management of traffic control. Especially in urban arterials, certain locations experience recurrent congestion due to the commute travels during peak hours and queues are formed when the vehicles on the road exceed the capacity. Thus, accurate estimation of queue lengths at these locations may help traffic engineers to develop Intelligent Transportation System (ITS) strategies to

alleviate the traffic congestion. Queue lengths near bottleneck location can be traditionally detected via input-output models or LWR shock wave model as similar in signalized intersection. The traffic data are generally collected from loop detectors or probe vehicle data.

More recently, Floating Car Data (FCD) has been used increasingly in urban network monitoring, mainly due to its lower cost and higher coverage. Today, it is commercially provided by a number of private companies such as, INRIX, TomTom, and Be-Mobile even in developing countries such as Turkey. The basic principle of FCD is to collect real-time traffic data by locating the vehicle via mobile phones or GPS over the entire road network, and to produce time-dependent average travel time (or speeds) for road segments. But, the format of the FCD depends on whether it is from an individually probe vehicle, or anonymously (and mostly commercially) processed data of multiple vehicles tracked for other purposes (such as from fleet data of taxis, trucks, etc.). While the former has capability to portray dynamics of the vehicle in a time-space diagram (i.e. location of queue join or exit, acceleration, deceleration, etc.), the latter mostly carries only average speed (or travel time) information determined over a given segment during a selected aggregation epoch time.

1.1. Research Objective

The main objective of this thesis is to propose a methodology for queue length estimation using commercial FCD speed. The FCD speed in this thesis was not obtained from probe vehicle data; instead, it was taken from a private company as processed data. In general, FCD speeds are provided with TMC (Traffic Message Channel) codes for the long road segments, varying from 500 m to 1500 m. The available data had road uniformly spaced road segment lengths with a maximum length of 50 m. This enabled to measure the queue lengths more precisely.

In addition to investigations carried out to assess its potential for queue length detection, the quality of commercial FCD speed for urban arterial was evaluated by performing a set of analysis to determine the current quality for speed and Level of Service (LOS) estimation and quantify its current penetration rate.

1.2. Scope of the Study

There is still no established methodology for FCD use in estimation of queue length in real life, as shockwave based queue length algorithms generally utilizes vehicle trajectories, which cannot be applicable for commercial FCD, as it carries an average speed data instead of individual vehicle time and location specifics; thus, it requires redefinition of “queue” and QL estimation using average speed information, which is the scope of this study.

For this purpose, analytical model was developed to estimate the queue lengths via commercial FCD. The model is mainly based on determination of speed threshold value for queue length estimation. Speed field, generated from FCD using 4-node quadratic interpolation technique, was used to create imaginary vehicle trajectory data and provided iso-speed contours in FCD. To control data quality, first, the model performance was tested in VISSIM environment by creating a hypothetical approach leg of a signalized intersection. Later, model performance was tested in two study corridors (uninterrupted urban arterial and signalized intersection) located in Ankara. To evaluate the model performance, Ground Truth (GT) data was also collected via video recording for both cases. For uninterrupted arterial, GT speed and flow data was obtained during two weekdays including morning and off-peak hours, which was used to

- i) evaluate the current quality of FCD in terms of speed and LOS estimation,
- ii) derive analytical relation between FCD speed and GT speed, which will be later used to estimate FCD speed threshold for queue length estimation.

Additionally, GT data was also collected for signalized intersection to observe actual queue lengths which was later used to compare the estimated queue lengths obtained from the proposed model. For all cases, Mean Absolute Percentage Error (MAPE) and root mean square error (RMSE) were selected as performance indicators to evaluate model performance.

1.3. Structure of the Thesis

Chapter 2 mainly presents the required background necessary to study FCD and queue length estimation. This chapter mainly consists of three sections. The first section includes the FCD studies in traffic engineering especially in traffic state estimation, traffic flow estimation and FCD quality evaluation. The second section covers the background information for traffic flow modeling concept and the final section includes the queue length estimation studies.

Before, discussing the proposed methodology for queue length estimation, Chapter 3 describes the structure of current commercial FCD and includes various analysis to evaluate the existing quality of FCD in terms of speed and Level of Service (LOS) estimation performance and its potential for urban traffic monitoring. Current penetration rate of the FCD is also discussed. Chapter 4 presents the proposed methodology for queue length estimation from FCD for signalized intersections and uninterrupted urban arterials, followed by simulation-based analysis results in Chapter 5. Chapter 6 includes the queue length estimation results for commercial FCD and followed by the conclusion section in Chapter 7.

CHAPTER 2

LITERATURE REVIEW

As a background for the proposed methodology and research findings, some key aspects of the available literature is summarized. The first part of the section provides the potential usage of FCD speed (obtained from either commercial companies or probe vehicle data) in traffic engineering studies especially for traffic state and traffic flow estimation for urban arterials. Furthermore, the studies regarding the effect of penetration rate of FCD for quality evaluation are also presented. The second part of the section mainly focused on traffic flow modeling concept and followed by the queue length estimation methods and related studies.

2.1. FCD Studies

The potential use of the FCD in traffic engineering studies is summarized by Leduc (2008) as follows:

- Detection focused: Congestion detection, traffic state estimation, incident detection, origin-destination matrix determination for commuter trips.
- Application focused: i) Optimization of existing infrastructures through a better use of the current road network, ii) dynamic network traffic control, iii) improved information services e.g. traffic information, dynamic route guidance, road message signs, etc., iv) improved vehicle fleet management especially for cargo companies, and v) shorten driving times to reduce costs.
- Planning and Policy focused: Plan for future investments, new perspectives in transport modelling: real-time data could be used to set up dynamic transport models capable to provide forecasts in a very short period of time.

Among the potential usage of FCD discussed above, the researchers in the literature more focused on the four main concepts to evaluate its potential for i) traffic state estimation, ii) traffic flow estimation, iii) quality evaluation and iv) queue length estimation as shown in Figure 2.1 and further discussed in the following subsections.

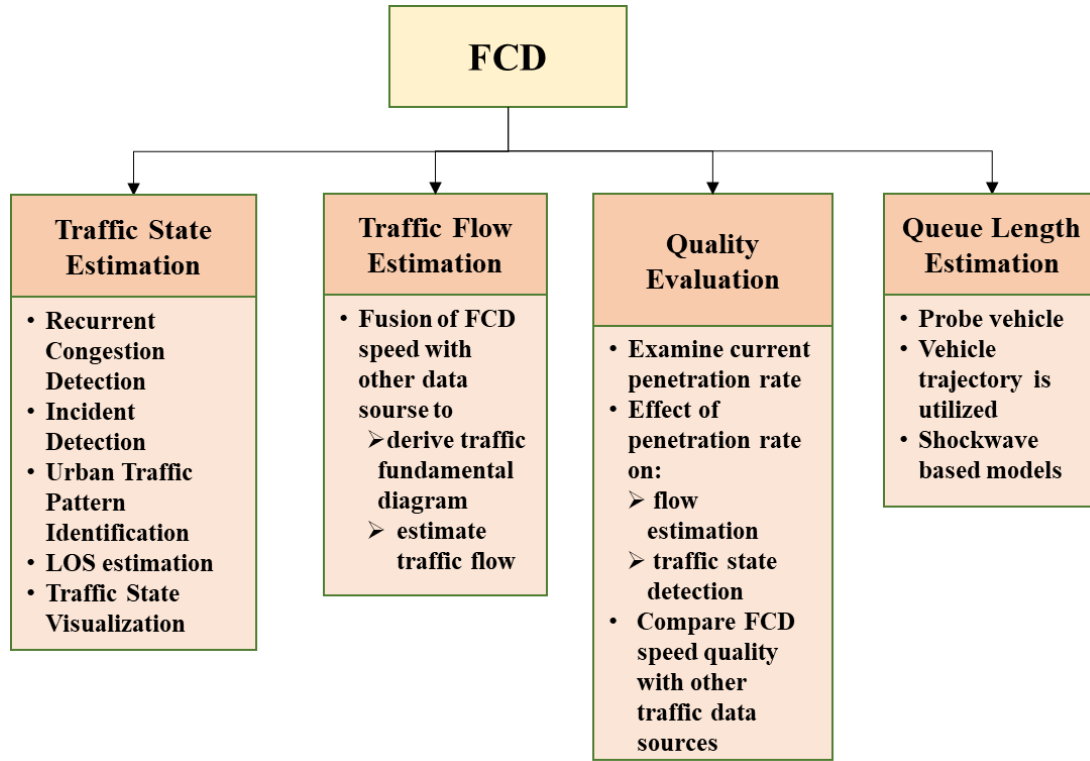


Figure 2.1. Floating Car Data (FCD) based studies.

2.1.1. Traffic State Estimation

In the absence of additional data sources, to detect traffic states, examining speed profiles of the selected corridor enabled to observe sudden changes amongst consecutive segments, as well as exploring the statistical distribution of speeds for each road segment (Quayle et al., 2010; Pan et al., 2011; Shoufeng et al., 2013; Wang et al., 2014). This will later be used to identify the recurrent/non-recurrent congestion locations or detection of the bottleneck locations (Xu et al., 2013; Li et al., 2012; Reinthaler et al., 2010).

Traffic state estimation studies have been performed either using historical data set or using real time traffic data (Petrovska and Stevanovic, 2015). Historical data analysis covers the examination of the speed distribution, statistical methods such as clustering, principal component analysis, etc. to capture the traffic states. Pongnumkul et al. (2013) used historical data set for examining the speed profiles and defined different congestion levels based on the different speed values to state traffic states. However, the authors did not clearly state how they determined these speed thresholds for the congested levels. Vasudevan et al. (2015) defined the congestion state based on the decrease in speed in accordance with the free flow speed. While, highly congested state was defined as the speed less than the $\frac{1}{3}$ of the free flow speed, uncongested state was specified as the speed greater than $\frac{2}{3}$ of the free flow speed.

Pascale et al. (2015) proposed the spatio-temporal clustering methods for the traffic state estimation in urban arterial. Clustering analysis resulted in 6 different states and threshold speed values were determined for each state. Later, selected urban arterial was visualized according the determined speed thresholds. On the other hand, Liu et al. (2015) defined speed threshold values for 5 different traffic states, but they did not discuss how they obtained these threshold values. Li et al. (2012) used 3 months of historical FCD to examine variabilities in average speeds, and attempted to determine congestion locations depending on sudden decreases in average speeds in consecutive road segments. Xu et al. (2013) highlighted the issues when dealing with the enormous historical data set when endeavoring to find meaningful traffic and congestion patterns. They obtained FCD from 12,000 GPS-equipped taxi fleets in Wuhan city, China. They proposed a statistical method for data analysis (data cube management) for congestion detection. Adu-Gyamfi and Sharma (2015) proposed time series data analysis to identify similar traffic patterns, especially congested one. Their model had a success of 74% accuracy for freeways, while this percentage was 63% for urban arterial.

Reinthal et al. (2010) used FCD from both taxi fleets and public transport in the German city of Dusseldorf. Public transportation-based data was found to provide more accurate results for speed and travel time values. Furthermore, they developed a model to integrate these two data sources for estimating traffic states and to identify the most congested locations. Altintasi et al. (2017) also proposed pattern search algorithm to detect 12 different traffic states (i.e. bottleneck release locations, congested flow, stable flow conditions etc.) from FCD and their algorithm successfully detect the traffic states for urban arterial. Different than these studies, Fabritiis et al. (2008) utilized real time FCD to estimate short term speed prediction (15-min and 30-min) as well as detecting the congestion location for the Roma Ring Road. FCD speeds were obtained for a one day with 3-min aggregation. A neural network-based model was proposed which estimated the short term speeds with 2% to 8% for 15-min and 3% to 16% for 30-min predictions. Furthermore, congested locations were detected with 90% accuracy.

2.1.2. Traffic Flow Estimation

Particularly for the determination of the relationship between traffic flow parameters, two of the three parameters (speed, density and flow) must be known, in order to explain the relationships between them. Since FCD provided only speed data, combining such data with other traffic data sources (such as the RTMS, inductive loops, video cameras, Automated Vehicle Identification systems etc.) enabled to establish traffic fundamental diagram. These kinds of studies involve data collection and implementation of well-known traffic flow models to best fit the data (Zhao et al., 2009; Anuar et al., 2015).

Few studies were performed to examine the potential of commercial FCD speed for developing fundamental diagram. More comprehensive study was conducted by Chase et al. (2012) by utilizing Inrix speed data (a private company providing FCD speed) and microwave radar sensor data to investigate speed-flow relationships. The authors

stated that due to systematic errors occurring in the FCD, the desired speed-flow relation could not be obtained. These systematic errors were the truncation of the speed at the posted speed limit in FCD and the low penetration rate.

Zhao et al. (2009) analyzed traffic flow characteristics on ring road expressways in Beijing using FCD and RTMS data. However, in this study, FCD speeds were obtained from probe vehicle trajectory data. While average speeds were obtained from both data types, whilst volumes were accessed from RTMS data only. Data were combined, in order to derive the flow-speed relationship in which Van Aerde traffic flow model was chosen the best model to explain this relation. Furthermore, results indicated that speeds of the two dataset were highly correlated with R^2 value of 0.98. Similar to this study, Anuar et al. (2015) used probe vehicle based FCD speed and loop detectors for traffic flow estimation. Four different traffic flow models were employed (Greenshield, Northwestern, Underwood and Van-Aerde) and Van Aerde traffic flow model was selected as the best one with 98 veh/h/ln RMSE.

2.1.3. FCD Quality Evaluation

Parallel to the increased use of FCD in traffic estimation, evaluating the quality of FCD has been the focus of many studies (Table 2.2 and Table 2.3). FCD quality was compared to speed from additional traffic data sources or to ground truth data, such as Bluetooth speed data, sensors or loop detectors. Studies showed that FCD presented different performance on freeways than urban arterials. Urban arterials had a more challenging environment due to traffic signals, intermediate access points, and other flow-interrupting situations (such as bus stops, speed enforcement points, etc.); thus, additionally requiring a higher penetration rate to detect traffic states (Hu et al., 2016; Cambridge Systematics, 2012).

Haghani (2010) compared the average speed of road segments obtained from FCD and Bluetooth data. Statistical evaluation was performed for 4 speed categories: i) below

30mph, ii) 30-45 mph, iii) 45 and 60 mph, and iv) speed above 60 mph. Bluetooth mean speeds were not found to be significantly different from the FCD speeds for each speed category. Zhao et al. (2009) compared the RTMS and FCD average speeds, and stated that RTMS speed values were generally 6% higher than FCD speed values. Chase et al. (2012) evaluated the reported speeds obtained from 3 different kinds of traffic data: i) FCD was obtained from Inrix with 5-minute aggregation. Travel time, speed, average speed and reference speed data were obtained; ii) Microwave radar sensors with 5-min aggregation speed data. Volume and occupancy values were collected from the same corridor for the same study period; iii) Radar sensors, for which only speed values were obtained. Speed profiles showed that all data types had a similar pattern. Speed differences obtained from Inrix and microwave radar sensor data were compared and differences were found normally distributed.

Inaccuracy of FCD speeds for urban arterial was attributed to low penetration rate of the FCD, while it was found to be successful for travel time estimation for freeways (Kondyli et al., 2016). Zhao et al. (2009) found a highly correlated linear relationship between RTMS and FCD speeds ($R^2=0.97$ for a freeway), but Hu et al. (2016) found a maximum $R^2=0.36$, when the ground truth speed was between 64.4-72.4 km/h for an urban arterial. Mean Absolute Percentage Error (MAPE) was reported to be rather high when the speed was below 15 km/h (209%), and the lowest MAPE obtained was between 72.4-80.5 km/h as 4.1%. Accuracy of FCD was found to be not acceptable for real-time traffic state estimation, but useful for long-term traffic characterization. Kim and Coifman (2014) showed that FCD responded to a sudden speed change 6-minute later, and quality of the data reduced for speeds lower than 56 km/h. Wang et al. (2014) reported that FCD produced a systematic bias and could not capture sudden changes in traffic states.

Table 2.1. *Studies comparing FCD with different traffic data sources on Freeways.*

Study	Data type	Length	Duration	GT Data	Measure of Effectiveness
Kondyli et al. (2016)	FCD (STEWART, INRIX, HERE) and Bluetooth	12.6km	1 day (15:30-18:30)	Probed vehicles	FCD overestimated the travel times
Zhao et al. (2009)	FCD(INRIX)	NA	5 days (06:00-10:00)	RTMS	Linear regression, $R^2=0.97$
Wang et al. (2014)	FCD(INRIX)	123.9km	7 days	License plate readers	A quick response for road closure
Adu-Gyamfi and Sharma (2015)	FCD(INRIX)	NA	1 month	Loop Detectors	Detect short term congestion events with 74% accuracy
Chase et al. (2012)	FCD(INRIX, TrafficCom and SpeedInfo)	3.2km	20 days	RTMS	Systematic errors observed in TrafficCom
Haghani et al. (2010)	Bluetooth	148.1km	9 days	FCD (INRIX)	Not significantly different for each speed bin
Latimer and Glotzbach (2012)	FCD(INRIX, TrafficCast and HERE)	32.2km	4 days (06:00-20:00)	Probed vehicles	INRIX had a less average absolute speed error
NA=Not Available					

Table 2.2. *Studies comparing FCD with different traffic data sources on urban arterials.*

Study	Data type	Length	Duration	GT Data	Measure of Effectiveness
Hu et al. (2016)	FCD (INRIX)	2.8km	1 month	Bluetooth	Up to 209% MAPE observed at congested hours
Kondyli et al. (2016)	FCD (HERE)	NA	1 day (15:30-18:30)	Probed vehicles	Not accurately estimated speed due to the small sample size
Kim and Coifman (2014)	FCD (INRIX)	22.4km	2 months	Loop detectors	Average absolute speed error of 4.8-9.6 km/h
Wang et al. (2014)	FCD	4.8km	7 days	License plate readers	Mean absolute percent error in speed as 17-73%
Adu-Gyamfi and Sharma (2015)	FCD (INRIX)	NA	1 month	Loop Detectors	Detect short term congestions with 63% accuracy
Anuar et al. (2015)	Probed vehicle	NA	1 day (10:00-18:00)	Loop detector	6.4% MAPE in average
Schneider et al. (2010)	FCD	14.4km	1 day (06:30-10:30/ 15:30-19:30)	Bluetooth	Not significantly different results
Brockfeld et al. (2007)	Taxi-FCD	2km	4 days (morning and evening peaks)	License plate readers	Short term speed drops were not captured
Quayle et al. (2010)	Bluetooth	1.28km	1 day (07:00-09:00)	FCD	Showed similar pattern
NA=Not Available					

2.1.4. Penetration Rate for FCD Quality

Quality of FCD depends certainly on the source of the GPS-based data feeding to as well as the nature of aggregation in FCD process. The impact of the FCD penetration rate was investigated mainly for different purposes as i) travel time reliability, ii) traffic state detection (such as, congestion or incident detection), and iii) speed prediction. Brockfeld et al. (2007) utilized a taxi-based FCD system in urban corridor with 2 km long in Nuremberg, Germany, to investigate the impact of FCD penetration rate for congestion detection. Due to the insufficient penetration rate, FCD travel time data was evaluated by aggregating 15-min intervals and compared with license plate recognition data collecting in 4 days. Results indicated that while long term congestion

was detected with a high reliability, short time congestion could not be captured precisely. However, the current penetration of FCD was not discussed for the study location. Kerner et al. (2005) investigated the minimum FCD penetration rate required for better traffic state estimation. The results showed that 1.5% FCD penetration rate enabled detection of an incident location with a 65% probability. When the FCD penetration was 2%, success rate was 85%. Vandenberghe et al. (2012) investigated the minimum penetration rate as well as the FCD time interval to be required for detecting incident and traffic congestion location in a simulation environment. While FCD with 1.0% penetration rate and 10 sec interval was successful to detect incident locations for highways, this rate was not adequate for urban arterials. Hong et al. (2007) also proposed minimum 2% penetration rate for traffic state detection by performing simulation based analysis.

For the speed prediction studies, while Herrera et al. (2010) specified 2-3% FCD penetration rate is enough for better speed prediction, Cheu et al. (2002) found this rate as 6% for their simulation based study. A more compressive study has been conducted by Klunder et al. (2017) regarding the effect of different FCD penetration rate for speed prediction in a 100 m urban road segment in Amsterdam, Netherland. Average absolute percentage errors (AAPE) have been computed for different penetration rates and they fit a curve showing the relationship between the penetration rate and corresponding estimation error. For 1% penetration rate, AAPE was not reported due to the higher error, but 10% penetration rate generated 5.6% AAPE value. Fabriitis et al. (2008) reported that at least 2.4% penetration rate was necessary for better speed prediction, while the current penetration rate was calculated as 1.7%. In an attempt to derive fundamental diagram using loop detector flow data and FCD speed data, Sunderrajan et al. (2016) created various scenarios with different FCD penetration rates; the minimum percentage of FCD was found as 5% for better estimation of this diagram.

2.2. Traffic Flow Modeling

2.2.1. Traffic Fundamental Diagram

For better management of traffic on urban arterials, it is essential to derive a fundamental diagram (FD), which is the mathematical representation of the relationships of the flow parameters of average speed (u), density (k) and flow (q) at a macroscopic level. Relations between $u - q - k$ for an urban corridor have a crucial effect on the arterial design and planning for effective solutions to urban arterial congestion problem (Van Aerde and Rakha, 1995). The basic relation between the traffic flow parameters is

$$q = uk \quad [2.1]$$

which captures the limiting traffic flow conditions such that there will be no flow, if average speed or density is zero. Relations between two parameters, such as $(u - q)$, $(u - k)$ or $(q - k)$ are necessary to further study the nature of traffic flow such as capacity.

The traffic flow simply defined as number of vehicles passing some designated roadway point during a time. In general traffic flow can be calculated as

$$q = \frac{1}{\bar{h}} \quad [2.2]$$

where; \bar{h} represents the average time headway in unit time per vehicle and calculated as follows:

$$\bar{h} = \frac{\sum_{i=1}^n h_i}{n} \quad [2.3]$$

where; h_i is the time headway between the passages of the front bumpers of successive vehicles at some designated highway point, and n is the number vehicles.

Space mean speed, on the other hand can be defined as the average speed of the vehicles based on the total time spent travelling over a given length of the roadway and calculated as

$$\bar{u} = \frac{1}{\frac{1}{n} \sum_{i=1}^n \frac{1}{u_i}} \quad [2.4]$$

where; u_i is the speed of the i^{th} vehicle.

If a 2-parameter relation is obtained from site observations, it is always possible to get the third parameter from Equation [2.1]. The traditional fundamental diagram representing the relationship between the flow and density is illustrated in Figure 2.2. Greenshields (1935) proposed a linear relationship between speed and density for uninterrupted traffic flows observed on highways, which produced a parabolic flow-density (and flow-speed) relationship. However, this model was not found reliable for congested traffic regimes (Zhao et al., 2009). To simulate realistic traffic flow, more complex models have been developed in recent decades. These models used nonlinear relationships between speed and density. Three different exponential functions, which have non-linear speed-density relations, were developed in Underwood (1961), Northwestern (1967), and Pipes (1967). Later, Van Aerde (1995) proposed a single traffic regime flow model that captured the different flow conditions both free flow and congested regimes in a single equation.

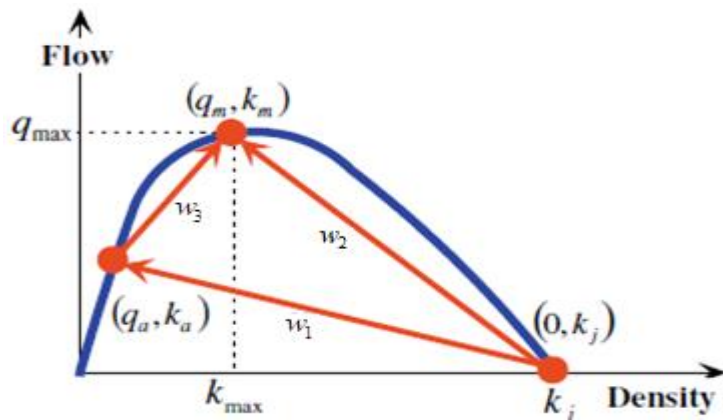


Figure 2.2. Shockwave speeds in fundamental diagram (Liu et al., 2011).

2.2.2. Queue Definitions for Interrupted and Uninterrupted Traffic Flows

What defines entering to or exiting from a queue is a very essential issue that's need to be clarified for both interrupted (such as, signalized intersection) and an uninterrupted urban arterial since they have different traffic flow characteristics. For the former one, HCM (2010) defined “Stopped-Vehicle State (or Queued State)” showing the state when a vehicle is in the queue. To determine the “Stopped-Vehicle State”, speed thresholds are used in which the selection of a near-zero speed threshold value would be more stable instead of selecting zero speed threshold. The report suggested to use 5 km/h speed threshold for entering the queue. An example vehicle trajectory data for signalized intersection is provided in Figure 2.3, showing the queue entrance and move locations more clearly.

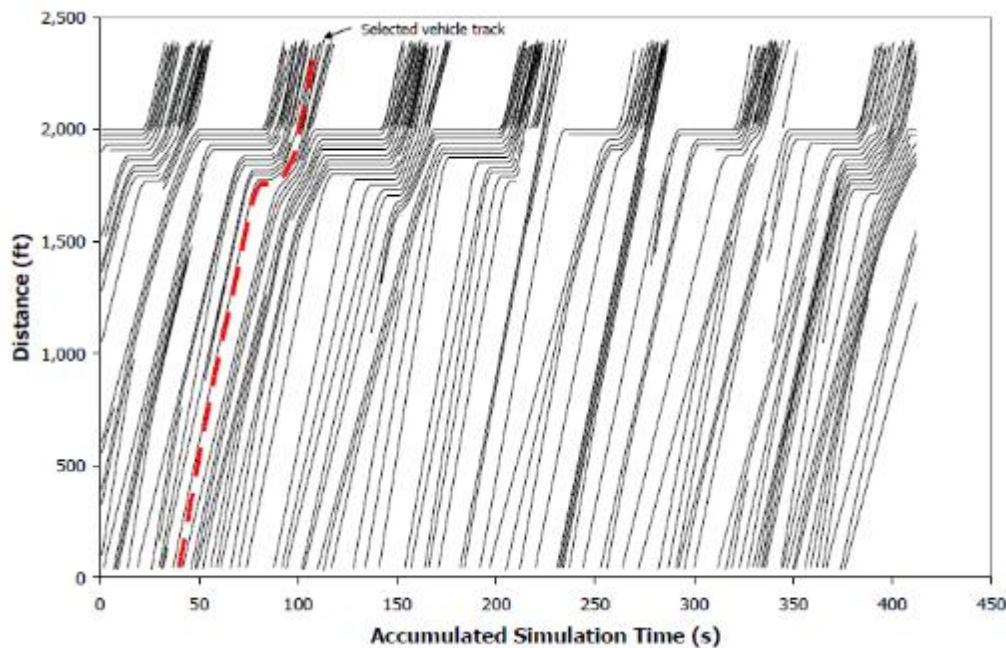


Figure 2.3. Space time diagram including vehicle trajectories for several signal cycles on a signalized approach (HCM, 2010).

Queue definition for uninterrupted flows is completely different since the traffic flow is continuous and is not interrupted with the signals. In other words, in this case no “Stopped-Vehicle State” occurs because the vehicle never came to stop. So, assuming 5 km/h speed threshold is not applicable. An example vehicle trajectory data for very congested segment is provided in Figure 2.4. As it can be seen from the Figure 2.4, the queue entrance and move locations are not clear as the interrupted flow condition.

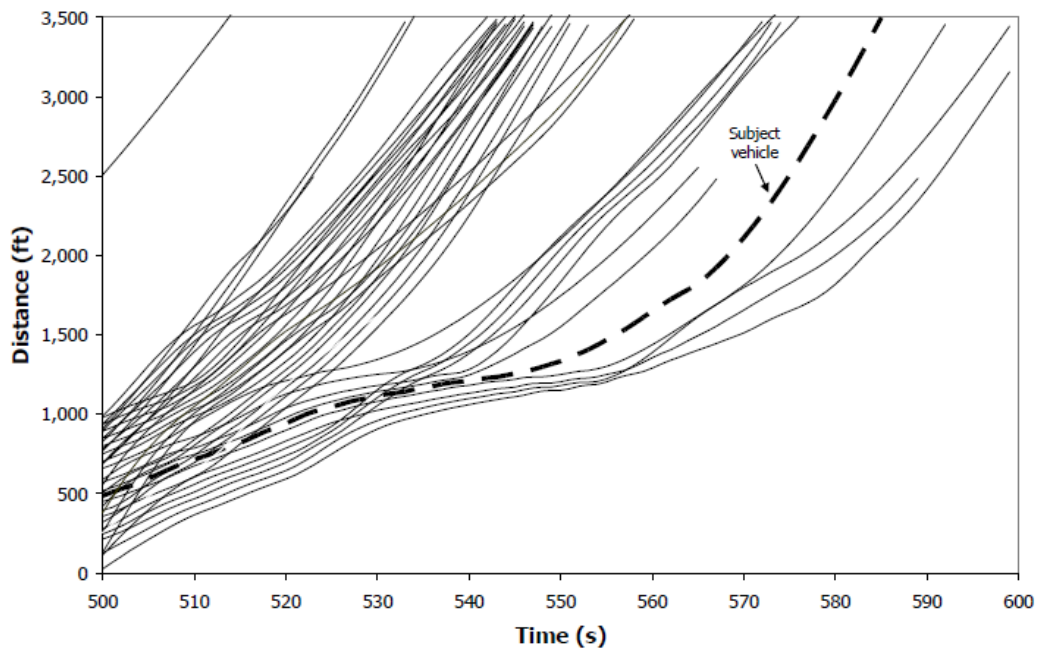


Figure 2.4. Space time diagram including vehicle trajectories for oversaturated road segments for uninterrupted flows (HCM, 2010).

On the other hand, for queue detection, derivation of traffic fundamental diagram is necessary to identify i) traffic flow parameters (such as, capacity flow, density and speed at capacity, jam density), ii) undersaturated and oversaturated regions based on the aforementioned parameters. HCM (2010) provided flow-density relationship for the different free-flow speed (FFS) values, separately for the uninterrupted flow condition (see Figure 2.5 for FFS of 75 mi/h). After determination of the capacity flow and density at capacity, the region where the density values lower than the density at capacity is depicted as the undersaturated region. The other side, however, is regarded

as the oversaturated region. Based on these information, “Moving-Vehicle State” concept was defined as follows:

- The uncongested state, in which a vehicle is moving in a traffic stream that is operating below its capacity
- The congested state, in which the traffic stream has reached a point that is at or slightly above its capacity, but no queuing is observed; and
- The severely congested state, in which downstream bottlenecks have affected the operation and queue occurs.

So, it is crucial to determine the speed value for severely congested state where the queues are observed.

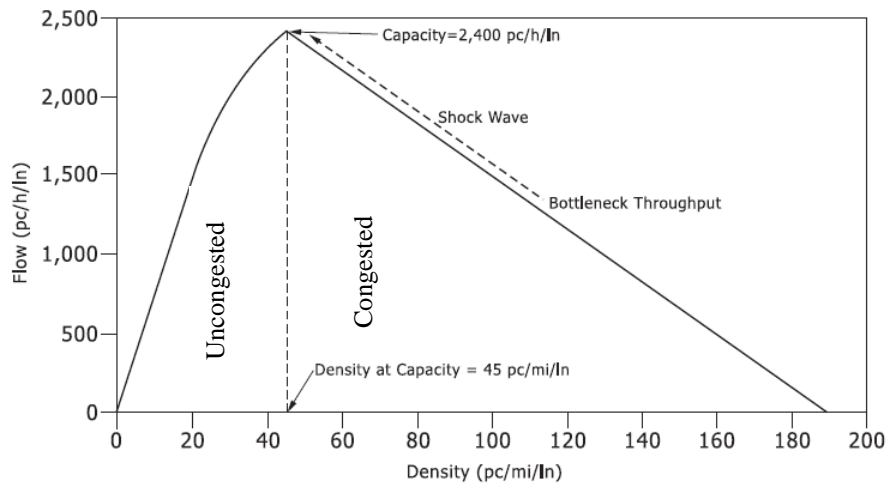


Figure 2.5. Flow-density relation for FFS of 75 mi/h (HCM, 2010).

A precise definition for distinguishing congested state and severely congested state required more complex algorithms (HCM, 2010) but the report suggested to select threshold speeds in which severely congested region could be specified when the speed is below one-third of the target speed. The target speed here, is the speed at which the driver prefers to travel. Other study conducted by Hall et al. (1992) generalized the speed-flow curve for collecting the traffic data during 52 days from multilane highway located in Ontario, Canada (see Figure 2.6). The authors divided

the speed-flow curve into three part as: i) the speed higher than the speed at capacity was named as uncongested region, ii) the traffic flow near the capacity was named as the queue discharge region (Segment 2 in Figure 2.6), and iii) the breakpoint at which speeds started to decrease from speed at capacity and this region was named as “within a queue”.

In addition to these information for queue detection, independent from the speed-flow curves, Elefteriadou et al. (1995) utilized loop detector data to identify the speed threshold limits to detect queue lengths near a bottleneck location on a freeway. Based on the 3-months of loop detector data the authors reported speed threshold limit of 35 km/h. In other words, the vehicle speed dropped below 35 km/h, regarded as entering the queue.

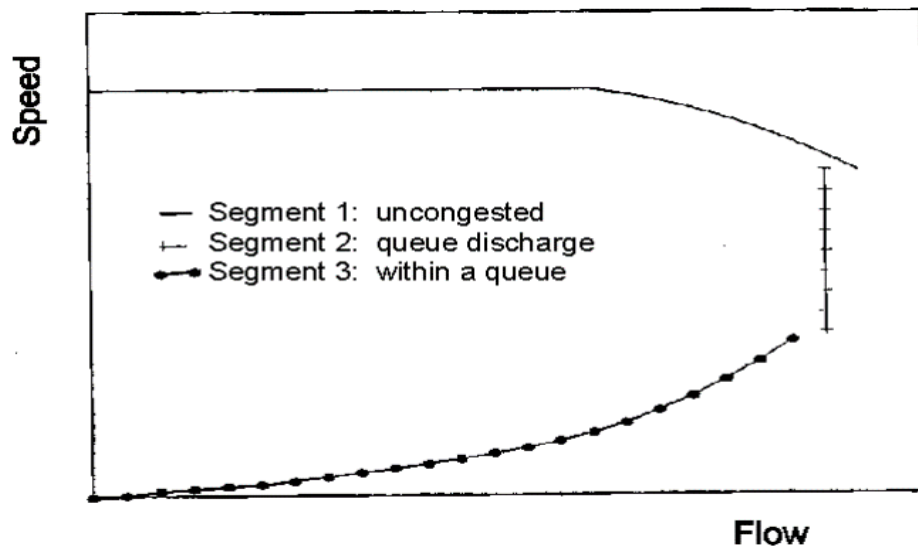


Figure 2.6. Generalized shape of speed-flow curve for uninterrupted flows (Hall et al., 1992).

2.2.3. Traffic Flow at Signalized Intersections

Before discussing the queue length estimation models and related studies, it is useful to discuss the key concepts and definitions used in the analysis of traffic at signalized

intersections. The first crucial concept is the saturation flow rate which represents the maximum number of vehicles that can pass through a signalized intersection if the intersection is green during one-hour (HCM, 2010). Saturation flow rate can be calculated as

$$s = \frac{3600}{h} \quad [2.5]$$

Where

s : saturation flow rate in veh/h,

h : saturation headway in sec/veh, and

3600: number of seconds per hour.

Based on HCM (2010), saturation flow can be determined by calculation of the saturation headway after the 4th vehicle following the beginning of a green time as shown in Figure 2.7. When a signal changes from red to green, the vehicles in the queue do not start moving simultaneously; there could be initial lag due to drivers reacting to the change of signal indication (Mannering et al., 2009). The drivers do not completely utilize the green time and causes some losses, namely start-up lost time (see Figure 2.7). HCM (2010) recommended to take 2 sec/phase as a start-up lost time. Furthermore, when the signal indication changes from green to yellow and if there is an all-red interval (AR), there could be another lost time, namely clearance lost time. Thus, the total lost time (t_L) can be calculated as

$$t_L = t_{sl} + t_{cl} \quad [2.6]$$

Where

t_L : total lost time for a movement during a cycle in seconds,

t_{sl} : start-up lost time in second, and

t_{cl} : clearance lost time in seconds.

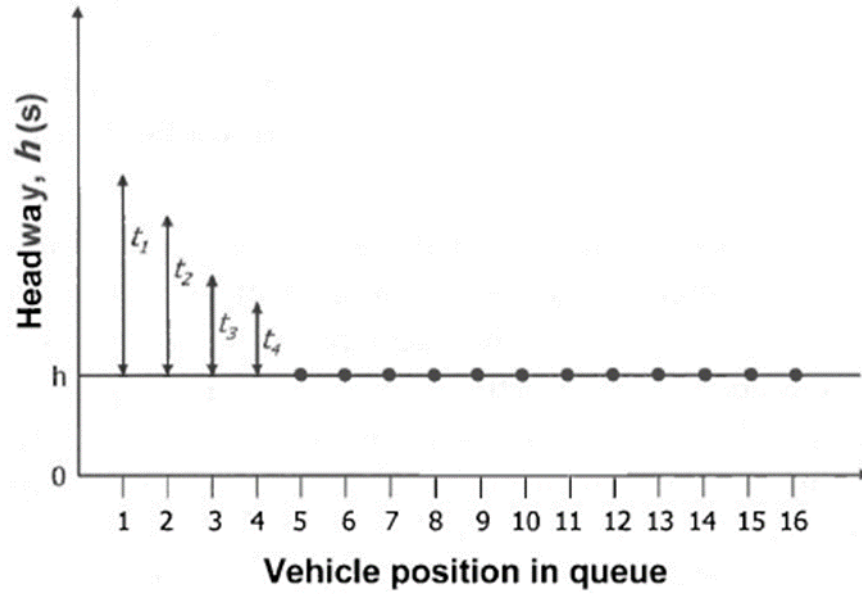


Figure 2.7. Saturation flow rate and lost time for a signalized intersection (HCM, 2010).

Another important parameter is the calculation of the effective green time (g) that represents the time which is effectively used by the traffic and calculated as follows:

$$g = G + Y + AR - t_L \quad [2.7]$$

Where

G : displayed green time for a traffic movement in seconds,

Y : displayed yellow time for a traffic movement in seconds,

AR : displayed all-red time in seconds.

Approach capacity is also crucial parameter for signalized intersections. The capacity of the approach represents the hourly volume that can be accommodated when the intersection approach had less than 100% green time (Mannering et al., 2009), and formulated as follows:

$$(c = s * g / C) \quad [2.8]$$

Where

c : capacity (maximum hourly volume of a movement) in veh/h,

s : saturation flow rate in veh/h,

g/C : ratio of effective green time to cycle length.

Finally, degree of saturation, denoted as X , can be calculated (see Equation [2.9]) showing the traffic condition of the approach, whether oversaturated or undersaturated as follows:

- If $X < 1$, arrival flow per cycle can be discharged in a single green period (undersaturated intersections), and when this value closes to one then the arrival flow reaches to capacity flow.
- If $X > 1$, then the approach is oversaturated and arrival flows per cycle can not be discharged in a single green period and residual queues could be observed.

$$X = \left(\frac{q / s}{g / C} \right) \quad [2.9]$$

2.2.4. Shockwaves in Signalized Intersections

The traffic data obtained from either loop detectors or probe vehicles, the Lighthill-Whitham-Richard (LWR) shockwave models are commonly most preferable for queue length estimation which uses the principles of conservation of vehicles and a traffic fundamental diagram that explains the flow-density relation (Mecit, 2012).

At signalized intersections, signal changes lead to the generation of various shockwave speeds as

$$w = \frac{\Delta q}{\Delta k} = \frac{q_2 - q_1}{k_2 - k_1} \quad [2.10]$$

which is the difference in flows of the two traffic states divided by the difference in densities. The shockwave speeds are illustrated on traffic fundamental diagram in Figure 2.2.

When the signal is in red interval, vehicles were forced to stop and generating backward moving shockwave speed (donated as w_1) and formulated as:

$$w_1 = \frac{0 - q_a^n}{k_j - k_a^n} \quad [2.11a]$$

where q_a^n and k_a^n represents the arrival flow rate and density, respectively for the cycle n . k_j represents the jammed density. Liu et al. (2009) specified the shockwave speed on an approach of an intersection more explicitly, as shown in Figure 2.8a. When the red time turns to green then the second shockwave speed is formed, discharge shockwave, and vehicles are assumed to discharge at saturation flow rate (Mecit, 2012) and formulated as:

$$w_2 = \frac{q_m - 0}{k_m - k_j} \quad [2.11b]$$

where q_m and k_m represents the saturation flow and density at saturation flow condition. The two shockwave speeds are overlapped at a time, showing the maximum queue length location. Later, new shockwave speed is formed which is defined as departure shockwave (see Figure 2.8c), w_3 , and formulated as:

$$w_3 = \frac{q_m - q_a^n}{k_m - k_a^n} \quad [2.11c]$$

For the oversaturated condition where the residual queue exists at the end of the green time, forth shockwave speed is formed (Figure 2.8d), w_4 , moving to upstream with a speed of

$$w_4 = \frac{0 - q_a^{n+1}}{k_j - k_a^{n+1}} \quad [2.12d]$$

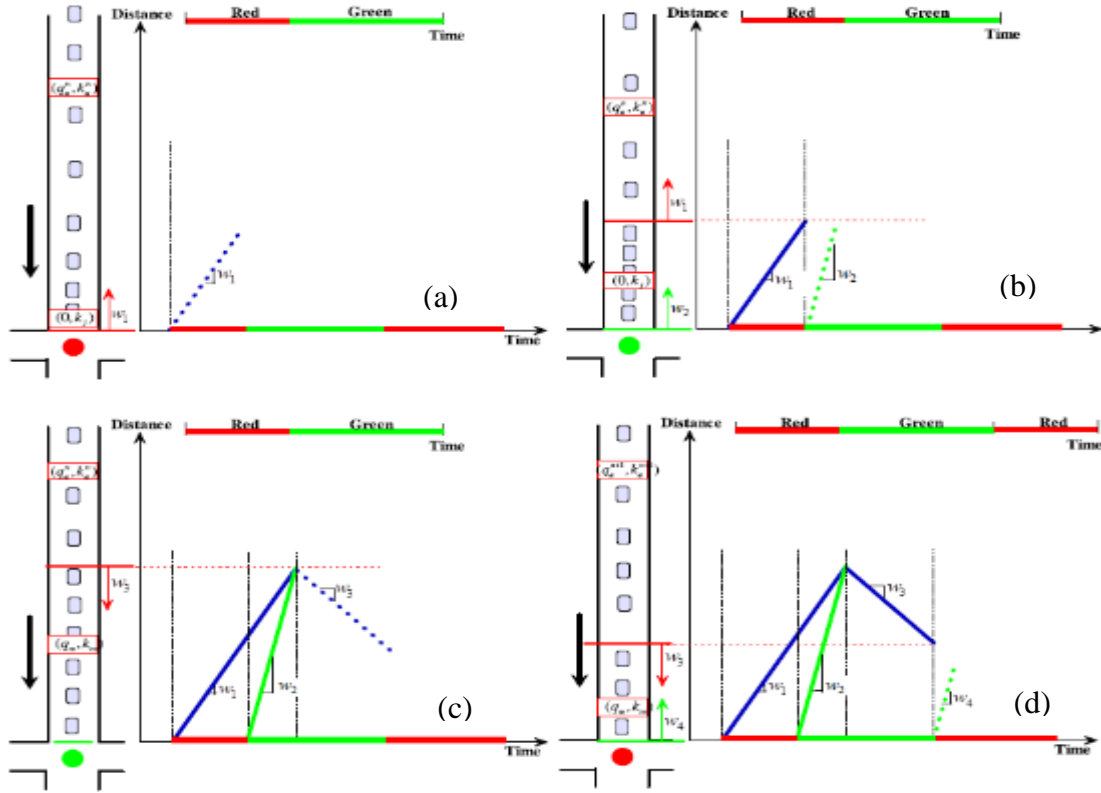


Figure 2.8. Shockwave speeds for a signalized intersection (Liu et al., 2009).

2.3. Queue Length Estimation Studies

For delay minimization based control, queue length of an approach is one of the main parameters (Tiaprasert et al., 2015). Typical methods for queue (which is also called maximum queue) length include either a cumulative traffic input-output model or a shockwave based model (Li et al., 2013). The former one was first proposed by Webster (1958) and utilized by many researchers for queue length estimation (Akcelik, 1999; Strong et al., 2006; Sharma et al., 2007). This model requires the determination of the cumulative arrival and departure flow continuously at intersections that cannot be always practical in real cases (Cai et al., 2014) when the rear of the queue exceeds the vehicle detector location. This leads to larger estimation error in queue estimation (Skabardonis, and Geroliminis, 2008). Furthermore, it could not provide spatio-temporal distribution of the queue length (Liu et al., 2009). On the

other hand, the most common technique is implementation of Lighthill-Whitham-Richard (LWR) shockwave model. For this model, it is crucial to measure the arrival traffic flow rate for each cycle which can be provided by either fixed-point sensors (i.e. inductive loop detectors) (Akcelik, 2001; Skabardonis and Geroliminis, 2008, Liu et al., 2009) or mobile sensors (Comert and Cetin, 2009; Ban et al., 2011). Unlike input-output model, LWR shockwave model provided the complicated queuing process in both temporal and spatial dimensions.

2.3.1. Queue Length Estimation with Loop Detector

Queue length estimation at signalized intersections studies traditionally required arrival flow data, which is generally provided by the loop detectors. Loop detectors provides reliable and more accurate traffic data (such as volume, occupancy, headway, and time gap) which are the essential parameters for the queue length estimation (Klein, 2006). However, the main drawback of this system is that when the queues exceed the detector location, then it could not be possible to collect arrival flow data. Thus, the location of the loop detector for the upstream of the intersection is necessary. According to the FHWA (2006) report, the location of the loop detector was associated with minimum green time interval and approach speeds for low-speed approaches while approach speed was used only parameter for high-speed approaches as shown in Table 2.3. On the other hand, SCOOTs, is a commercial company for performing adaptive signal control systems, stated that the loop detector should be located 8-12s travel time from the upstream of the intersection.

Existing studies regarding queue length estimation from loop detectors generally have not been depended on such distances. For example, Liu et al. (2009) proposed a shockwave based queue length estimation model for oversaturated intersections by defining different break points from detector occupancy and time gap data. The loop detector was located 120 m distance from the stop line. In their study, queue length for each cycle exceeded the detector location, and the authors defined three break

points (A, B, and C as shown in Figure 2.9) which represent the times that the traffic flow changes at the detector location.

Table 2.3. Loop detector location and related parameters for urban signalized intersections (FHWA, 2006).

Low Speed Approach	Approach Speed		Loop detector location from stop line	Minimum green time
	mi/h	km/h	meter	second
	15	24	12	9
	20	32	18	11
	25	40	24	12
High Speed Approach	Approach Speed		Loop detector location from stop line	
	mi/h	km/h	meter	
	35	56	77	
	40	64	87	
	45	72	100	
	mi/h	km/h		
	50	80	108	
	mi/h	km/h		
	55	88	118	

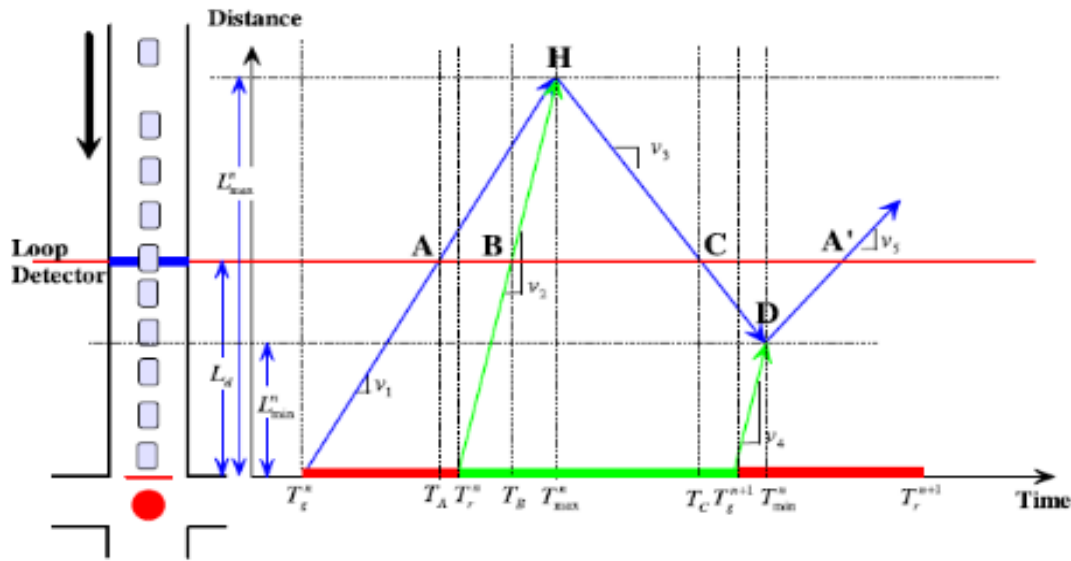


Figure 2.9. Shockwave speeds and break points at an intersection (Liu et al., 2009).

The break point A and B was calculated from the detector occupancy time by assuming the 3 s occupancy time was a threshold value as shown in Figure 2.10a. Thus the time, T_A in Figure 2.9 was recorded when the detector occupancy was greater than 3 sec and by performing simple mathematical operations backward moving shockwave was

calculated. Similarly, discharge speed was determined by determining T_B , which is the time that detector occupancy was less than 3 s. Thus, the point H, which is the maximum queue location, can be determined by solving equation of the two lines. On the other hand, Point C, was calculated from time gap data as shown in Figure 2.10b, later be used to calculate residual queue location which is Point D in Figure 2.9. Their model had a MAPE value of 9.34% to 22.03% with an average of 14.93%.

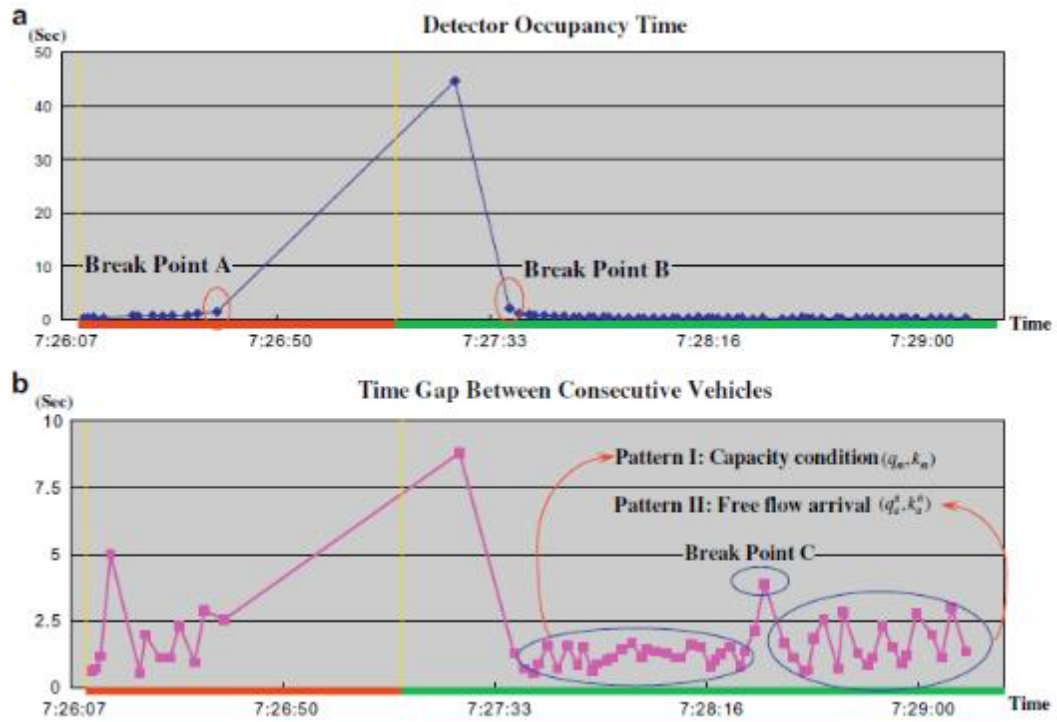


Figure 2.10. a) Detector occupancy time, b) time gap data for a one cycle (Liu et al., 2009).

Similar study conducted by Geroliminis and Skabardonis (2008) that the authors proposed shockwave based model by utilization of real time 30 sec aggregated loop detector data. While the occupancy and time gap values were utilized to estimate maximum queue location, the aggregation of these values made it harder to determine the time gap data between consecutive vehicles. While the model had a great success for estimating maximum queue length in uniform arrival pattern, the model had limited success when fluctuations in arrival traffic flow was observed. On the other hand,

Muck (2002) proposed a linear regression model instead of using shockwave based model to estimate queue lengths when the queue exceeded the detector location. The model had a success of estimating maximum queue location even the queues ten times far away from the detector location. However, no performance measures were defined to quantify the errors.

For undersaturated cases, Badillo et al. (2012) performed a simulation based study which utilized a fine-grained loop detector data (every 1s occupancy and time gap data were taken) located in 228 m from the upstream of the intersection. The authors defined a “Look Ahead Interval Time” for arrival flow calculation. The arrival flow (q_a) and corresponding density value (k_a) were obtained from detector data based on “Look Ahead Interval Time”; however, q_j and k_j values were assumed to be constant value according to the empirical observations. Shockwave model was implemented to identify the maximum queue length locations.

2.3.2. Queue Length Estimation with Probe Vehicle Data

Since vehicle-to-vehicle and vehicle-to-infrastructure communications are growing, data obtained from probe vehicles gain importance to develop new methods in queue length estimation (Mecit, 2012). Probe vehicle data provides probe trajectory, which means location and speed of the vehicle is known over time. Thus, it is possible to identify the time when the vehicle join the queue, and similarly the time when the probe vehicle leaving the queue by assuming 5 km/h threshold speed as recommended in (Mecit ,2012, Cai et al., 2014).

Comert and Cetin (2009) focused on the importance of the probe vehicle data for real time queue length estimation at signalized intersections. The proposed analytical model evaluated how the queue length changed at the near the intersections and conditional probability distribution of the queue length was derived. The authors reported that time and location of the last probe vehicle should be utilized to estimate

queue length if more than one probe vehicle is joined the queue. Furthermore, they defined an error range for the different penetration rate of the probe vehicle data.

Cetin (2012) developed a mathematical model that utilized the position and time coordinate of at least one probe data for estimating the queue lengths at oversaturated intersections. The position and time coordinates of the probe vehicle when joining the back of the queue was utilized to estimate the evaluation of back of the queue as well as the critical points (such as, maximum queue and residual queue locations). The model was tested with different penetration rate as well. While the model was successful even for 5% penetration rate, it could not estimate the queue length, when a probe vehicle was not captured in a cycle. A follow up study, for undersaturated condition, Unal and Cetin (2014) examined queue dynamics from probe vehicle data using shockwave model, which estimated the queue length location with mean absolute percentage error of (MAPE) 23.6% for 10% probe vehicle penetration.

In Neumann (2010), examined frequencies of the probe vehicles near the signalized intersections, statistical method was proposed to estimate the daily queue lengths. Ban et al. (2011) utilized travel time data obtained from the mobile sensors (treated as FCD) between predefined virtual points before and after the intersection for estimating the real time queue length. The model was tested in both simulation environment and a field that the distance between two virtual points were selected as 860 m. The estimation was based on the observation of the critical pattern changes of travel time. Sharp increase or decrease in travel time of the probe vehicle in a location was spotted and regarded as the joining/leaving the queue location. Later, shockwave based model was implemented to estimate the queue length. The effect of penetration rate of probe vehicle on queue length estimation was also tested. Under full penetration rate, the model had a success rate of 80%-90%, while the success rate was 15%-32% for 20% penetration rate. The authors reported that at least 40% penetration rate was necessary for reliable queue length estimation.

Cheng et al. (2011) also utilized only probe vehicle trajectory for cycle-by-cycle queue length estimation. Similar to the aforementioned studies, joining and leaving the queue locations were detected from space-time diagram and shockwave model was implemented. Three different data sources were used as NGSIM (Next Generation Simulation), simulation based and probe vehicle data equipped with GPS. NGSIM provided real vehicle trajectory data from video recordings. The results of the observed 12 cycle indicated that the queue length estimations from NGSIM data were found with an MAPE of 22.26% while GPS equipped vehicle produced MAPE of 25.49%. Simulation-based analysis have been created both representing undersaturated and oversaturated traffic condition, which resulted in MAPE value of 17.46% and 19.23%, respectively.

Implementing shockwave model is not always necessary for queue length estimation from probe vehicle data. For example, Li et al. (2013) performed simulation-based study in VISSIM and utilized probe trajectory and signal timing data without information of arrival traffic flow and other essential parameters for queue length estimation. In their model, location and time information of the last probed vehicle that joined the queue in a cycle was determined. Later this information was used to calculate the queue increase rate since start of red time was known. Similarly, location and time information of this probe vehicle was recorded when this vehicle leaved the queue. Thus, queue discharge speed was calculated. Then maximum queue location was determined based on these two parameters. The effect of probe vehicle penetration rate showed that MAPE was found as 4.29% for 90% penetration rate, while this value was raised to 60.82% for 10% penetration.

Similarly, Tiaprasert et al. (2015) presented a mathematical model for real time queue length estimation from probe vehicle data for actuated and fixed control signalized intersections tested in a simulation environment. The model utilized the position of the last probe vehicle joining the queue for each cycle. The model was applicable

without arrival flow rate, signal timing data and queue characteristics information. To overcome the big estimation error from the low penetration rate, the study proposed a discrete wavelet transform algorithm to improve the model accuracy. The results indicated a RMSE value of 8 vehicles (corresponding to approximately 40 m) when the penetration of the probe vehicle is 10%. For the full penetration, RMSE was found as 3 vehicles (approximately 15 m).

2.3.3. Queue Length Estimation by Fusing Loop Detector with Probe Vehicle Data

To enhance the accuracy of the queue estimation at signalized intersections, fusing loop detector with probe vehicle trajectory data have been focused of many studies. This fusion could be performed either using data fusion algorithms such as Kalman filtering or combined the two data sources jointly to determine the shockwave speeds as well as the queue lengths. For the former, Li et al. (2013) estimated the queue length by utilizing Kalman filtering method for probe vehicle and loop detector data separately. Later, weighted combination of the queue length was calculated according to these two data source, which resulted in the estimated queue length. The model was tested in VISSIM simulation environment under varying penetration rate of probe vehicle. The author stated that significance of the data fusion was observed under low penetration rate, but still the model produced rather high MAPE value as more than 60% for 10% penetration.

Cai et al. (2014) examined the real time cycle-by-cycle queue lengths by using loop detector (located 50 m from the upstream of the intersection) and probe vehicle trajectory data obtained from mobile sensors in an urban arterial in China. The mathematical formulations were developed for three different cases separately, which were based on the LWR shockwave model. The representation of three cases are illustrated in Figure 2.11. For Case 1, the queue exceeds the detector location (marked as Point A in Figure 2.11a) and probe vehicle was joined and leaved the queue at Points B₁ and C₁ respectively. To calculate the maximum queue location, which is

Point D, the two shockwave speeds were calculated based these points. Since the location of the detector is known, the time when the detector was occupied (Point A) was calculated from the detector occupancy data by assuming 3 sec as a threshold limit. Since the location and time information of the Point B₁ are known from probe trajectory, backward moving shockwave can be calculated from equation of the line. Similarly, discharge shockwave can be calculated from the line equation.

For Case 2, probe vehicle was assumed to join the queue after the detector location. Same procedure was implemented to estimate the maximum queue location. On the other hand, in Case 3, Point A did not exist since the queue did not exceed the detector location (see Figure 2.11b). In this case, detector data was utilized to obtained arrival flow and density data, and probe trajectory data information was utilized to calculate the Point D. The results indicated that while the MAPE values were found as 11.60% and 9.98% for Case 1 and 2, respectively, this value was 26.40% for the Case 3. For their model, at least one probe vehicle was necessary to estimate the queue length.

Wang et al. (2017) also presented a similar methodology for queue length estimation that traffic states (arrival flow, arrival density etc.) were identified from loop detectors and location of stop and move of the probe vehicles were used to implement LWR model. The model had a capability of estimating queue length with MAPE of 17.09% among 11 cycles from site observation, but failed in estimating the residual queues for oversaturated condition.

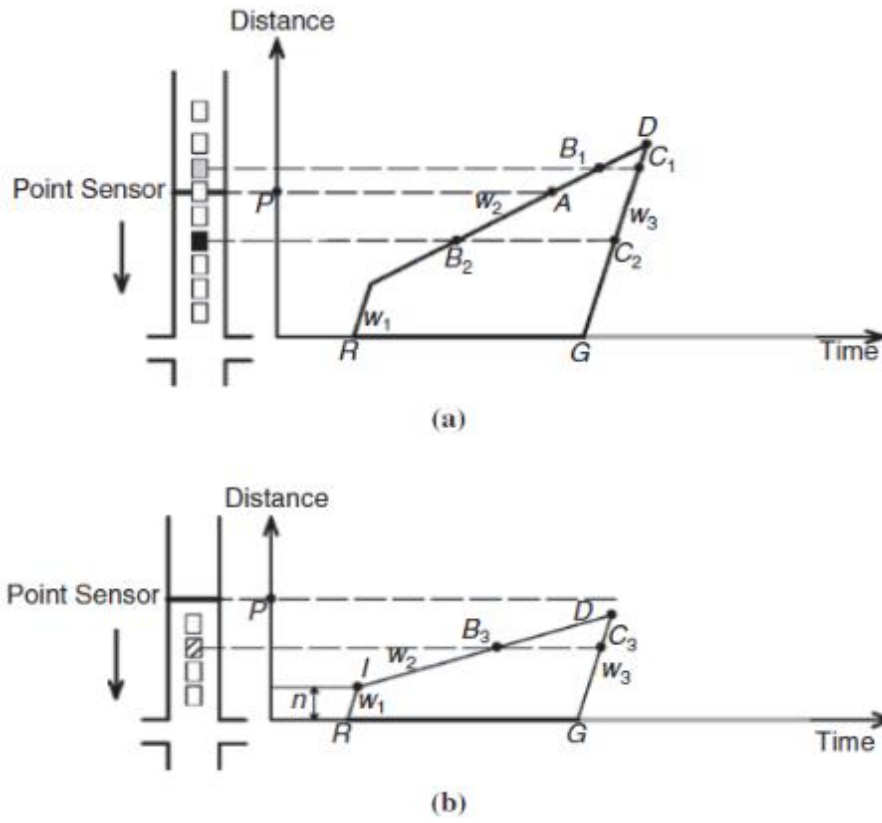


Figure 2.11. Representation of scenarios a) Case 1 and Case 2, b) Case 3 for Cai et al., (2014) study.

CHAPTER 3

FCD STRUCTURE AND QUALITY

In this chapter, the structure of the commercial FCD in Turkey will be discussed first, and followed by the description of the study corridors. The forth section mainly focuses on the evaluation of quality of the existing FCD in terms of i) speed estimation, ii) Level of Service (LOS) estimation and iii) LOS-based urban traffic monitoring by carrying out a set of analysis. The current penetration rate of FCD was also determined by performing Monte Carlo simulations in the final section.

3.1. FCD Structure

FCD used in this study included “real-time average speed data” published at 1-minute intervals for predefined road segments by a private company, Be-Mobile. FCD for Turkey comes from 600,000 GPS equipped vehicles (among the total 19 million registered vehicles), which corresponds to approximately 3% penetration rate. With such penetration, FCD has become a major traffic data source for urban arterials, along which there existed almost no traffic data sources or counts before. Today, real-time broadcasted FCD has provided traffic data for almost 5,000 segments (road segments less than 50 m) in Ankara (see Figure 3.1a), which covers almost 250 km of road network, and requires storage capacity of 8GB area per day.



Figure 3.1. a) Location of two study corridors in Ankara (Be-mobile, 2018); bi-directional location of some of the FCD segments in b) Dumlupınar Boulevard, c) Muhsin Yazıcıoğlu Street.

For efficiency, the invariant portion of the data (Segment ID, Length, Road Class Type, Speed Limit, Optimal Speed, and Local Coordinates) was shared once in a static table (see Table 3.1). The dynamic part of the data included attributes Segment ID, Date, Time, Speed (\bar{u}_{FCD}^t), Travel Time, and Coverage (Table 3.2); and the segment ID was the repeated parameter connecting the two parts of the data. In this data, as \bar{u}_{FCD}^t was equal to “Length (from static part)” divided by “Travel Time (from dynamic part)” – it was not a parameter observed independently. However, evaluation of the FCD for the many corridors in Ankara showed that published \bar{u}_{FCD}^t never exceeded the speed limit defined in the static part; thus, it was a truncated value. “Coverage” was explained by the data provider as “number of probe vehicles included in the average speed calculation” and the maximum value was observed as 10 in the study corridor data, suggesting “inclusion of data from 10 probed vehicles”. However, the details of the averaging function have not been clearly stated, such as, if 10 vehicles were observed at time t , or within a certain time interval before it, which was more likely the case; thus, it has not been regarded as a very reliable measure. Optimal speed was a parameter created by the FCD provider based on some archival evaluation, but not clearly defined. The FCD static data table was augmented to include a Local ID, showing the consecutiveness of the segments along the study corridor.

Table 3.1. *Static information of sample road segments located in the Dumlupınar Blvd. Corridor.*

Segment Id	Length (m)	Road Class	Optimal Speed	Speed Limit	Start Coordinate	End Coordinate	Local Id
676110	40.33	1	70	70	32.734701, 39.9065	32.735171, 39.906523	19
676111	40.33	1	70	70	32.735171, 39.906523	32.735642, 39.906545	20
676107	49.36	1	70	70	32.735642, 39.906545	32.736104, 39.906564	21
676108	49.36	1	70	70	32.736104, 39.906564	32.736565, 39.906594	22
676109	49.36	1	70	70	32.736565, 39.906594	32.737025, 39.906627	23

Table 3.2. *Sample dynamic attributes for the “676111” road segment.*

Segment Id	Day	Time	Travel Time (s)	Speed	Coverage
676111	01.07.2016	8:00	2.48	70.00	10
676111	01.07.2016	8:01	2.48	70.00	8
...					
676111	01.07.2016	8:59	2.54	69.79	10
676111	01.07.2016	9:00	2.89	61.34	10
...					

3.2. Study Corridor 1

Two study corridors were selected for this thesis (see Figure 3.1). The first study corridor has an approximately 3.6 km stretch along Dumlupınar Blvd. in Ankara, a major arterial in the form of a multilane urban highway corridor, with three lanes in each direction (see Figures 3.2a, 3.2b, 3.2c). The study corridor consists of 82 FCD segments in one direction which delivers real-time average speed data in 1-minute periods for a fine and almost uniform segmentation with maximum length of 50 m. The static information of the road segments for this corridor is given in Table A.1.

The corridor includes two main interchanges of J1 (located between segments 10 and 19) and J2 (located between segments 72 and 82) and an electronic speed enforcement at Segment 26. Note: Although recently the speed limits were raised to 82 km/h for passenger cars (in practice, this meant 90 km/h due to tolerance in enforcement) and 70 km/h for commercial vehicles for this corridor, the FCD network data still showed 70 km/h as the coded limit and thus FCD speed values were truncated at this limit in the published data. Although this created some inaccuracy in the evaluation of traffic conditions, the error was observed on the uncongested regimes and caused minimal inconvenience in the evaluation of congested periods and bottlenecks.

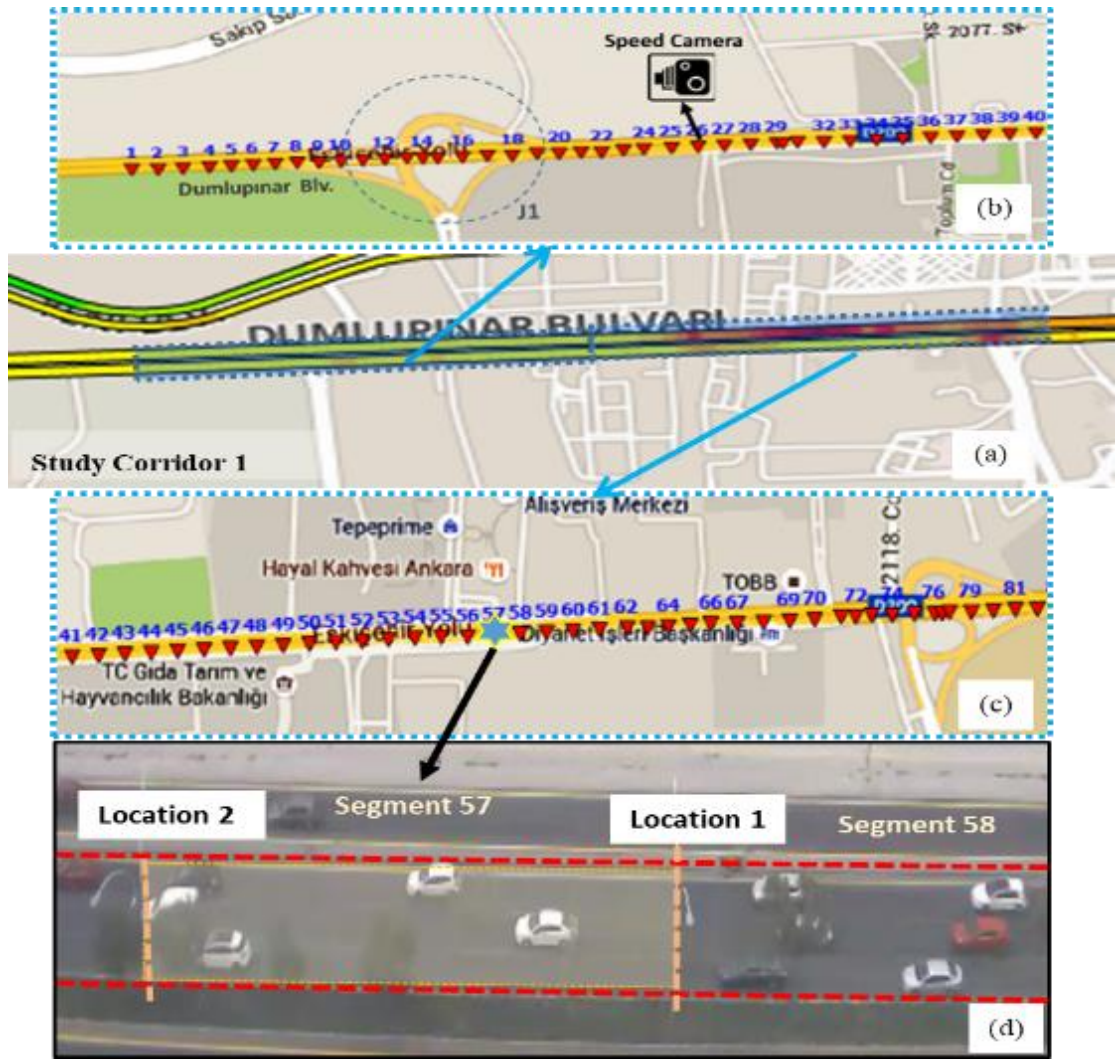


Figure 3.2. a) Locations of Study Corridor 1 of 3.6 km length b) with 40 FCD segments in the eastern part, c) 42 FCD segments in the western part d) with a close look-up on the control Segment 57 with GT data.

3.2.1. Ground Truth Data

In order to evaluate the quality of existing FCD from different aspects for different traffic conditions, Ground Truth (GT) data was collected. In order to collect GT data, a video camera was installed at a high-rise building along the study corridor to record traffic on a specific segment (Seg. 57 in Figure 3.2d) for two days (Friday October 21, 2016 and Tuesday October 25, 2016). The video camera view provided clear visibility

of the segment (49.15 m) for all three lanes. The analysis time period, T , was 07:30 to 16:00, (during which daylight was available for data processing) and included the morning peak and noon off-peak hours. Using a MATLAB code, the video camera was processed twice manually to obtain values of i) 1-minute traffic flow and ii) speed for each lane separately. The flow was determined by counting vehicles crossing a virtual line at Location 1 in Figure 3.2d. While determining the speed of a vehicle i , entry and exit times were recorded at Locations 1 and 2, respectively. First, spot speed of the vehicle, u'_i , was calculated, but it was then converted to space mean speed for the segment, \bar{u}' , by taking the harmonic mean to be comparable with the \bar{u}'_{FCD} value. As detecting u'_i required tracking of the vehicle i between the two observation points, the next vehicle for speed data, vehicle $i+1$, was selected as the first vehicle observed at Location 1, when vehicle i passed Location 2; this caused a lower sampling rate for speed data compared to full flow observation in the GT values. Furthermore, as the FCD speed values were published for segments, not for each lane separately, lane-based traffic data (flow and speed values) were combined to obtain segment-based traffic flow and speed values. Figure 3.3 shows 1-minute flow and speed volumes for both counting days, which illustrate the sampling in the speed data.

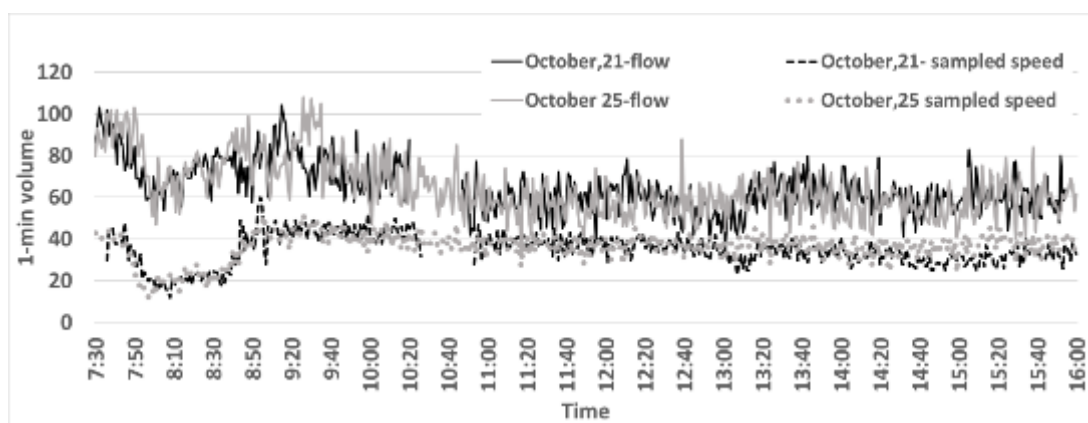


Figure 3.3. Traffic counting results of two counting days.

3.3. Study Corridor 2

The second corridor is located in Muhsin Yazıcıoğlu Street in Cukurambar and composed of two consecutive signalized intersections as shown in Figure 3.4. The first one is located at the intersection of the Muhsin Yazıcıoğlu and Ufuk University Street, and the second one is almost 327 m far away from the upstream of the first intersection. The direction from Muhsin Yazıcıoğlu to Ufuk University Street, labelled as Approach 1, has four lanes in which the inner most lane is designated to right turn movements and remaining lanes are for through movements with 3.75 m lane width and 50 km/h desired speed. For the reverse direction, labelled as Approach 2, it has three lanes in which the inner most lane reserves for parking area and the other two lanes have a width of 3.75 m and 50 km/h desired speed. 8 FCD segments for this study corridor were defined from Be-Mobile bi-directionally and FCD segment lengths varied from 38.85 m to 41.43 m. Static information of the FCD segments are provided in Table A.2.

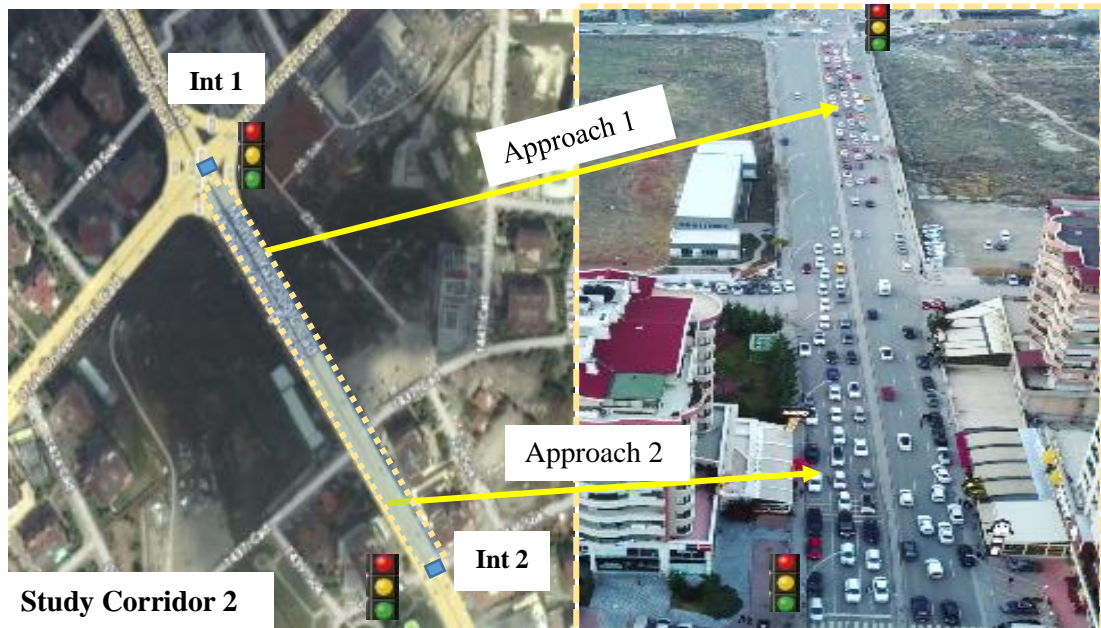


Figure 3.4. Study Corridor 2 located between 2 signalized intersections of length 327 m covered in 8 FCD segments.

3.3.1. GT Data for Muhsin Yazıcıoğlu Street

GT data was collected via video records obtained from drone to examine the queue lengths over time for the Approach 1 and Approach 2 as shown in Figure 3.5. Queue lengths from video records were detected for each lane separately for every 5 sec. Duration of the video was 11 minutes covering 6 and 7 cycles for Approach 1 and 2, respectively. Queue length profile of the approaches indicated that queue lengths were around 210 m for Approach 1 while they were in between 75 m and 125 m for the other approach (see Figure 3.5).

Further analysis have been carried out to determine critical parameters of the approaches such as saturation flow rate, capacity and degree of saturation. Based on the HCM (2010) procedure discussed in Section 2.2.3, saturation flow rate was calculated by taking the average headway of the vehicles after the 4th vehicle passing through from the stop line. This process was implemented for all lanes separately. Then, calculated lane-based average headway was put into the Equation [2.5] and resulted in saturation flow rate of 2018 veh/h, 1866 veh/h and 1860 veh/h for Lane 1, Lane 2 and Lane 3, respectively (see Table 3.3). For the Approach 2, the saturation flow rate for the lanes showed very similar values which was around 1900 veh/h. Furthermore, lane-based arrival flow rate was also determined for the analysis period as shown in Table 3.3 for the two approaches. To calculate the capacity, it is first necessary to determine the effective green time (see Equation [2.7]) in which signal timing information of the approaches as follows:

- Approach 1: $G=24$ sec, $R=84$ sec, $Y=2$ sec, $AR=2$ sec, $C=110$ sec
- Approach 2: $G=28$ sec, $R=63$ sec, $Y=2$ sec, $AR=2$ sec, $C=93$ sec

Assuming start-up lost time as 2 sec (HCM, 2010) and clearance lost time as 3 sec, total lost time (t_L) was calculated as 5 sec/phase. Using Equation [2.7], effective green times (g) were found 23 sec and 27 sec for the Approach 1 and 2, respectively. Finally, lane-based capacity flow values were obtained using Equation [2.8] as shown in Table 3.3. It is clearly seen that for all lanes of Approach 1, arrival flow rate was greater than

the capacity which resulted in degree of saturation (X) of 1.50, 1.52 and 1.32 for Lane 1, Lane 2 and Lane 3, respectively, which were oversaturated. On the other hand, Approach 2 was not oversaturated for all lanes in which X were calculated as 0.86 and 0.80 for the Lane 2 and Lane 3, respectively.

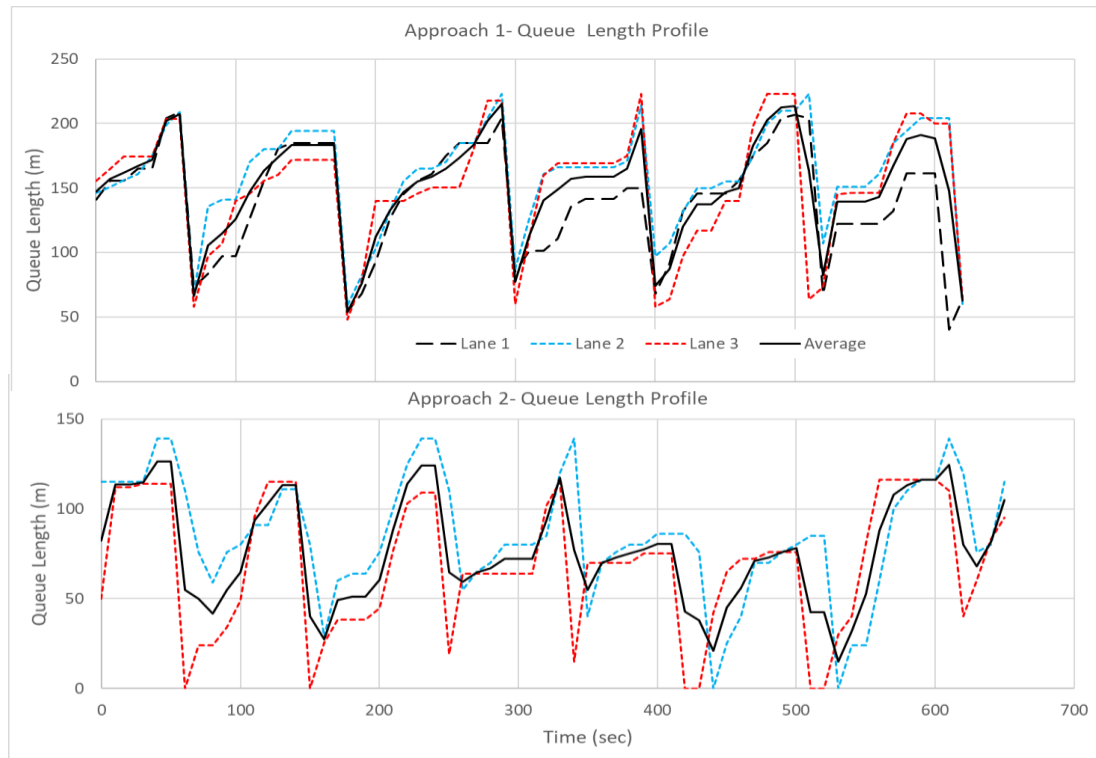


Figure 3.5. Lane based as well as average observed queue lengths for Approach 1 and 2.

Table 3.3. Traffic analysis results of the Approach 1 and 2.

	Saturation Flow (s) (veh/h)	Traffic Demand (q) (veh/h)	Capacity (veh/h) ($c = s * g / C$)	Degree of Saturation $X = \left(\frac{q / s}{g / C} \right)$
Approach 1				
Lane 1	2018	632	422	1.50
Lane 2	1866	594	390	1.52
Lane 3	1860	516	389	1.32
Approach 2				
Lane 2	1854	464	538	0.86
Lane 3	1912	444	555	0.80

3.4. FCD Quality in Turkey

The quality of commercially available FCD was evaluated for Dumlupınar Blvd. in terms of i) descriptive evaluation, ii) speed estimation performance, iii) LOS estimation performance and iv) urban traffic monitoring. The methodological framework for evaluating the quality of FCD speed was presented in detail in Appendix B. This section only provides the analytical results based on the proposed methodology.

3.4.1. Descriptive Evaluations

GT speed profiles for the two study days were very similar; sudden drops were observed after 07:30 indicating severe congestion until 09:00 (see Figure 3.6). No congestion was detected until the end of the study period, which did not include the evening peak due to early sunsets in October. During off-peak period, vehicle spot speeds varied between 40 km/h- 130 km/h and had an average speed range of 70 km/h -80 km/h. During the peak period, range between the maximum and minimum spot speeds was smaller as expected. (Note: video camera data was not available between 10:23-10:53 for October 21, 2016).

Plotting FCD speed, \bar{u}_{FCD}^t , profile in juxtaposition with GT values, \bar{u}_t , showed that \bar{u}_{FCD}^t mostly followed the average \bar{u}^t (see Figure 3.6), sometimes underestimating or overestimating it. Key findings are summarized as follows:

- When traffic states changed from uncongested to congested regime (or vice versa), \bar{u}_{FCD}^t did not respond to the sudden drop/increase in speed at the same rate.
- In the congested regime, FCD overestimated the speeds.
- Since \bar{u}_{FCD}^t was truncated at 70 km/h, it was not possible to observe speeds beyond this limit, particularly during off-peak hours. However, for \bar{u}_t values

close to but not exceeding 70 km/h, \bar{u}_{FCD}^t underestimated the speeds, which may be due to the probed vehicles traveling slowly through the segment.

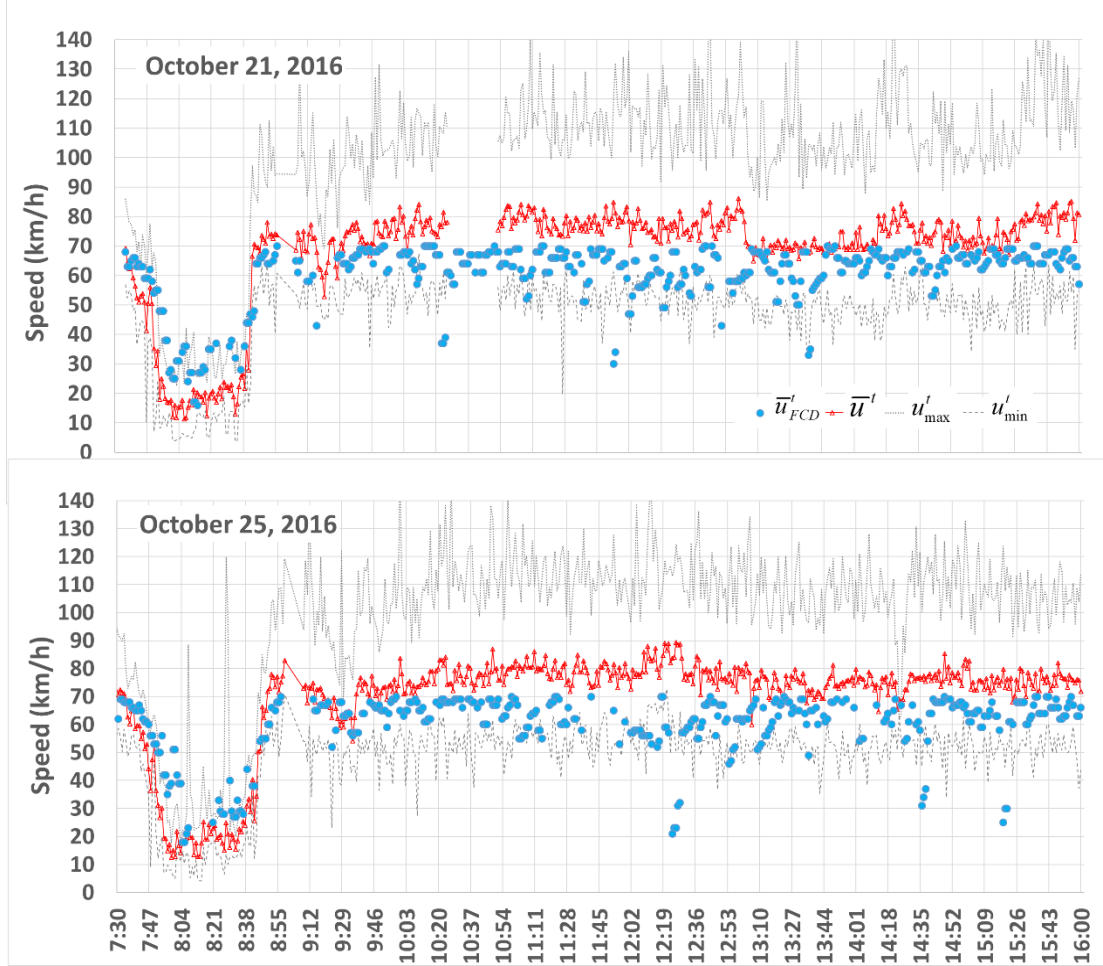


Figure 3.6. Speed profile of the \bar{u}_{FCD}^t and \bar{u}_t as well as u_{max}^t and u_{min}^t for the two weekdays between 07:30-16:00.

GT-based fundamental diagram with q^t and \bar{u}_t was plotted as shown in Figure 3.7. Van Aerde fit to the GT data suggested a free flow speed limit of 91.7 km/h and a speed value of 47.4 km/h producing the highest capacity (which also falls within LOS C range). When \bar{u}_{FCD}^t was as a surrogate measure for real speed values in this diagram (see Figure 3.8), there was a large variability and scattered distribution in the FCD-based fused diagram. Besides the sharp border in the uncongested region due to the

speed limit truncation, overestimations in the congested region were clearly visible, similar to the conclusions stated by Chase et al. (2012).

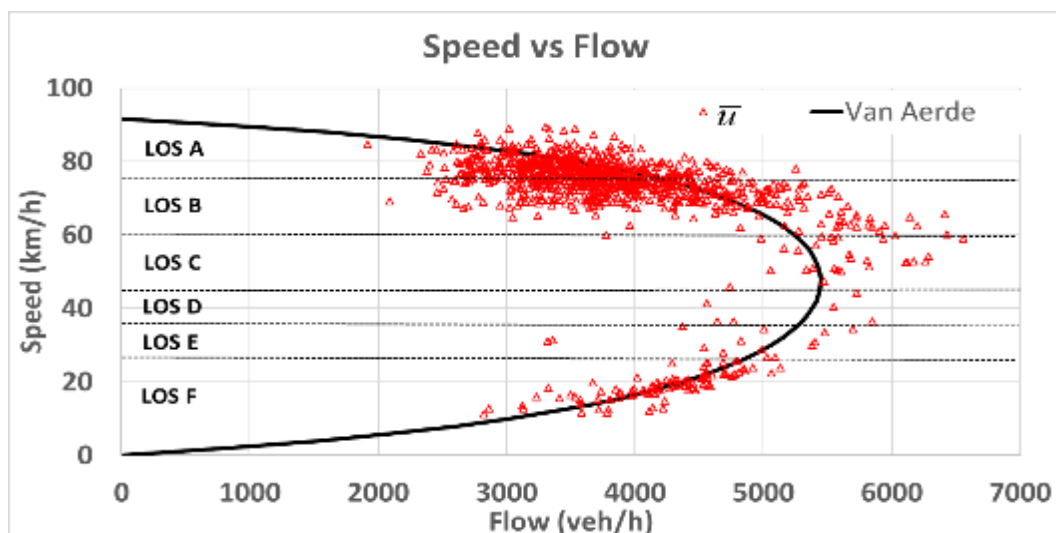


Figure 3.7. Fundamental diagram and LOS threshold limits of GT data.

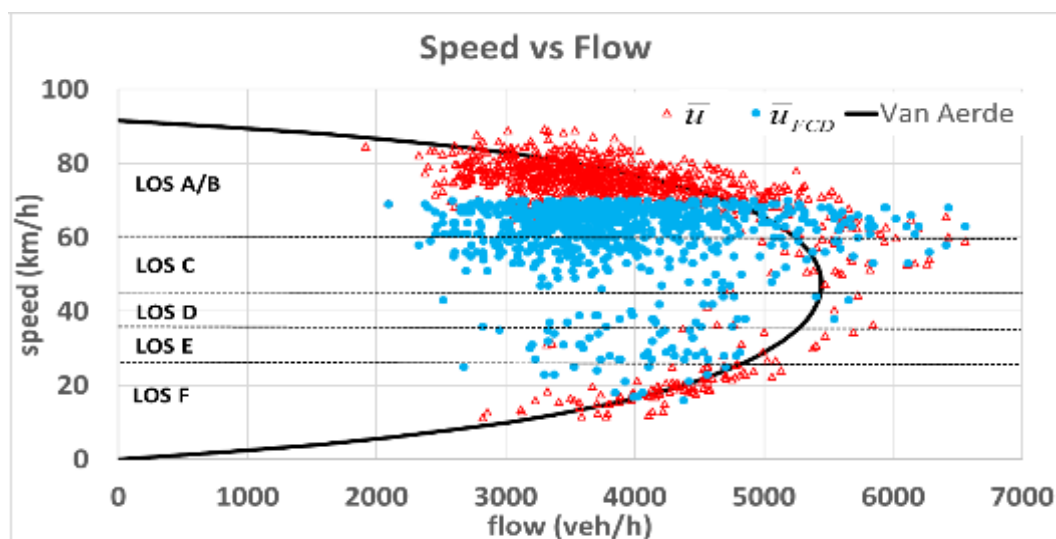


Figure 3.8. Fundamental diagram and LOS threshold limits of GT data and FCD speeds.

3.4.2. Speed Estimation Performance

As shown in Table 3.4, the daily speed data sample sizes were very close summing up to a total 802 in the aggregated data set. Following the data preprocessing step

described in Appendix B, 27 FCD speed values were eliminated as outliers and left a total of 775 values in the filtered dataset. When two days were examined separately, no significant difference was observed in the performances measures. Based on the aggregated 2-day results, speed estimation $MAPE_u$ and $RMSE_u$ values were calculated as 16.64% and 10.85 km/h, respectively, with raw FCD speeds. However, these errors were reduced to 14.19% and 8.71 km/h, respectively, when filtered FCD speed dataset were used. Majority of the error stemmed from morning peak speed values, which showed $MAPE_u$ and $RMSE_u$ values of 42.29% and 12.12 km/h, respectively. Significant deterioration in $MAPE_u$ values despite a small increase in $RMSE_u$ can be explained by a) time lag in FCD response to congestion entry/exit, which was captured in descriptive evaluations, and b) magnification in percentage calculation with small speed values. Thus, $MAPE$ -based performance evaluation during for low-speed regimes should be made with caution. The lowest $MAPE_u$ and $RMSE_u$ for speed estimations were obtained at the off-peaks, which showed that FCD speeds were only 8.83% different than real values on average, and had an average difference of 7.89 km/h.

Table 3.4. FCD speed performance based on $MAPE_u$, $RMSE_u$ and R^2 measures.

Analysis Time Period	Raw FCD			Filtered FCD		
	$MAPE_u$ (%)	$RMSE_u$ (km/h)	R^2	$MAPE_u$ (%)	$RMSE_u$ (km/h)	R^2
October 21, 2016 (n=396) (n=384)						
Whole study period	16.10	9.38	0.61	15.10	8.83	0.71
AM peak	49.94	13.56	0.79	45.68	12.28	0.82
Off-peak	9.55	9.22	NA*	8.77	7.91	NA*
October 25, 2016 (n= 406) (n= 391)						
Whole study period	17.22	11.67	0.45	13.65	8.73	0.68
AM peak	47.52	13.87	0.76	36.94	11.72	0.82
Off-peak	11.07	11.17	NA*	9.03	8.01	NA*
Aggregated 2-day results (n= 802) (n=775)						
Whole study period	16.64	10.85	0.53	14.19	8.71	0.71
AM peak	49.22	13.69	0.76	42.29	12.12	0.82
Off-peak	10.28	10.20	NA*	8.83	7.89	NA*
* Due to almost constant speed values during off-peaks, estimation of R^2 measure was not appropriate.						

A transformation function to estimate speeds from FCD speed was developed using a regression analysis. When truncated GT speeds, \bar{u}_{tr}^t , were regressed against FCD speeds (\bar{u}_{FCD}^t) using aggregated 2-day dataset, results showed a non-linear best-fit with a rather low R^2 value of 0.53 (see Table 3.4) for the whole analysis period (see Figure 3.9a) and provided the speed transformation function, \hat{u}_{FCD} , in the form of

$$\hat{u}_{FCD} = 13.672e^{0.025(\bar{u}_{FCD})} \quad [3.1a]$$

But, the speed transformation relation in Fig 3.10a with

$$\hat{u}_{FCD}^{AM} = 6.841e^{0.033(\bar{u}_{FCD}^{AM})} \quad [3.1b]$$

had an improved success for morning peak hours with $R^2=0.76$ (see Table 3.4). When the same analysis was repeated with filtered FCD speeds, the success of the speed transformation was improved even more with

$$\hat{u}_{FCD*} = 9.8115e^{0.0302(\bar{u}_{FCD*})} \quad (R^2 = 0.71) \quad [3.1c]$$

$$\hat{u}_{FCD*}^{AM} = 7.0159e^{0.0333(\bar{u}_{FCD*}^{AM})} \quad (R^2 = 0.82) \quad [3.1d]$$

as shown in Figure 3.9b and 3.10b. (Note: Most of the outliers were observed during the off-peak periods at high GT speeds more than 60 km/h. The high impact of filtering can be clearly seen comparing Figures 3.9a and 3.10a).

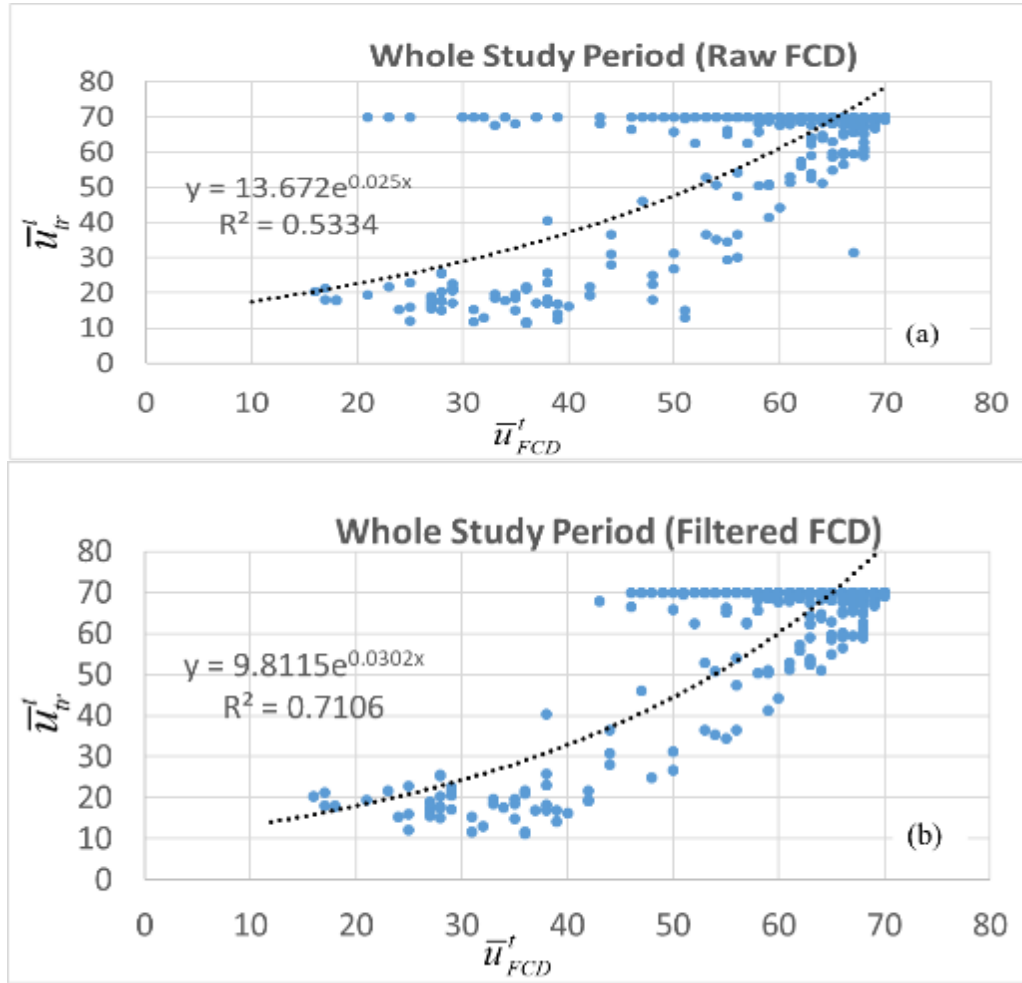


Figure 3.9. Speed estimations using a) raw FCD speeds, \bar{u}_{FCD}^t , b) filtered FCD speeds, \bar{u}_{FCD*}^t , for the whole study period.

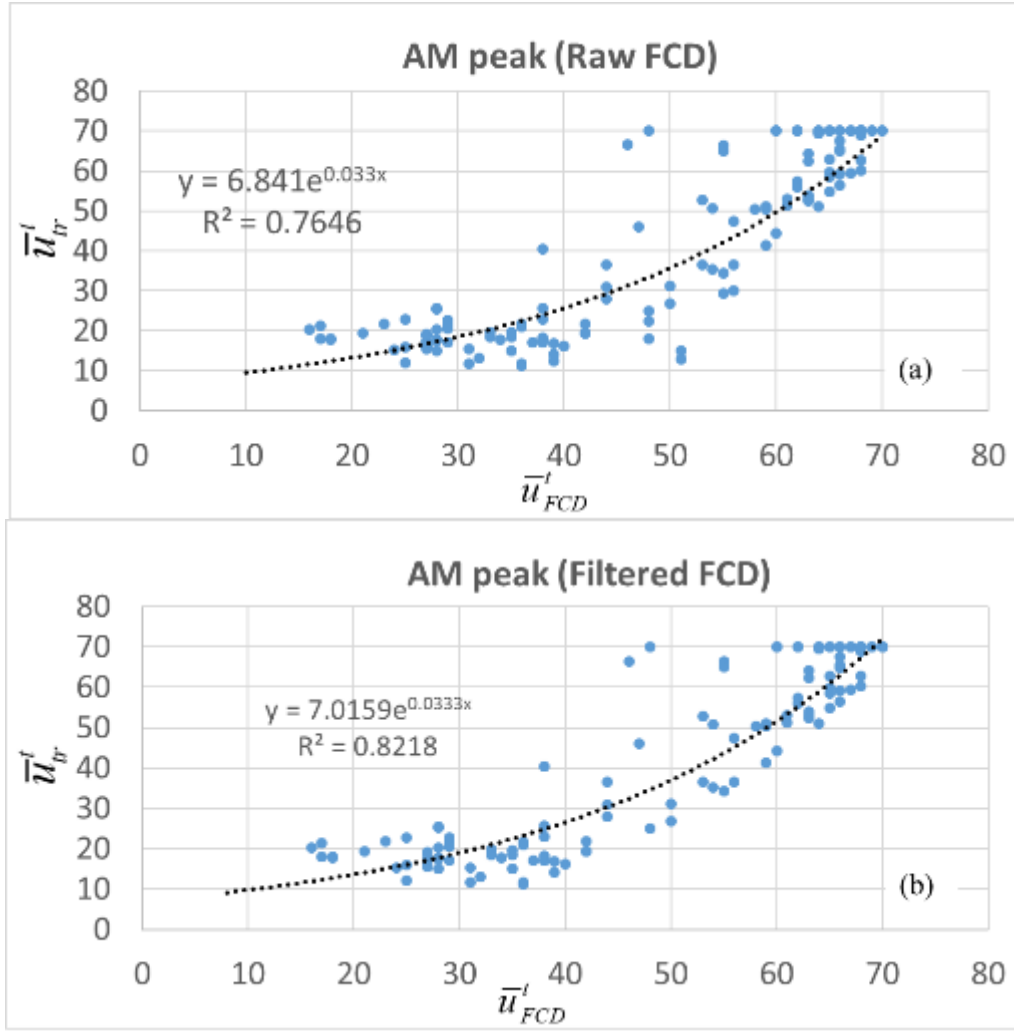


Figure 3.10. Speed estimations using a) raw FCD speeds, b) filtered FCD speeds for the AM peak.

As seen above, the quality of FCD speed estimation varied significantly under different regimes; thus, a further breakdown of $MAPE_u$ and $RMSE_u$ for different speed intervals as proposed by (Wang et al. 2014; Hu et al. 2016) was presented in Table 3.5. Speed intervals were selected based on the LOS threshold limits as shown in Table B.1, which were also used in the LOS estimation. Due to longer off-peak periods in the data, the majority of the \bar{u}' was in LOS A or LOS B categories (702 samples out of 802 speed values). For 278 records with speeds within LOS A range (266 observations in filtered data) $MAPE_u$ and $RMSE_u$ were observed as high as 22.47%

and 20.42 km/h, respectively, which is clearly a problem due to speed limit truncation in FCD. In LOS B range, these values dropped to 12.60% and 11.40 km/h, sharply.

Table 3.5. $MAPE_u$ and $RMSE_u$ distribution in HCM-based LOS speed intervals (2-day analysis).

LOS	GT Speed Interval	Sample Size	$MAPE_u$ (%)	$RMSE_u$ (km/h)	Sample Size	$MAPE_u$ (%)	$RMSE_u$ (km/h)
		Raw FCD ($n=802$)			Filtered FCD ($n=775$)		
From raw GT							
A	$\bar{u}' \geq 77$	278	22.47	20.42	266	20.56	17.47
B	$60 \leq \bar{u}' < 77$	424	12.60	11.40	417	11.88	10.23
From truncated GT							
A/B	$\bar{u}'_{tr} = 70^a$	600	10.27	10.26	583	8.92	8.07
	$60 \leq \bar{u}' < 70$	102	8.30	8.28	100	7.46	6.86
C	$45 \leq \bar{u}' < 60$	25	13.05	7.69	25	13.05	7.69
D	$36 \leq \bar{u}' < 45$	6	33.93	14.58	6	33.93	14.58
E	$27 \leq \bar{u}' < 36$	8	70.01	22.79	5	54.67	17.67
F	$\bar{u}' < 27$	61	85.99	16.82	56	75.25	14.79
^a Errors due to the truncations were calculated separately for the joint LOS value							

To create a fair comparison, truncated GT speeds were used to determine the $MAPE_u$ and $RMSE_u$ values for the 600 truncated speed values ($\bar{u}'_{tr} = 70$ km/h), which were found as 10.27% and 8.92 km/h, respectively, showing the contribution of truncation in FCD resulting in overestimation of performance measure values significantly (see Table 3.5). For 102 observations between 60 km/h and 70 km/h, $MAPE_u$ and $RMSE_u$ dropped to 8.30% and 8.28 km/h, respectively. Within the LOS C range, two performance measures had similar values of 13.05% and 7.69 km/h, respectively. However, for speed values within LOS D to LOS F levels, FCD had increasing $MAPE_u$ and $RMSE_u$ values, reaching 75.25% and 14.79 km/h, suggesting that available FCD could not estimate speed values reliably and was not capable of capturing real-time congestion, as also indicated in Wang et al. (2014) and Hu et al. (2016). (Note:

$MAPE_u$ and $RMSE_u$ values dropped slightly when extreme values in FCD were filtered, but did not change the characteristics within different LOS levels).

3.4.3. LOS Estimation Performance

To test the quality of FCD for LOS estimation, GT and FCD speeds, \bar{u}^t and \bar{u}_{FCD}^t , were used to estimate LOS levels directly based on HCM definitions given in Table B.1. Consistency between these two sets of LOS values were illustrated in Table 3.6a showing that majority of the time traffic flew in high-speed regime (>60 km/h) and constituted LOS A/B conditions, which was also determined by FCD speeds. On the other hand, for low-speed regimes during peak hours, FCD could not estimate the LOS F values correctly (Table 3.6a). The performance measures were determined as $MAPE_{LOS} = 27.15\%$ and $RMSE_{LOS} = 0.80$; a correlation coefficient value of only 0.50. Elimination of the outliers only (see Table 3.6b), brought down the $MAPE_{LOS}$ and $RMSE_{LOS}$ values to 19.80% and 0.60, respectively, and increased the R^2 value to 0.71.

Using the speed transformation function derived above, two more sets of LOS values were obtained which were compared to the GT LOS as shown in Table 3.6c and 3.6d. Transformation of raw FCD speeds enabled significant improvement in LOS estimation, especially correcting FCD speeds during low-speed regimes with LOS F; while R^2 value was raised to 0.67, the $MAPE_{LOS}$ and $RMSE_{LOS}$ scores dropped to 26.80% and 0.7, respectively (see Table 3.6c). Additionally, speed transformation over filtered FCD speeds improved LOS estimation performance up to the level of $R^2 = 0.81$, $MAPE_{LOS} = 15.4\%$ and $RMSE_{LOS} = 0.5$ (see Table 3.6d).

Table 3.6. Comparison of GT- and FCD-based LOS estimations for Segment 57 (2-day analysis).

(a)		LOS (\bar{u}_{FCD})					Total	(b)		LOS (\bar{u}_{FCD^*})					Total
		A/B	C	D	E	F				A/B	C	D	E	F	
LOS	A/B	552	130	6	10	4	702	LOS	A/B	552	130	1			683
	C	17	8				25		C	17	8				25
	D	1	3	2			6		D	1	3	2			6
	E	3	3	2			8		E		3	2			5
	F		7	16	27	11	61		F		2	16	27	11	56
Total		571	158	27	37	15	802	Total		570	146	21	27	11	775
R ² =0.50 MAPE _{LOS} =27.15%; RMSE _{LOS} = 0.8								R ² =0.71 MAPE _{LOS} =19.80%; RMSE _{LOS} = 0.6							
(c)		LOS(\hat{u}_{FCD})					Total	(d)		LOS(\hat{u}_{FCD^*})					Total
		A/B	C	D	E	F				A/B	C	D	E	F	
LOS	A/B	552	125	6	15	4	702	LOS	A/B	552	129	2			683
	C	16	5	2	1		24		C	16	7	2			25
	D		2	2	1	1	6		D		3	1	2		6
	E			4	4		8		E			3	2		5
	F			2	8	52	62		F			1	4	51	56
Total		568	132	16	29	57	802	Total		568	139	9	8	51	775
R ² =0.67 MAPE _{LOS} =26.80%; RMSE _{LOS} = 0.7								R ² =0.81 MAPE _{LOS} =15.40%; RMSE _{LOS} = 0.5							

3.4.4. FCD Performance for Urban Corridor Monitoring

Though it is valuable to evaluate FCD at a control segment over different performance measures, the availability of such detailed GT for an urban corridor is very challenging. However, based on the intuition gained over the control segment evaluation, it is possible to estimate speed and LOS over a longer urban stretch. As an application, LOS mapping over the study corridor with 82 segments shown in Figure 3.2 was performed for a morning period of 07:30-09:00 for October 21 (see Figure 3.11a) and October 25 (see Figure 3.12a). LOS mapping with raw FCD speeds suggested a queue formation at J2 starting at Segment 72 around 8 am that spilled back to Segment 36 by 8:30 am corresponding to a maximum queue length of 1.8 km. This queue dissipated by 9 am, suggesting a morning congestion effect of the interchange.

However, existence of LOS D and LOS E along this queue formation may be due to noise in FCD, which was eliminated in LOS estimations using transformed speed values in Figures 3.11b and 3.11c, which showed a clearer spatio-temporal queue formation (see Figures 3.12b and 3.12c for October 25). A much smaller but persistent congestion was also detected at the interchange J1, and decrease in LOS was observed due to electronic enforcement at Segment 26, temporarily between 8 am and 9 am, which was more visible with the speed transformation. The free flowing conditions in the upstream of J1 (segments 1-15) were captured consistently.

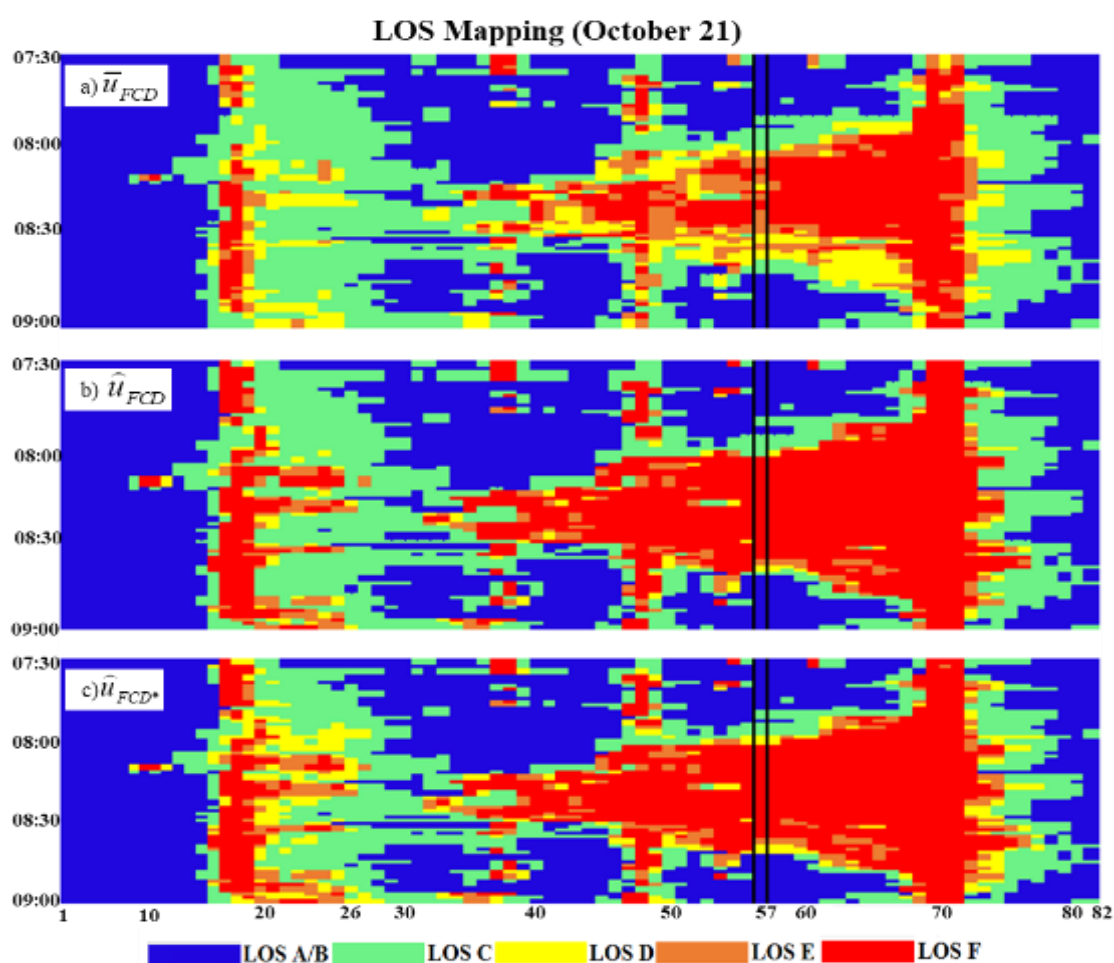


Figure 3.11. LOS estimations for the study corridor using a) raw FCD speeds, b) transformed FCD speeds, c) transformed filtered FCD speeds for the day of October 21.

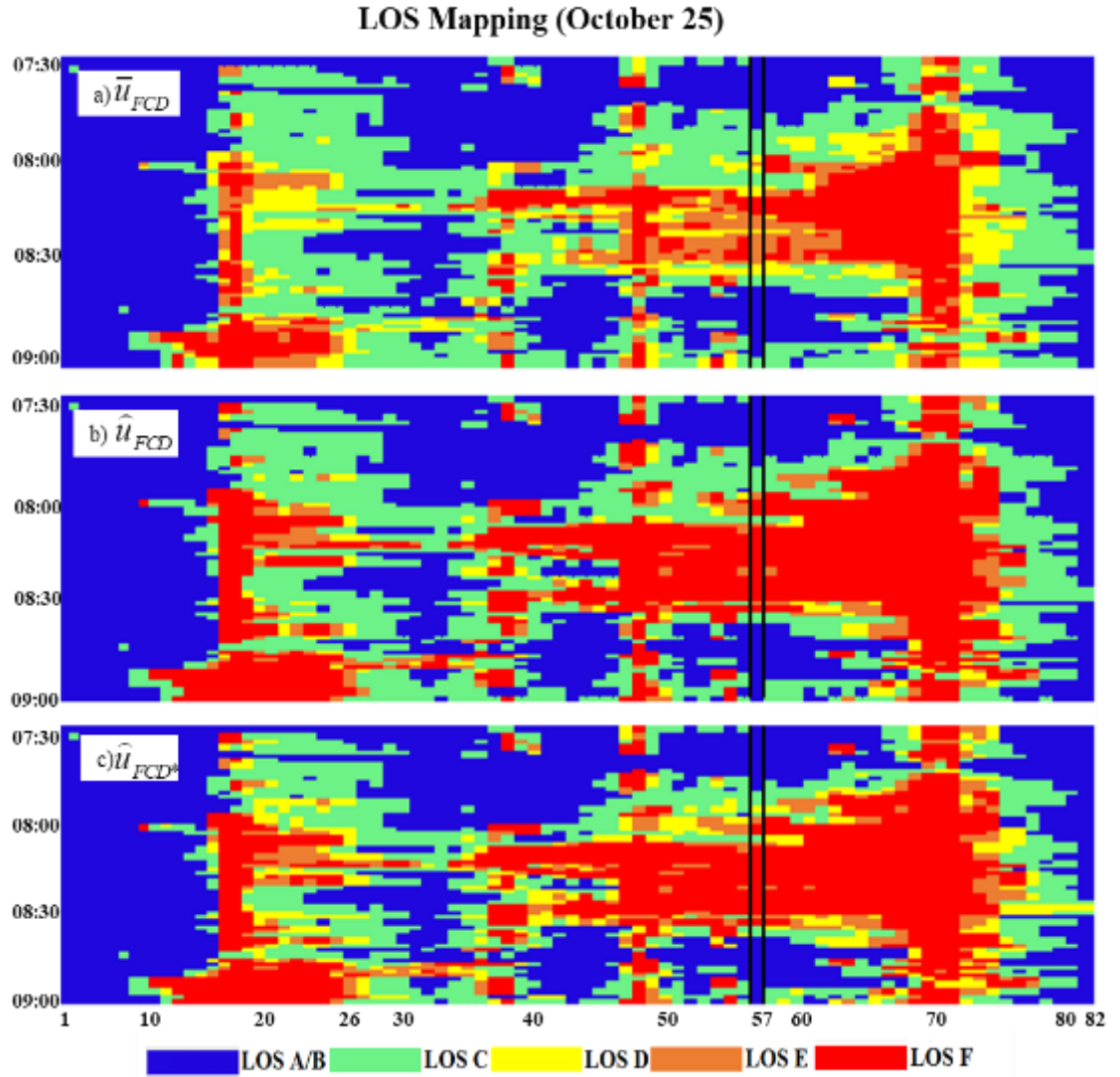


Figure 3.12. LOS estimations for the study corridor using a) raw FCD speeds, b) transformed FCD speeds, c) transformed filtered FCD speeds for the day of October 25.

As a check, the LOS values from all three LOS maps for the control Segment 57 were displayed in juxtaposition to the GT LOS values for the two days, which suggested that FCD always lagged responding to sudden regime changes, and had noise in the data during congestion (see Figure 3.13).

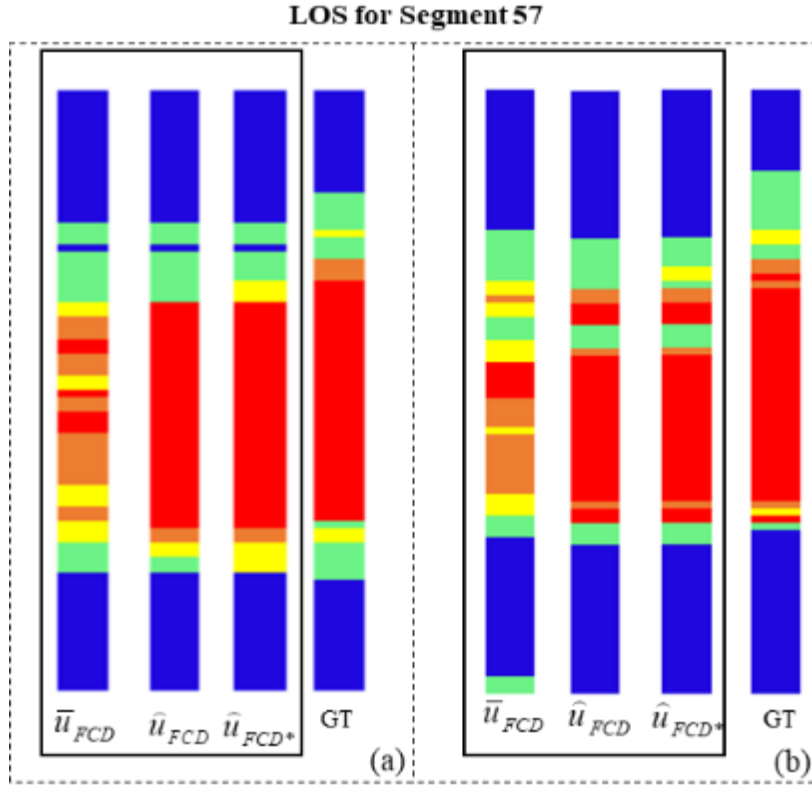


Figure 3.13. Comparison of LOS estimations for Segment 57 for a) October 21, b) October 25 data.

Furthermore, a clearer picture could be taken when a longer duration FCD-based LOS data was analyzed for the whole weekdays in October, 2016 as shown in Figure 3.14. Disregarding the spatio-temporal fluctuations among segments and observation times, when dominant traffic states at each segment for each observation time (which is 1-min) defined as the state that were observed more than 50% of the 24 weekdays in October, corridor characteristic was detected from the FCD, such that there was an recurrent bottlenecks at Segment 72, Segment 48 and Segment 17. The queue caused by Segment 72 was expected to spill back to Segment 56 with more than 50% probability, whereas uncongested regime was expected on segments 1-15 with the same probability.

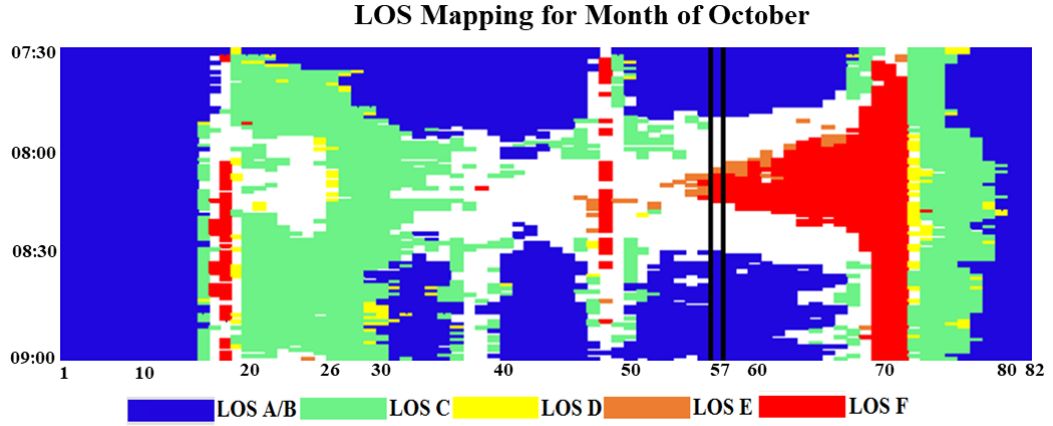


Figure 3.14. Dominant traffic states (more than 50% probability) for October month.

3.5. Evaluation of Current FCD Penetration Rate

The quality of FCD under varying penetration rates was evaluated by creating various FCD subsets from GT speed dataset using Monte Carlo (MC) simulations. This analysis enabled to derive both FCD quality-penetration rate relation and the current penetration rate of the existing FCD. The framework for deriving this relationship was explained in more detail in Appendix C.

The plots showing the relationship between FCD penetration rates and error measures in Figures C.4, C.5 and C.6 suggested a strong logarithmic relation. Logarithmic functions developed for $MAPE_u$ (or $RMSE_u$) in Table 3.7 were used as a guide to estimate the current penetration rates at the study location. For the whole study period, measured $MAPE_u$ of 17.22% obtained from raw FCD data from the whole study period (see Table 3.4), corresponds to an FCD penetration rate between 0.76% (from $MAPE_{u,max}^\delta$) to 0.35% (from $MAPE_{u,min}^\delta$) with an average of 0.54% penetration. A much lower error value of 13.65% (see Table 3.4) determined from the filtered FCD speeds suggested FCD penetration rates between 1.87% and 1.02%.

Table 3.7. Estimated level of FCD penetration, $\tilde{\delta}_{FCD}$, from speed data for different analysis periods (Oct. 25, 2016).

Error-Penetration Rate Relation	R ²	Estimated FCD Penetration Rate ($\tilde{\delta}_{FCD}$) in %	
		Raw	Filtered
Whole			
$MAPE_{u,max} = -3.944\ln(\delta_q)+16.128$	0.99	0.76	1.87
$\overline{MAPE}_u = -3.678\ln(\delta_q)+14.991$	0.99	0.54	1.44
$MAPE_{u,min} = -3.376\ln(\delta_q)+13.710$	0.99	0.35	1.02
AM Peak			
$MAPE_{u,max} = -7.377\ln(\delta_q)+26.654$	0.98	0.06	0.25
$\overline{MAPE}_u = -4.359\ln(\delta_q)+17.343$	0.99	0.00*	0.01
$MAPE_{u,min} = -3.580\ln(\delta_q)+13.875$	0.96	0.00*	0.00*
Off-peak			
$MAPE_{u,max} = -3.921\ln(\delta_q)+15.808$	0.99	3.35	5.63
$\overline{MAPE}_u = -3.528\ln(\delta_q)+14.329$	0.98	2.52	4.49
$MAPE_{u,min} = -3.019\ln(\delta_q)+12.518$	0.99	1.62	3.17
Whole			
$RMSE_{u,max} = -3.769\ln(\delta_q)+14.843$	0.99	2.32	5.06
$\overline{RMSE}_u = -3.421\ln(\delta_q)+13.514$	0.99	1.71	4.05
$RMSE_{u,min} = -3.179\ln(\delta_q)+12.532$	0.99	1.31	3.31
AM Peak			
$RMSE_{u,max} = -5.878\ln(\delta_q)+18.456$	0.96	2.18	3.14
$\overline{RMSE}_u = -2.206\ln(\delta_q)+7.9339$	0.99	0.07	0.18
$RMSE_{u,min} = -1.500\ln(\delta_q)+5.6015$	0.99	0.00*	0.02
Off-peak			
$RMSE_{u,max} = -3.958\ln(\delta_q)+15.887$	0.99	3.29	7.34
$\overline{RMSE}_u = -3.550\ln(\delta_q)+14.334$	0.99	2.44	5.94
$RMSE_{u,min} = -3.163\ln(\delta_q)+12.885$	0.99	1.72	4.67
*Estimated FCD penetration rate value was less than 0.005%			

Repeating the same analysis for the $RMSE_u$ suggested a range for the current penetration rate, $\tilde{\delta}_{FCD}$, equivalent to errors in penetration rates of 1.31% to 5.06%. Analyzing errors in peak and off-peak periods separately suggested that:

- During the peak period, estimated FCD penetration rate, $\tilde{\delta}_{FCD} < 1\%$ (except for the 3.14% based on $RMSE_{u,max}$ formulation)
- Off-peak FCD quality suggested a penetration rate, $\tilde{\delta}_{FCD} = [2.44\%; 5.94\%]$.

3.6. Potential use of FCD for Monitoring Urban Traffic in Ankara

In the light of the research findings described above, the comparison of FCD speeds against a ground truth data for a control segment on an urban study corridor in Ankara, Turkey showed that

- FCD speed mostly followed the GT speed profiles except for a few outliers, and had free flowing speed values.
- truncation of FCD speeds at the posted speed limits, a common practice in commercial data to prevent speed enforcement traps on the roads, brings a permanent error mostly for the off-peak periods, but, truncation at the free flow conditions rarely affect LOS estimations negatively.
- data filtering in FCD can significantly improve speed and LOS estimations for urban corridors
- the regression results between the GT and FCD speeds may be non-linear suggesting different relations during congested and uncongested regimes.
- it is critical to work with multiple performance measures (MAPE, RMSE, R^2 , etc.) to monitor FCD quality, as neither of them can assess the quality successfully alone.
- major queue formations and dissipations can be observed in FCD-based LOS monitors.

All these results showed that FCD could serve as a useful surrogate measure for urban speed monitoring at a macro level, such as LOS estimation. On the other hand, when used as the only traffic data source to monitor urban corridors in developing countries, it is very important to evaluate the quality of FCD regularly in space (separately for every urban corridor), even if it is against a short term GT data, to develop speed

transformation functions properly, which would improve corridor monitoring performance. Furthermore, it is helpful to repeat these evaluations over time, as penetration rate of GPS-equipped vehicles may increase which would increase the quality of FCD inherently. However, data clean up would always be necessary due to errors in data processing which is kept as a black-box in the commercial sector. Filtering can be carried out on a statistical basis, on either historical FCD availability or simply distribution of errors between FCD and GT values. Thus, it is crucial to keep a good archive of FCD speeds to have an understanding of speed distributions, which can be used to develop filters to detect outliers in real-time use.

The use of FCD speeds in a predefined fundamental flow-density relation, etc. can provide flow estimation, but errors due to truncation and laggings in FCD speeds must be handled carefully. Such an application will definitely require data fusion of FCD speed and flow (or density) from other traffic data sources. In this case, it is also important to check data quality of both sources and develop more probabilistic relations considering quality levels of the FCD speeds and the other parameter.

CHAPTER 4

METHODOLOGY FOR DETECTING QUEUE LENGTH USING FCD

As discussed in literature review part, FCD speed can be obtained from either probe vehicles or processed data of the multiple probe vehicles, which produced average speed data over a given segment. For the former one, since space-time diagram of the vehicle could be derived, it could be possible to identify time and location information of the vehicle when join and leave the queue by assuming a speed threshold value (commonly assumed as 5 km/h for signalized intersections). Based on these information, shockwave based models are implemented to estimate the maximum locations (Comert and Cetin, 2009; Cheng et al., 2011; Mecit, 2012; Li et al., 2013). On the other hand, when processed FCD speed can be considered, existing models cannot be appropriate since this data encompass the average speed of both moving and stopping vehicles. So, it is necessary to redefine the queue definition by selecting an speed threshold, v_{QL} , value representing the maximum queue length. This methodology provides how this speed threshold is selected to estimate queue lengths (see Figure 4.1).

FCD speed for a defined road segment s , epoch time λ (equals to 60 sec in commercial FCD) and at time interval t , denoted as $u_s^{t,\lambda}$, was only input parameter for the proposed model. Independent from the traffic condition, whether signalized or uninterrupted flows, the framework of the proposed methodology mainly consists of two parts including i) speed field estimation and ii) queue length estimation process as shown in Figure 4.1.

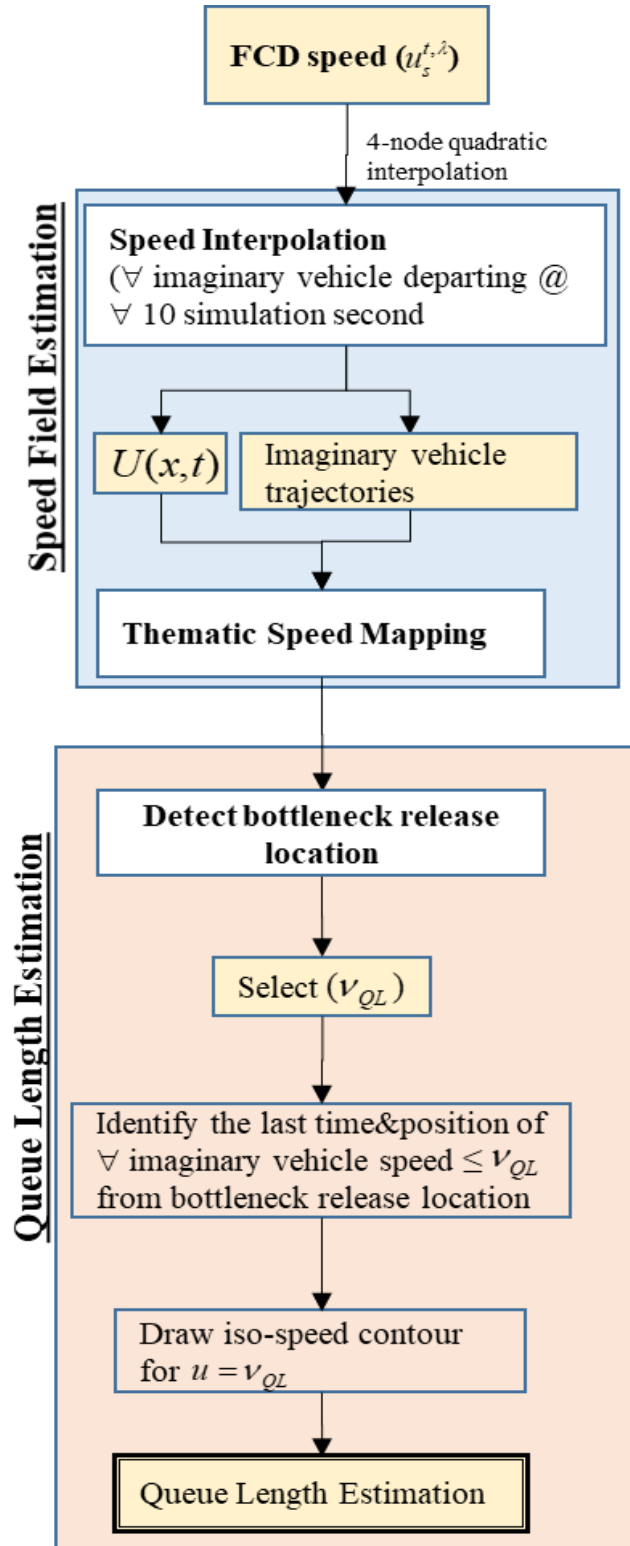


Figure 4.1. Framework for queue length estimation from FCD.

4.1. Speed Field Estimation from FCD

Average FCD speeds, $u_s^{t,\lambda}$, were employed in a 4-node quadratic interpolation to generate a estimated speed value, $U(x,t)$, for any given location x and time t as

$$U(x,t) = \sum_{m=1}^4 N_m(x,t) u_m^{t,\lambda} \quad [4.1]$$

where; N_m : node-specific interpolation function for the m^{th} node such that

$$N_1 = \frac{(t - \Delta t)(x - \Delta x)}{\Delta x \Delta t}, \quad N_2 = \frac{-t(x - \Delta x)}{\Delta x \Delta t}, \quad N_3 = \frac{-tx}{\Delta x \Delta t}, \quad N_4 = \frac{-(t - \Delta t)x}{\Delta x \Delta t}$$

Sending an imaginary vehicle j from the midpoint location of the first segment of the road corridor at time $\lambda / 2$, the next location of the vehicle was calculated by assuming a travel distance traversed at speed of $U(x,t)$ for the assumed time step ε_t .

Similarly, at any given point x_j of the imaginary vehicle trajectory, the next location (x_j') of the imaginary vehicle would be

$$x_j' = x_j + U(x_j, t) * \varepsilon_t \quad [4.2]$$

at the next time step $t' = t + \varepsilon_t$, where $U(x,t)$ value is calculated using relations in Equation [4.1]. ε_t was taken as 0.1 sec, which means it could be possible to have an location and time information of imaginary vehicles for every 0.1 sec. Imaginary vehicle trajectory generation stops when the updated position is beyond the midpoint of the last FCD segment of the corridor. In this study, imaginary vehicles were created at every 10 sec, and imaginary vehicle generation was terminated at the end of analysis period. Example imaginary vehicle trajectory data for the study corridor 1 (Dumlupınar Blvd) are shown in Figure 4.2a. Based on the imaginary vehicle trajectory data, Figure 4.2a gives an idea about the existing bottleneck location which is Segment 72 (around 3293 m far from the initial segment in Figure 4.2a) and slope of the lines before and after this location draw a conclusion about the speed changes

around this location. Using the location and time (x, t) information augmented with the speed $U(x, t)$, thematic speed maps were obtained as shown in Figure 4.2b.

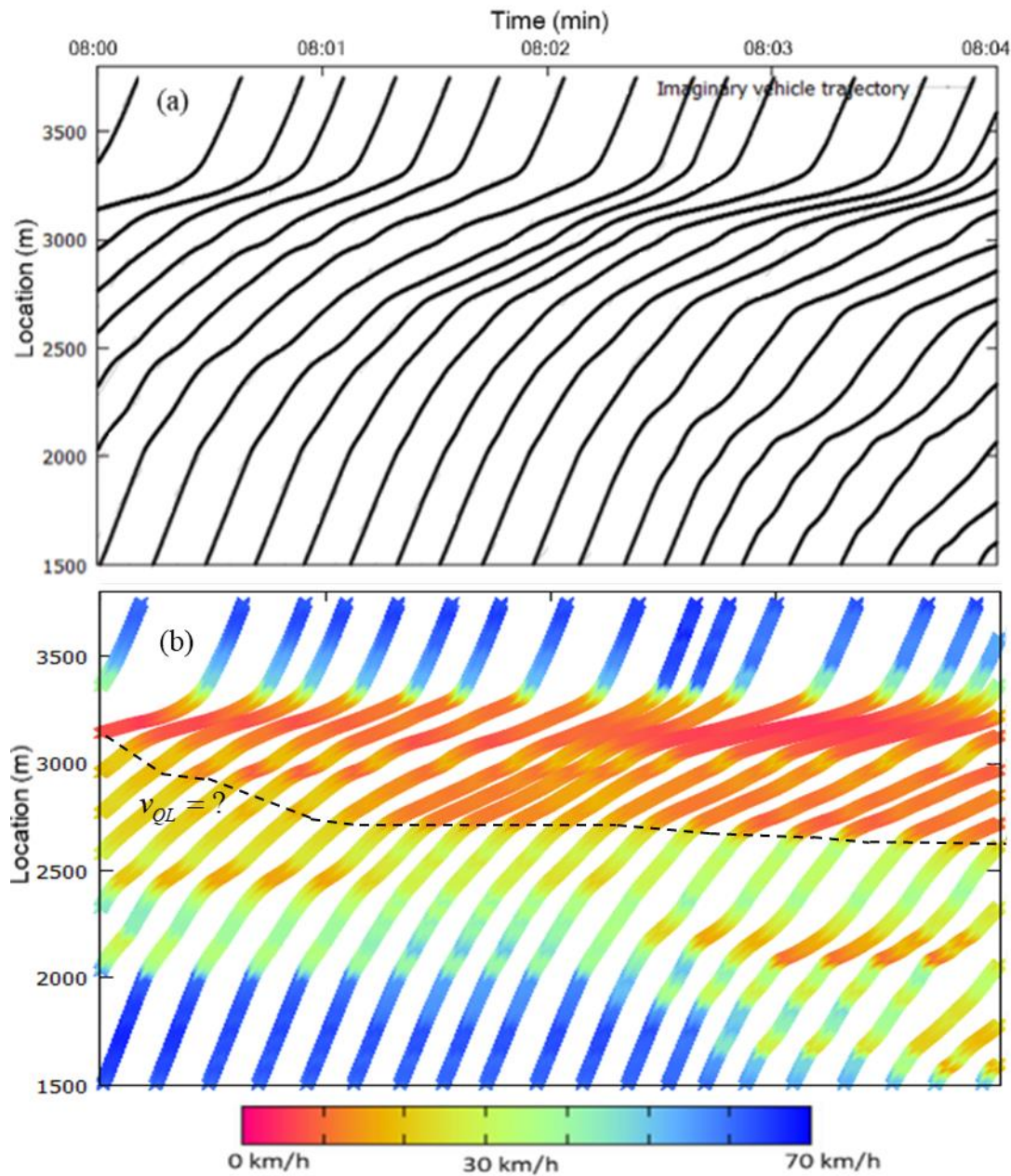


Figure 4.2. a) Imaginary vehicle trajectory data generation, b) thematic speed map for the study corridor 1.

After obtainment of thematic speed maps, accurate selection of speed threshold, v_{QL} , and drawing iso-speed contours based on the selected v_{QL} value enabled to estimate the possible queue length profile over time (see Figure 4.1). To draw iso-speed contours, 4-node quadratic interpolation method was revised in a way that time and position information of sending imaginary vehicle was recorded when its speed first dropped to selected v_{QL} near bottleneck location. Repeating same procedure for every imaginary vehicle provided queue entry location and connecting this location with a line enabled to form iso-speed contours as shown in Figure 4.2b. However, the critical issue here is how to determine the v_{QL} for providing minimum queue length estimation error.

4.2. Selection of Speed Threshold for Queue Length Estimation

Selection of v_{QL} for queue length estimation for uninterrupted flows requires the identification of the severe congested states (where the queue occurs) as described in Section 2.2.2. As recommended in HCM (2010), severe congested state can be determined by taking the one-third of the target speed. The target speed was defined as the speed at which the driver prefers to travel. So, based on the GT speed profile presented in Figure 3.6, the target speed was taken as 82 km/h which was also the speed limit of the study corridor. Thus, taking one-third of the 82 km/h resulted in 27.3 km/h which meant the speeds below 27.3 km/h were assumed to join the queue. So, v_{QL} value can be selected as 27.0 km/h for queue length estimation. On the other hand, it could be possible to select another v_{QL} by implementing transformation functions in Equations [3.1b] and [3.1d] separately to obtain corresponding FCD speeds. When the transformation function in Equation [3.1b], showing the relationship between GT speed and raw FCD speed, was used, corresponding FCD speed was calculated as 41.97 km/h. Similarly, Equation [3.1d] resulted in FCD speed of 41.56 km/h, which is quite similar values. So, two v_{QL} values were selected for queue length

detection for the study corridor 1 as considering the transformed FCD speed, 42.0 km/h, and without the transformed speed as 27.0 km/h.

On the other hand, for signalized intersections, since FCD speed in this study was averaged for the predefined road segments, selecting v_{QL} as 5 km/h is not valid for defining maximum queue location. Determination of v_{QL} value for signalized intersection can be determined by collecting Ground Truth data to observe the actual queue length for each cycle in real time and to determine the corresponding FCD speeds from thematic speed maps when the maximum queue length is achieved. Alternatively, it can be determined by utilization of VISSIM simulation environment. It could be possible to generate a signalized intersection and a synthetic FCD speeds for the defined segment lengths of the approach leg. Selecting different speed threshold values, v_z , and calculating the queue length estimation errors provided to derive error-speed threshold function and minimum value of this function provided the optimum speed threshold value which is donated as v_{opt} .

CHAPTER 5

QUEUE LENGTH ESTIMATION WITH FCD IN VISSIM ENVIRONMENT

5.1. Signalized Intersection in VISSIM Environment

To evaluate the performance of the proposed model in signalized intersection, VISSIM simulation was utilized to generate a road corridor with a signalized intersection. The framework for queue length estimation is composed of five parts: i) VISSIM simulation for ground truth and synthetic FCD data generation, ii) speed field estimation, iii) queue length observation, iv) queue length estimation and v) performance evaluation (see Figure 5.1). VISSIM simulation data was processed multiple times with different FCD penetration rate (δ) and speed aggregation epoch time (λ). Using VISSIM COM Interface, a MATLAB code has been developed to track the vehicles in the network for each 0.1 simulation second and generated vehicle trajectory data (Task T1 in Figure 5.1), which composed of vehicle identification, a sequence of time, position, speed data and whether the tracked vehicle is FCD vehicle or not. An example vehicle trajectory for the study segments in VISSIM environment is provided in Figure 5.2, which was used to extract time and position of a vehicle i) joining the queue, and ii) leaving the queue by assuming 5 km/h threshold speed limit. For each cycle, “Joined Queue Data Set” and “Leaved Queue Data Set” were created (Task T2) in which the former was later be utilized to extract the position and time information of the last vehicle that joined the queue in Task T6.

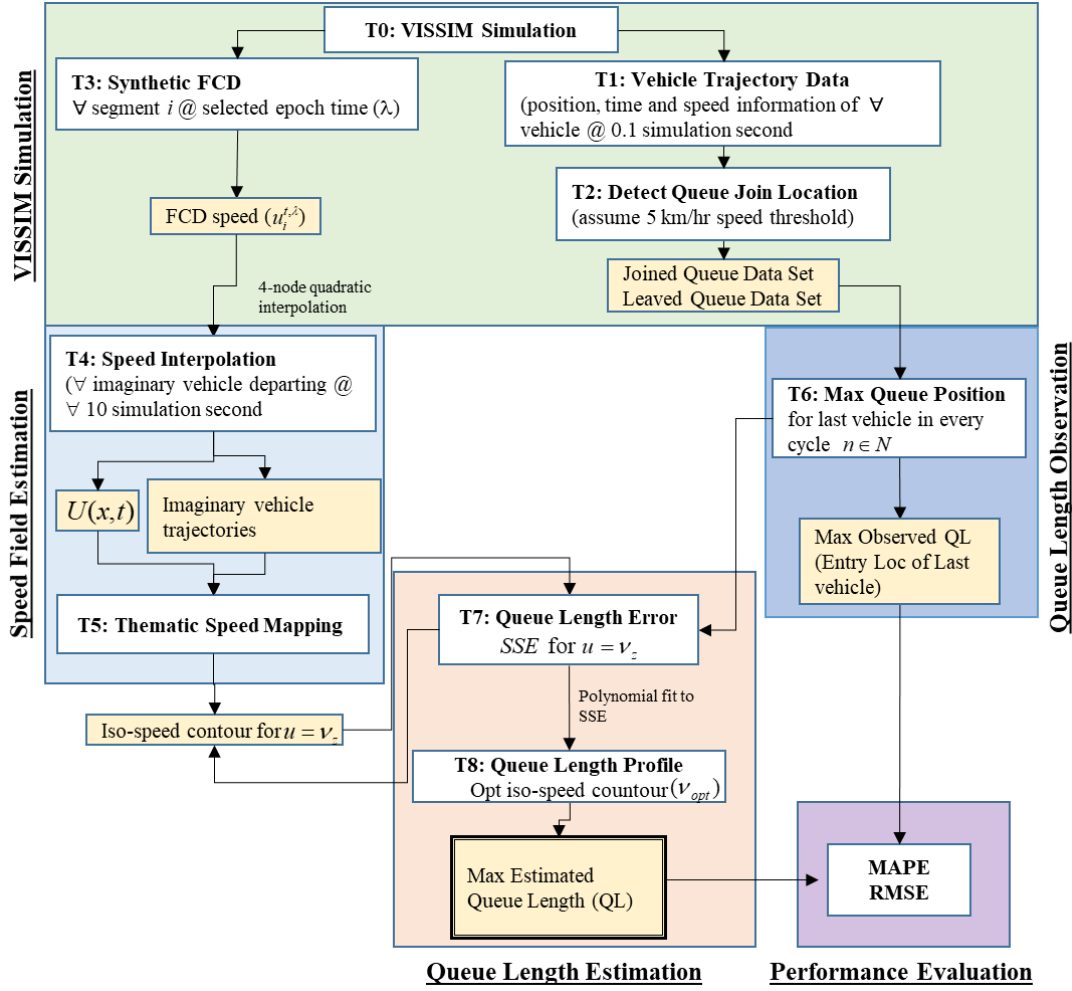


Figure 5.1. Framework for simulation-based queue length estimation from FCD.

In Task T3, to generate the synthetic FCD speed, $u_s^{t,\lambda}$, individual vehicle travel times over for the road segment s during the epoch time λ , were measured by sensors in VISSIM. Finally $u_s^{t,\lambda}$ was determined by dividing the segment length by the average travel time at time interval t , and assumed to represent the speed at the midpoint of a space-time finite element as shown in Figure 5.3 (superscript λ was omitted to simply the figure). (Note: Synthetic FCD for shorter epoch times of $\lambda = 30$ sec and 15 sec were created, to evaluate sensitivity to potential FCD precision in the future FCD formats).

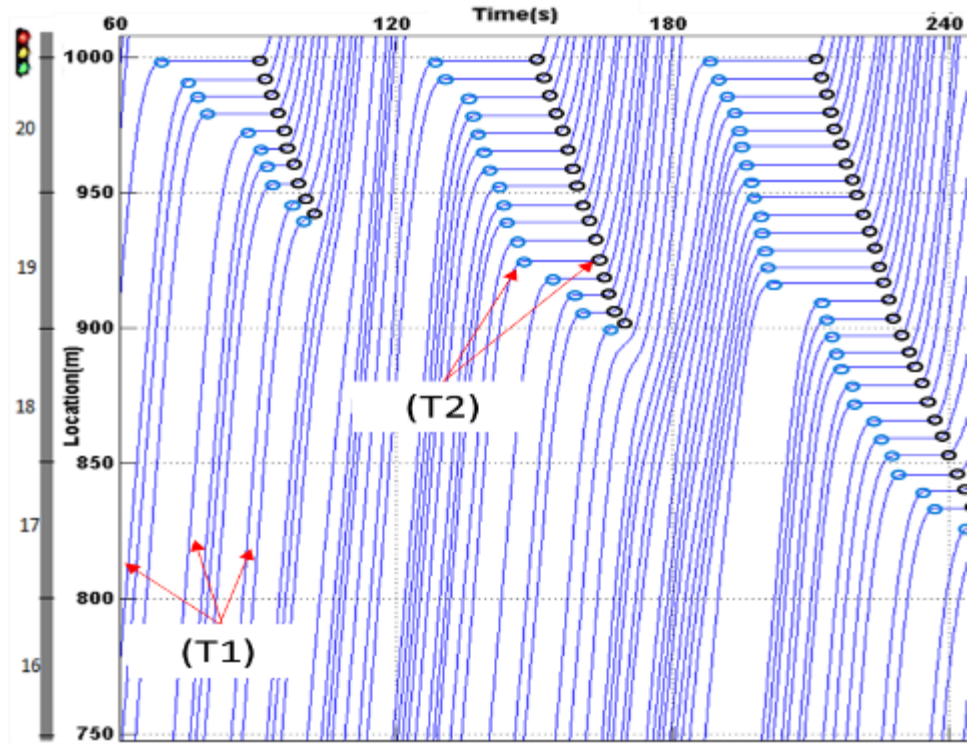


Figure 5.2. Vehicle trajectory data with Joined/Leaved Queue Data Set in VISSIM.

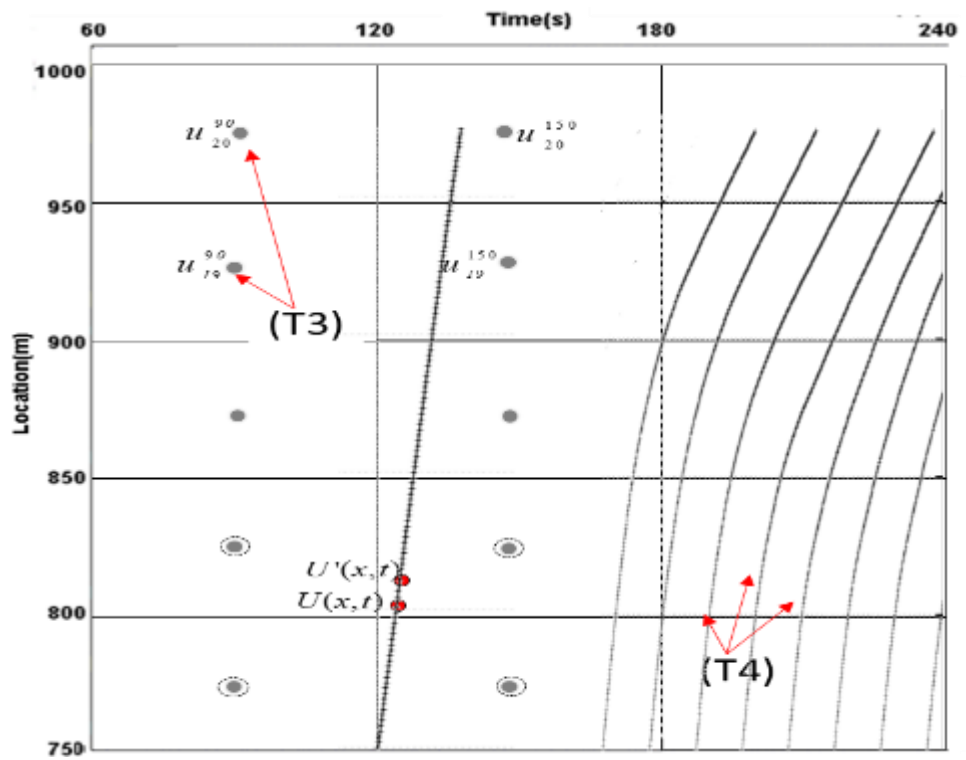


Figure 5.3. FCD speed and imaginary vehicle trajectory data generation.

In T4, using 4-node interpolation method discussed in Section 4.1 was employed to synthetic FCD speed to generate imaginary vehicle trajectory data as well as the thematic speed maps. Imaginary vehicles were created at every 10 sec, and imaginary vehicle generation was terminated at the end of $T=3600$ seconds. Using the location and time (x,t) information augmented with the speed $U(x,t)$, thematic speed maps (defined in T5) were obtained as shown in Figure 5.4.

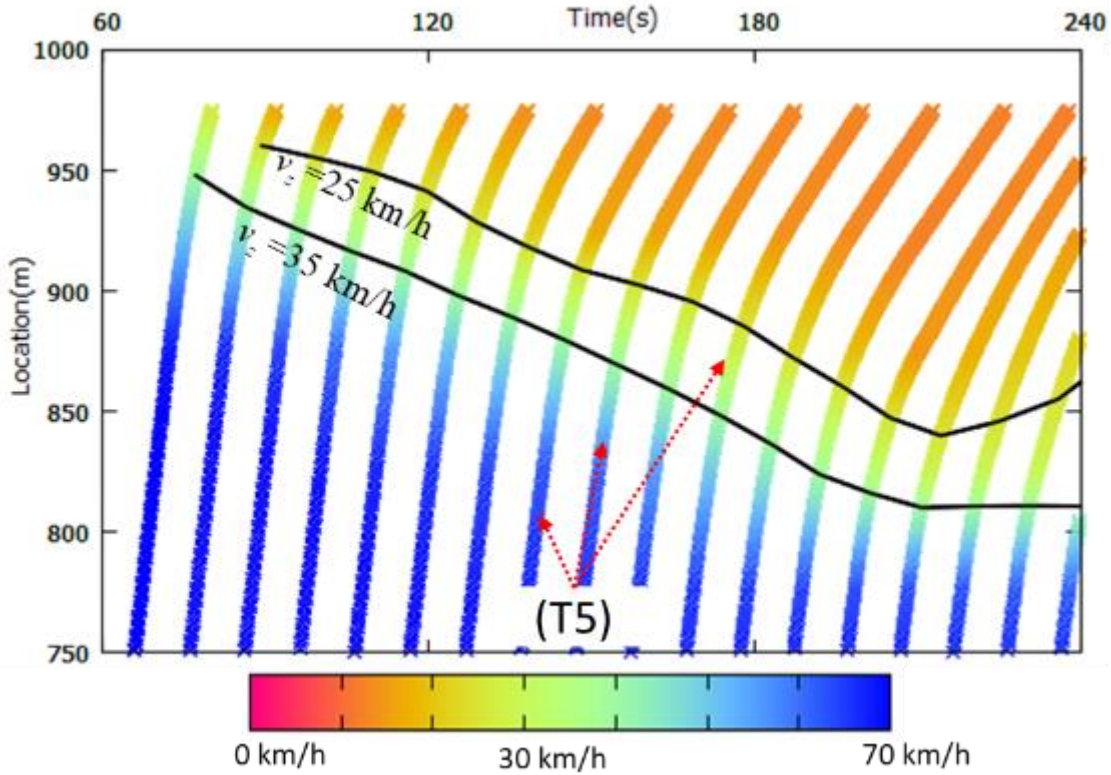


Figure 5.4. Thematic speed maps with iso-speed contours.

5.1.1. Determination of Optimum Speed Threshold

To determine the v_{opt} , different speed threshold values, v_z , were selected for drawing iso-speed contour lines during the simulation period (see Figure 5.4). Selected v_z for this study were $\{20 \text{ km/h}, 25 \text{ km/h}, 30 \text{ km/h}, 35 \text{ km/h}, 40 \text{ km/h}\}$. For this purpose, 4-

node quadratic element interpolation method has been revised in a way that when each imaginary vehicle speed drops to selected V_z , the algorithm ended and recorded the time and location information. Therefore, during the simulation period, the time and location for each imaginary vehicle were connected a line to form an iso-speed contour (see Figure 5.4).

“Joined Queue Data Set” matrices were utilized to determine position and time information of the last joined vehicle for each cycle from simulation (T6). The last joined vehicle was defined as the last vehicle that joined the queue for the cycle n (see Figure 5.5). According to the time information of the last joined vehicle, the position of the iso-speed contour line were determined for each cycle, and sum of square error (SSE) has been computed in Equation [4.1] and denoted as $SSE_{e,z}$. This process was re-repeated for every selected speed threshold.

$$SSE_{e,z} = \sum_{n=1}^N \mathcal{E}_n = \sum_{n=1}^N (x_e^n - x_{e,z}^n)^2 \quad [5.1]$$

where,

x_e^n : the location of last vehicle joined the queue at signal cycle n , $n=1,2,..N$

$x_{e,z}^n$: the location of iso-speed contour line z when the last vehicle entering to queue at signal cycle n , $n=1,2,..N$

Thus, minimization of the $SSE_{e,z}$ enabled to determine the v_{opt} for the possible queue length estimation profile.

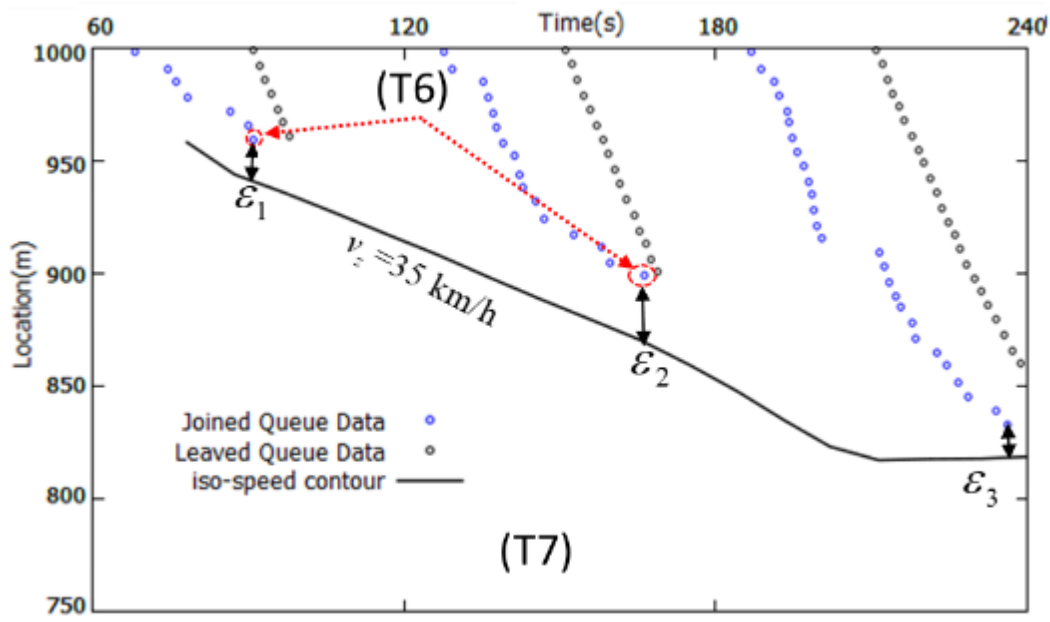


Figure 5.5. Iso-speed contour with Joined/Leaved Queue Dataset for error calculation.

5.1.2. Performance Evaluation

The model performance was evaluated by $MAPE_Q$ and $RMSE_Q$ by comparing the actual queue lengths with the estimated ones from Equation [5.2] and Equation [5.3], respectively.

$$MAPE_Q = \frac{1}{N} \sum_{n=1}^N \left| \frac{\hat{Q}_n - Q_n}{Q_n} \right| * 100 \quad [5.2]$$

$$RMSE_Q = \sqrt{\frac{1}{N} \sum_{n=1}^N (\hat{Q}_n - Q_n)^2} \quad [5.3]$$

5.2. VISSIM Scenarios

To estimate the queue length from FCD speed data, a simple synthetic network has been created in simulation environment VISSIM. A single one-lane link of approximately 1 km was created, and a signal head was located at the end of the synthetic network and segment lengths were designed as 50 m lengths. All vehicles are assumed passenger cars with the desired speed of 70 km/h and they enter the network at a constant rate but randomly. All other parameters are kept at the default values built within VISSIM and simulation time was set to 3600 sec. To test the efficiency of the model three set of simulation runs have been performed by considering different traffic conditions and cycle times as shown in Table 5.1. Based on the design parameters discussed above, saturation flow rate of the approach was determined as 2160 veh/h in which the capacity of the approach for different traffic conditions are illustrated in Table 5.1. The capacity was calculated as 1032 veh/h for the Condition 1 (C1) and Condition 3 (C3), while it was 1008 veh/h for C2. Degree of saturation (X) for C1 was calculated as 0.60 representing undersaturated traffic condition, while the others were very close to 1, showing the mixed traffic condition (see Table 5.1). For this analysis, the model performance was tested under full penetration of FCD vehicle, and its strength was also tested in various penetration rate which will be discussed in the following section.

Table 5.1. *Traffic conditions and corresponding input parameters for simulation based queue length estimation.*

Traffic condition	Traffic Demand	Cycle Length (sec) (Green/Red)	Capacity (c)	Degree of Saturation (X)
Condition (C1): Undersaturated	650 veh/h	90 sec (45 sec/45 sec)	1032 veh/h	0.60
Condition (C2): Mixed (Undersaturated+ Oversaturated)	950 veh/h	60 sec (30 sec/30 sec)	1008 veh/h	0.94
Condition (C3): Mixed (Undersaturated+ Oversaturated)	950 veh/h	90 sec (45 sec/45 sec)	1032 veh/h	0.92

5.2.1. Undersaturated Condition

To examine the strength of the proposed model for the undersaturated condition, the traffic demand was set to 650 veh/h with a cycle length of 90 sec as shown in Table 5.1. At end of the simulation, simulated FCD speeds obtained for each segment were discretized to generate imaginary vehicle trajectory data and speed field data by using the finite element method as described in the methodology section.

Use of 4-node quadratic interpolation method in speed field estimation provided the thematic speed maps shown in Figure 5.6 on which Joined and Leaved Queue Data sets (as obtained from ground truth data) were displayed jointly. For $\lambda = 60$ sec, thematic speed maps provided some insights about extension of queue lengths over time depicted by an enveloping lower speed zones (< 30 km/h) around maximum queue points, despite lack of precision on formation and dissipation of them in each cycle (see Figure 5.6a). The queue dynamics were slightly more observable when λ was selected as 30 sec as shown in Figure 5.1b, which were further improved with $\lambda = 15$ sec (see Figure 5.6c); though a traditional 5 km/h threshold was not appropriate (nor reached sometimes) for queue detection in FCD speeds. To determine v_{opt} , several speed thresholds, v_z , were selected (Figure 5.7a for $\lambda = 60$ sec case) and errors in $SSE_{e,z}$ were determined. Plotting $SSE_{e,z}$ vs v_z values as shown in Figure 5.8 produced an error-speed threshold function; minimum value of which would produce the optimum speed threshold in FCD, v_{opt} , defining the queue length. For $\lambda = 60$ sec (see Figure 5.7a for the iso-speed contours), the minimum error in queue length estimation was achieved if v_{opt} of 32.0 km/h was selected (see Table 5.2). This produced $MAPE_Q$ and $RMSE_Q$ of 28.6% and 15.2 m, respectively.

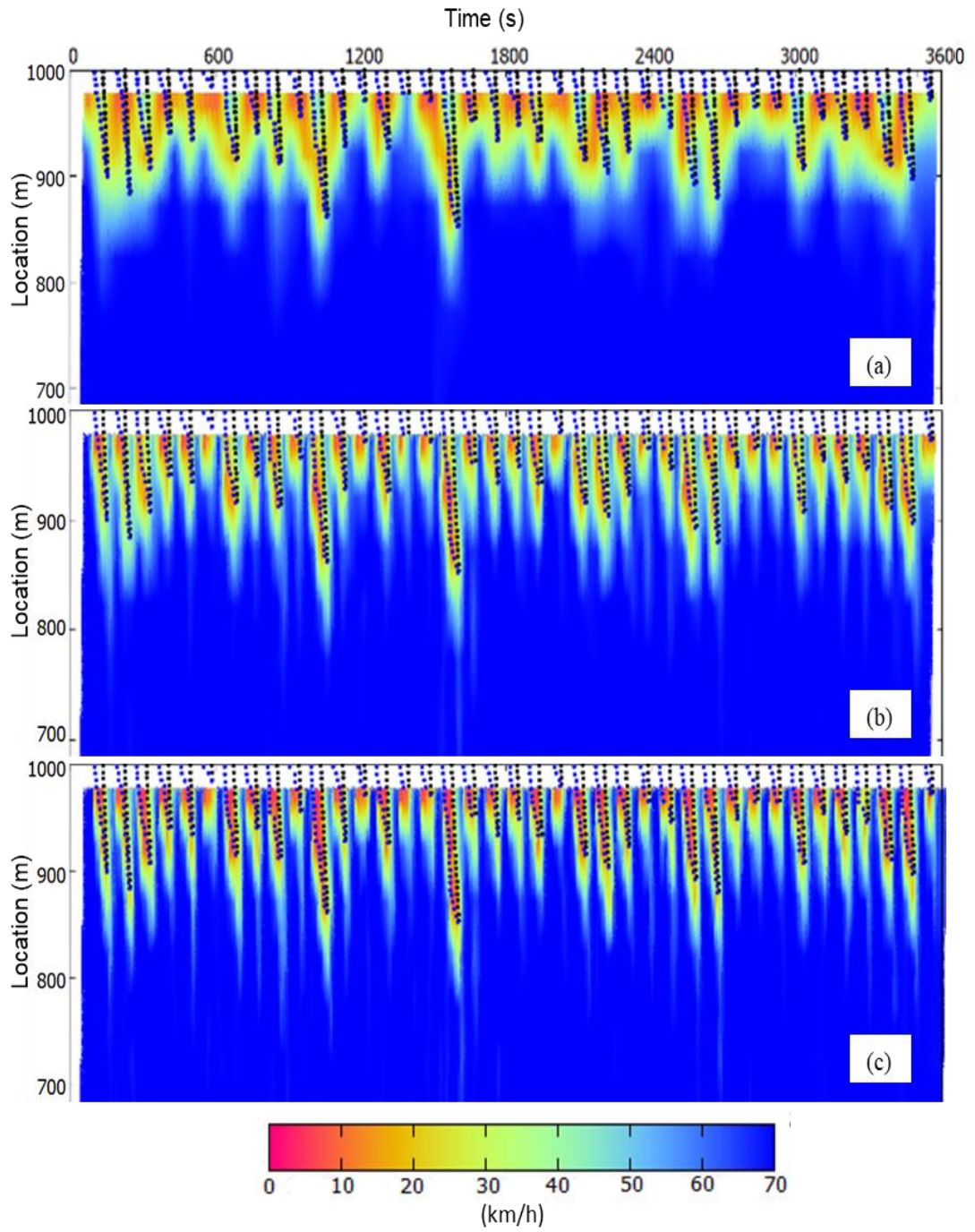


Figure 5.6. Comparison of the queue lengths obtained from vehicle trajectory data and speed thematic map for FCD with a) 60 sec b) 30 sec, c) 15 sec epoch times for C1.

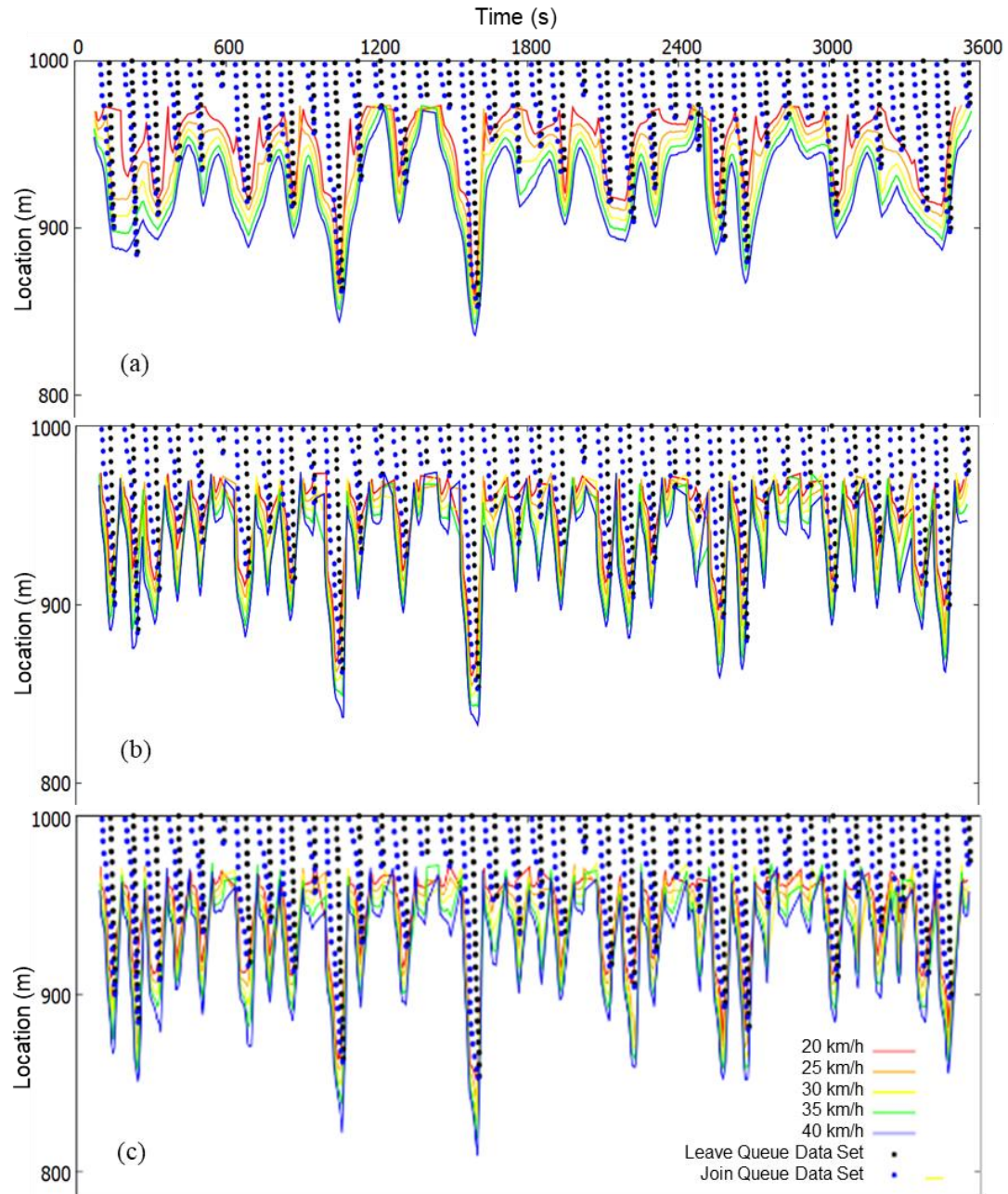


Figure 5.7. Iso-speed contours for a) 60 sec, b) 30 sec and c) 15 sec epoch times with observed queue lengths obtained from vehicle trajectory data for C1.

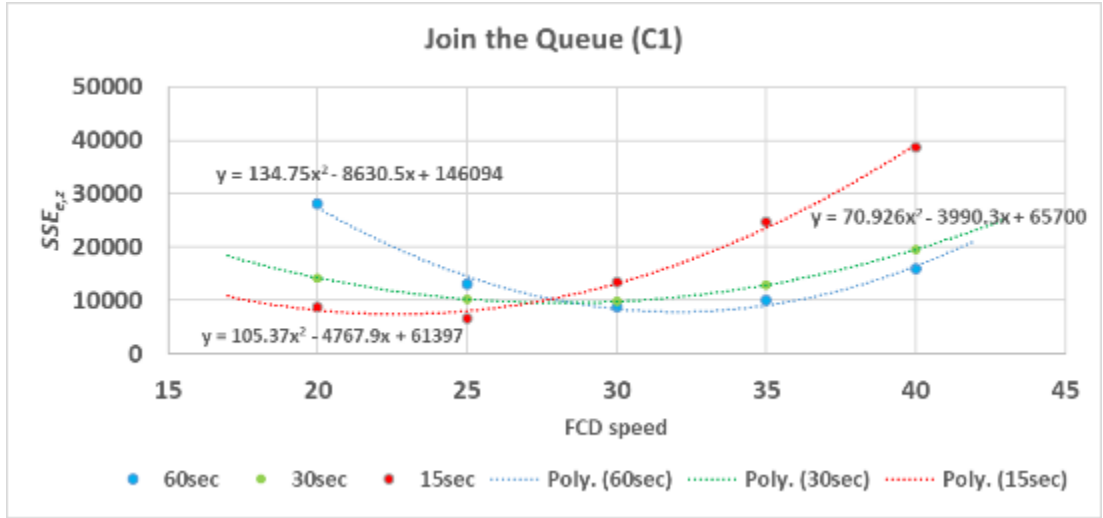


Figure 5.8. Derivation of $SSE_{e,z}$ and V_z function for V_{opt} determination for C1.

Table 5.2. V_{opt} and corresponding $MAPE_Q$ and $RMSE_Q$ values for different λ values for C1.

δ (%)	Last Join Queue Speeds	V_{opt} (km/h)	$MAPE_Q$ (%)	$RMSE_Q$ (m)
100 ($\lambda = 60\text{sec}$)	32.0 km/h	32.0	28.6	15.2
100 ($\lambda = 30\text{sec}$)	28.1 km/h	28.1	23.7	14.7
100 ($\lambda = 15\text{sec}$)	22.6 km/h	22.6	21.9	12.3

When the same analysis was repeated with $\lambda = 30$ sec, selected speed threshold defining queue length was found as 28.1 km/h, which had a $MAPE_Q$ and $RMSE_Q$ values of 23.7% and 14.7 m, respectively. The V_{opt} valued dropped to 22.6 km/h for $\lambda = 15$ sec case which also slightly improved $MAPE_Q$ and $RMSE_Q$ values. To understand the real success in the two performance measures, it is helpful to display the observed and estimated queue lengths for every cycle as shown in Figure 5.9.

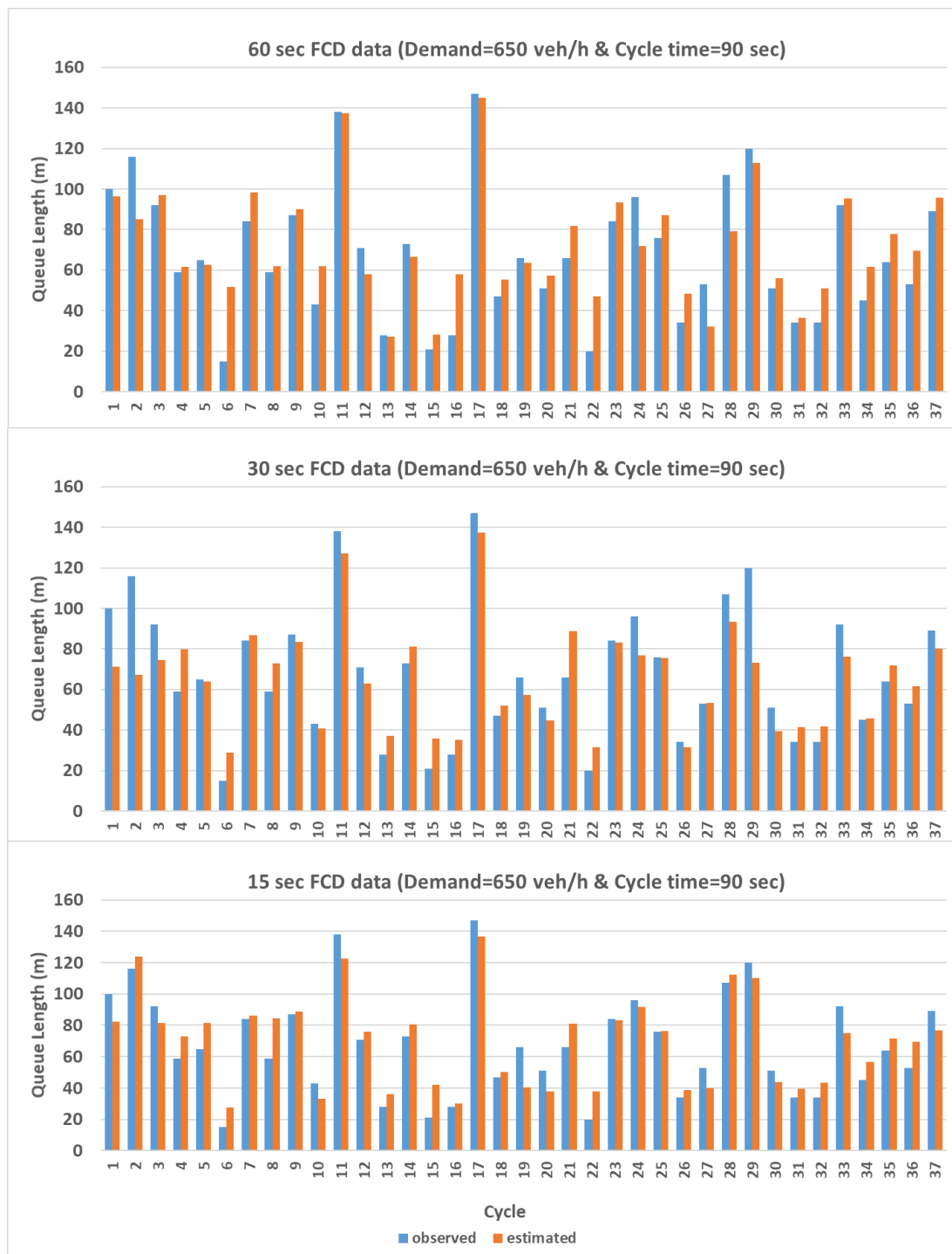


Figure 5.9. Comparison of the cycle based estimated queue lengths with observed ones for C1.

5.2.2. Mixed Condition

To evaluate the model performance under both undersaturated and oversaturated cases, two sets of simulation have been performed under different cycle times with the same demand (see Table 5.1). Implementation of the 4-node quadratic interpolation method in speed field estimation provided the thematic speed maps as shown in Figure 5.10 and Figure 5.12 for the C2 and C3, respectively. Similar to the C1, thematic speed maps provided insights about where the queue extends in each cycle for each λ 's. As expected, due to the big aggregation of the FCD speed ($\lambda = 60$ sec), it could not possible to observe the queue dynamics (see Figure 5.10a and Figure 5.12a) for the C2 and C3, whereas the queue dynamics were more observable when $\lambda = 15$ sec (see Figure 5.10c and Figure 5.12c).

Drawing iso-speed contours for the C2 and C3 (see Figure 5.11 and Figure 5.13, respectively) and deriving the error-speed threshold function (see Figure 5.14 and Figure 5.15), gives v_{opt} and corresponding $MAPE_Q$ and $RMSE_Q$ values as follows:

- When $\lambda = 60$ sec,
 - minimum error in queue length estimation was achieved if $v_{opt} = 30.8$ km/h for C2, which produced $MAPE_Q$ and $RMSE_Q$ of 21.8% and 14.2 m, respectively (see Table 5.3).
 - v_{opt} was determined as 35.3 km/h for C3 with $MAPE_Q$ and $RMSE_Q$ of 9.7% and 12.6 m, respectively, which produced less estimation error when compared to C2.
- When $\lambda = 30$ sec,
 - v_{opt} value was almost same for C2 and C3 (Table 5.3) as 29.5 km/h and 29.9 km/h, respectively. $MAPE_Q$ was found as 21.9% for the C2, while it was only 9.2% for C3.

- $RMSE_Q$ values were calculated as 15.3 m and 11.1 m, which were very close to each other.
- When $\lambda = 15$ sec,
 - v_{opt} was 24.3 km/h and 27.9 km/h with $MAPE_Q$ of 20.8% and 9.1% for C2 and C3, respectively.

Finally, observed and estimated queue lengths for every cycle are illustrated in Figures 5.16 and 5.17 for C2 and C3, respectively. It is concluded that selecting lower λ 's provides to examine the queue dynamics more precisely and only changes the selected v_{opt} . However, it does not significantly change queue length estimation errors.

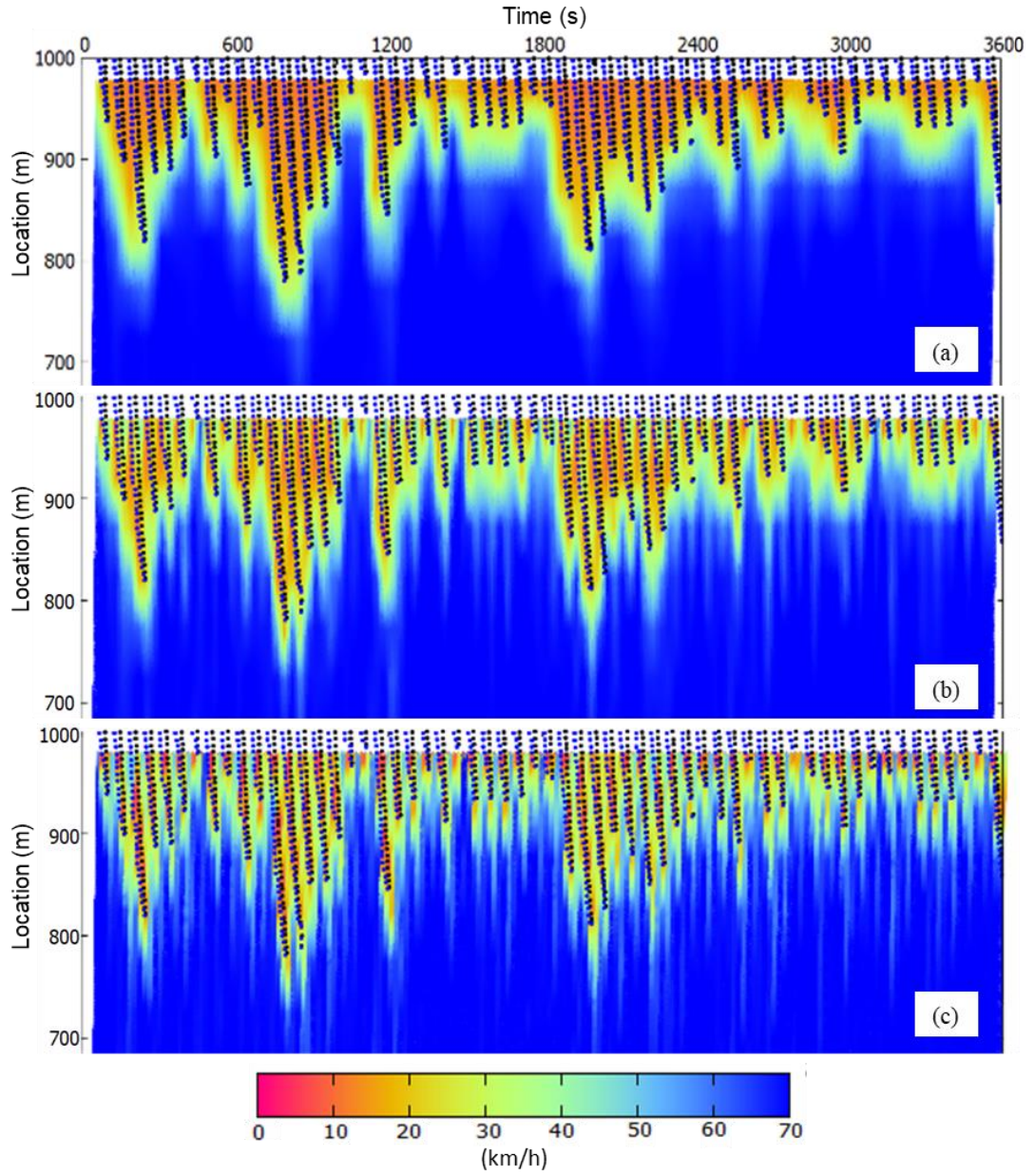


Figure 5.10. Comparison of the queue lengths obtained from vehicle trajectory data and speed thematic map for FCD with a) 60 sec b) 30 sec, c) 15 sec epoch times for C2.

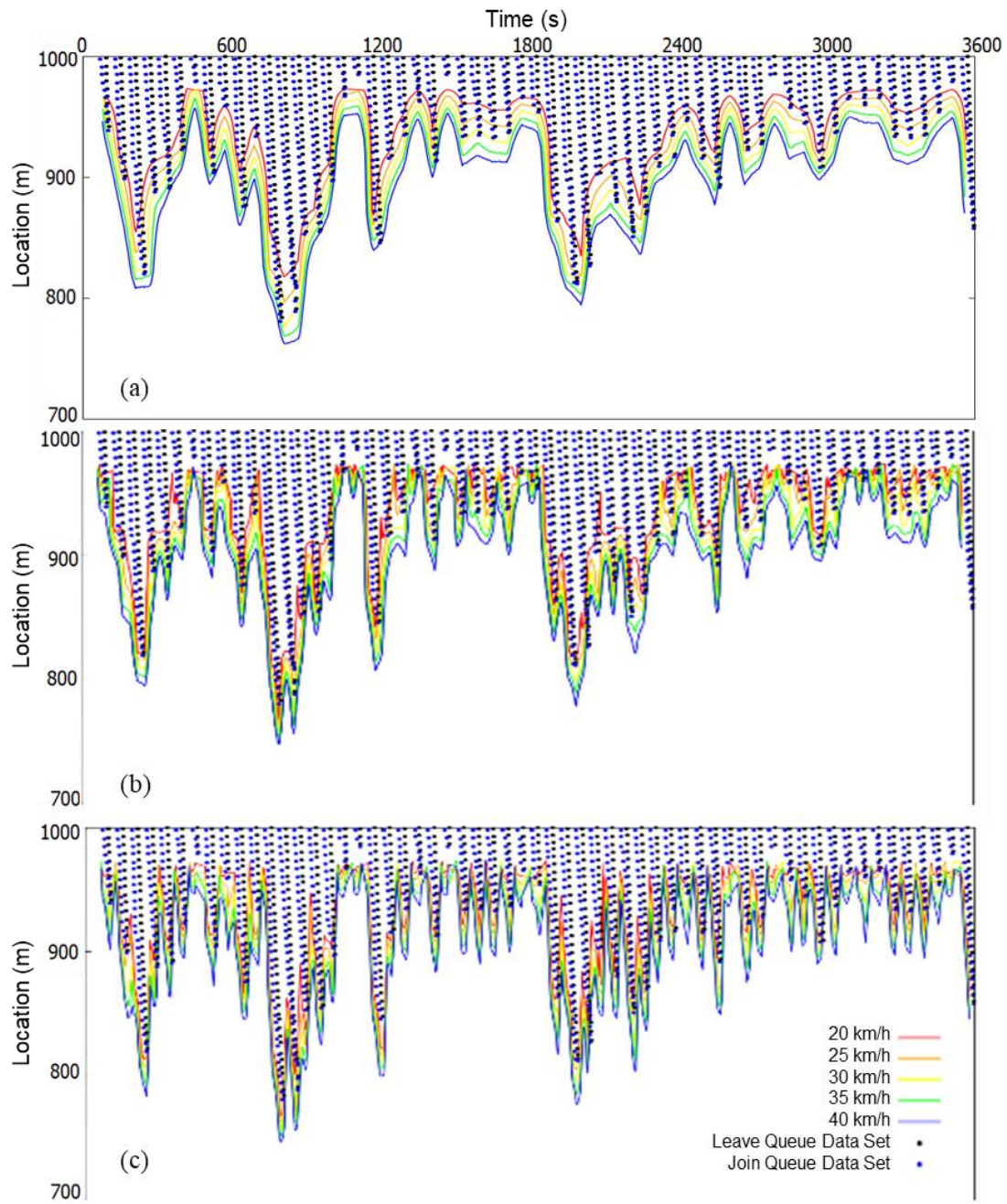


Figure 5.11. Iso-speed contours for a) 60 sec, b) 30 sec and c) 15 sec epoch times with observed queue lengths obtained from vehicle trajectory data for C2.

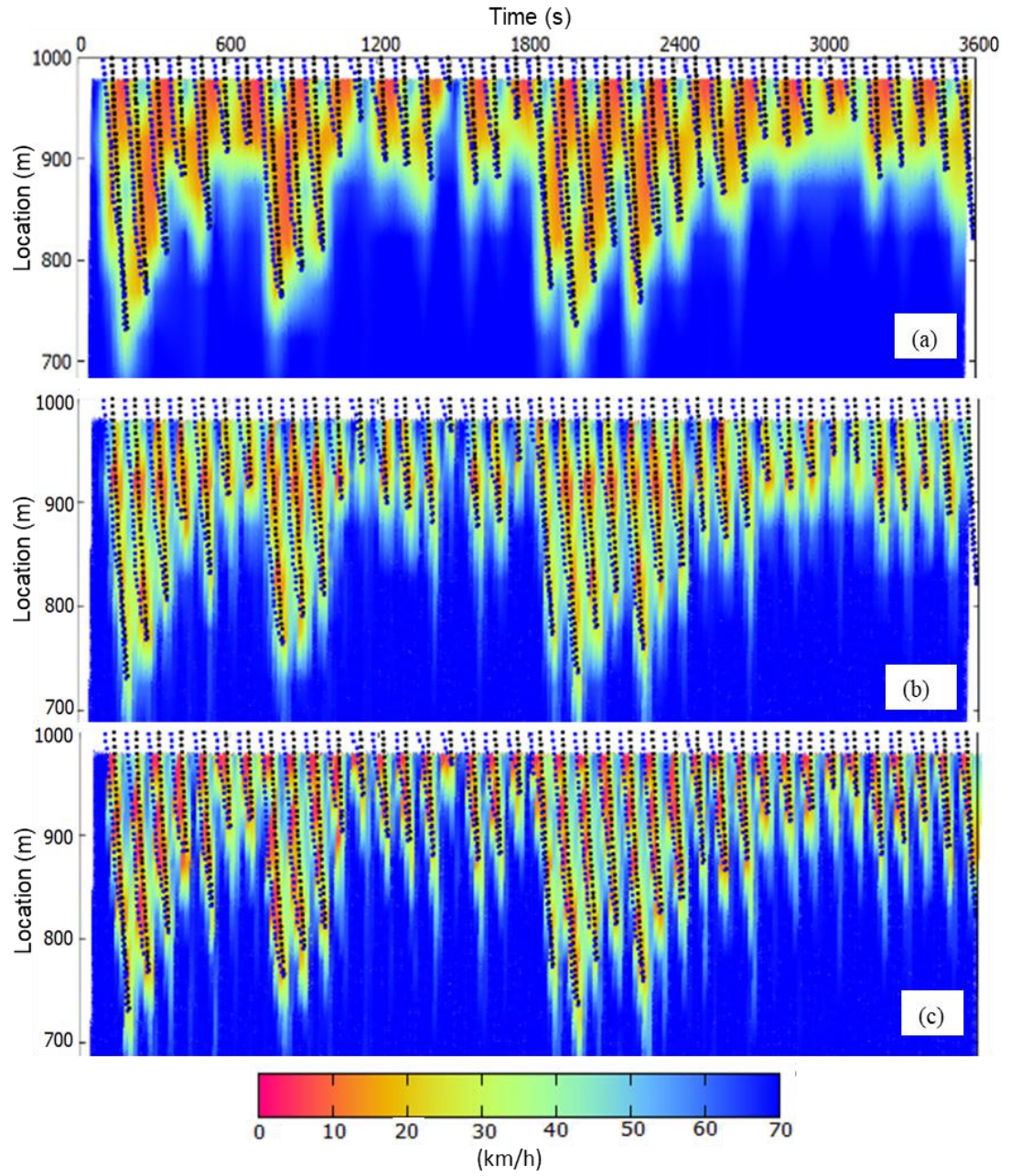


Figure 5.12. Comparison of the queue lengths obtained from vehicle trajectory data and speed thematic map for FCD with a) 60 sec b) 30 sec, c) 15 sec epoch times for C3.

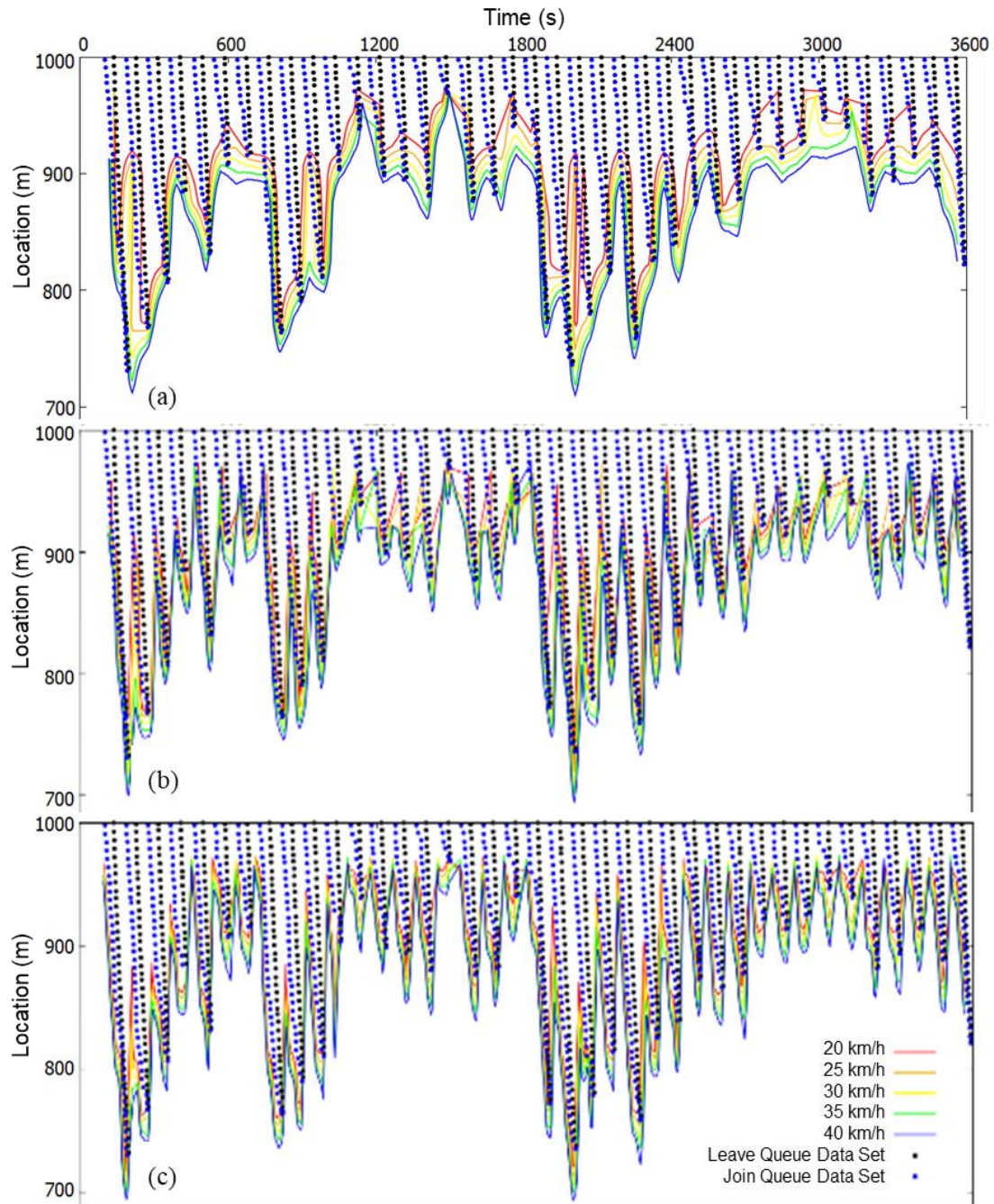


Figure 5.13. Iso-speed contours for a) 60 sec, b) 30 sec and c) 15 sec epoch times with observed queue lengths obtained from vehicle trajectory data for C3.

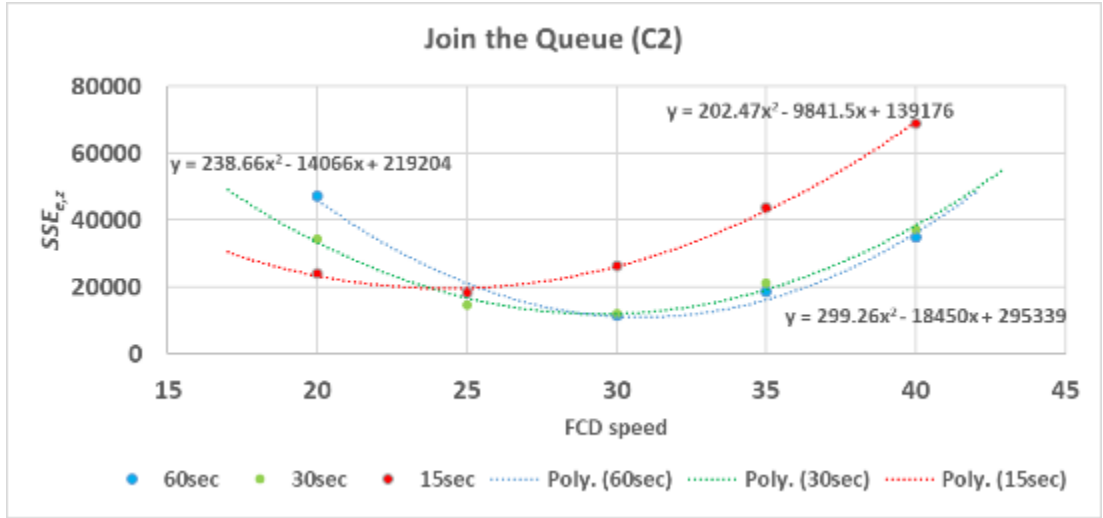


Figure 5.14. Derivation of $SSE_{e,z}$ and V_z function for V_{opt} determination for C2.

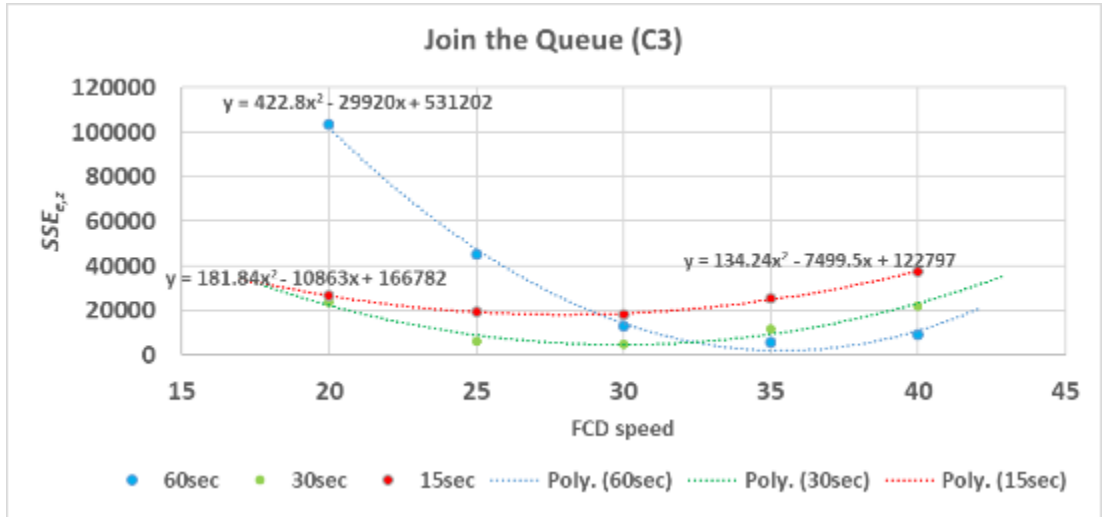


Figure 5.15. Derivation of $SSE_{e,z}$ and V_z function for V_{opt} determination for C3.

Table 5.3. v_{opt} and corresponding $MAPE_Q$ and $RMSE_Q$ values for different λ values for C2 and C3.

δ (%)	Last Join Queue speeds	v_{opt} (km/h)	$MAPE_Q$ (%)	$RMSE_Q$ (m)
C2				
100 (λ =60sec)	30.8 km/h	30.8	21.8	14.2
100 (λ =30sec)	29.5 km/h	29.5	21.9	15.3
100 (λ =15sec)	24.3 km/h	24.3	20.8	15.1
C3				
100 (λ =60sec)	35.3 km/h	35.3	9.7	12.6
100 (λ =30sec)	29.9 km/h	29.9	9.2	11.1
100 (λ =15sec)	27.9 km/h	27.9	9.6	12.7

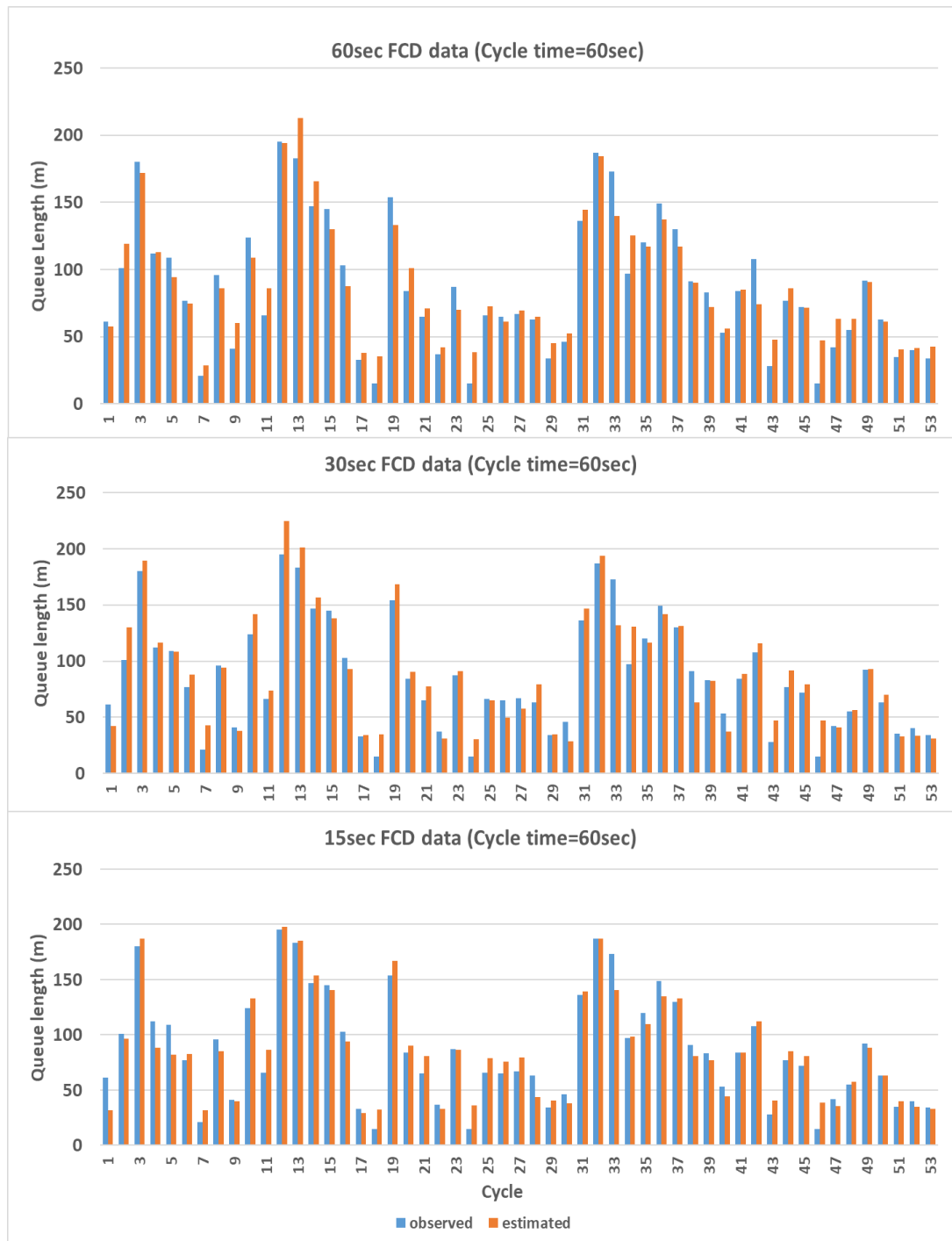


Figure 5.16. Comparison of the cycle based estimated queue lengths with observed ones for C2.

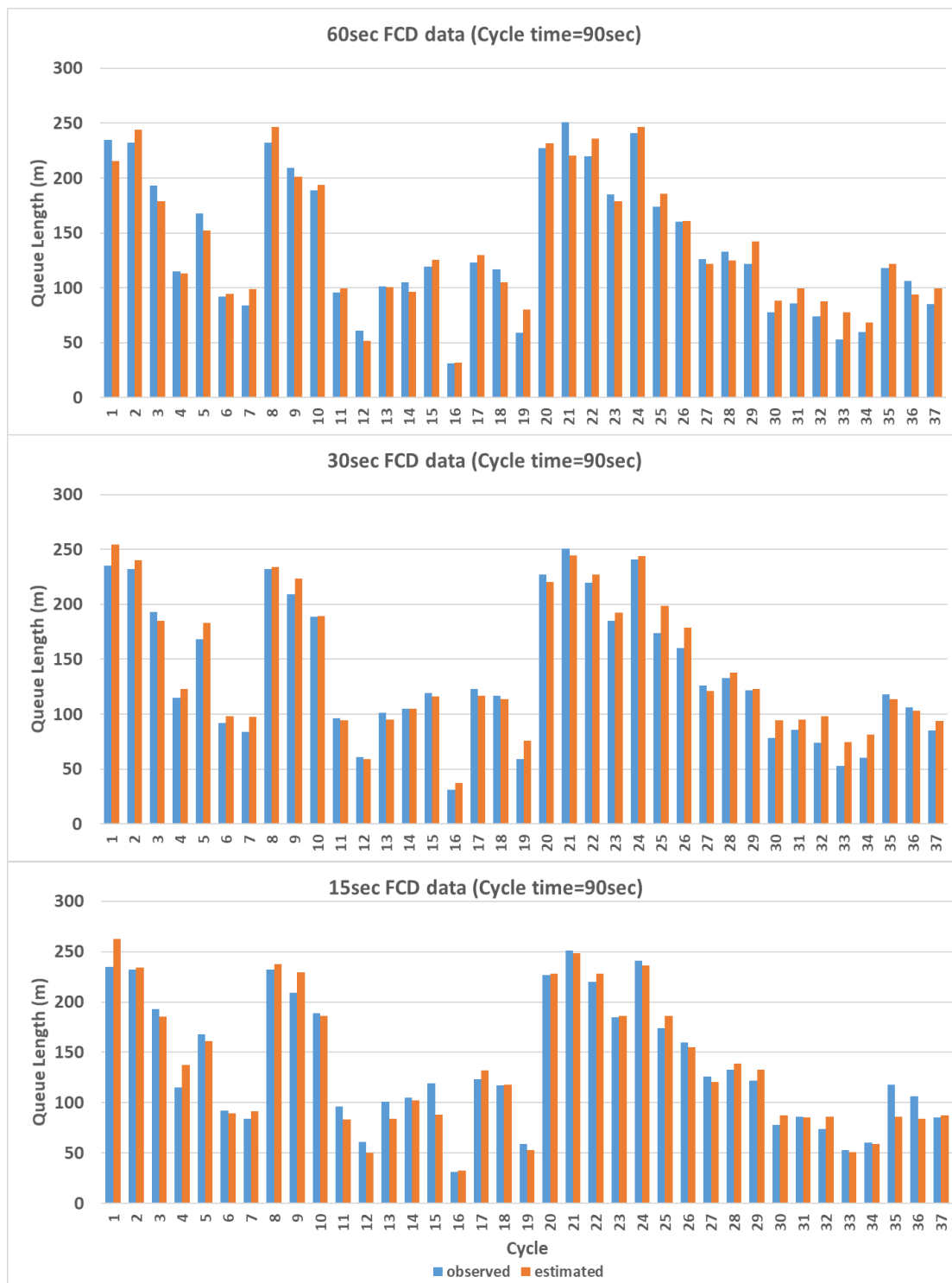


Figure 5.17. Comparison of the cycle based estimated queue lengths with observed ones for C3.

5.2.3. Generalized Relation

For the same test network, in addition to calculation of the v_{opt} and corresponding queue length estimation error for different traffic conditions separately, it could be useful to derive only one v_{opt} value for the test network and evaluate the estimation errors for each condition. To determine generalized v_{opt} for the test network, $SSE_{e,z}$ values obtained from each three condition were summed up to get only one value for a speed threshold value, v_z . Later, plotting the v_z with the $SSE_{e,z}$ provided the speed threshold-error function as shown in Figure 5.18 and v_{opt} value was determined. The overall results are provided in Table 5.4. v_{opt} value was calculated as 33.3 km/h for $\lambda = 60$ sec and produced $MAPE_Q$ and $RMSE_Q$ of 30.6% and 15.7 m for C1, respectively. This showed almost 2% increase in $MAPE_Q$ value and 0.7 m increase in $RMSE_Q$ value when compared the estimation results in Table 5.2. While $MAPE_Q$ value raised from 21.8% to 27.8% for C2, $RMSE_Q$ increased only 2.7 m. On the other hand, slightly increase in errors were observed in C3 that $MAPE_Q$ and $RMSE_Q$ were found as 9.9% and 13.7 m, respectively. v_{opt} was determined as 29.4 km/h and 25.0 km/h for $\lambda = 30$ sec and $\lambda = 15$ sec, respectively and $MAPE_Q$ and $RMSE_Q$ values showed slightly increase and providing acceptable estimation errors as shown in Table 5.4.

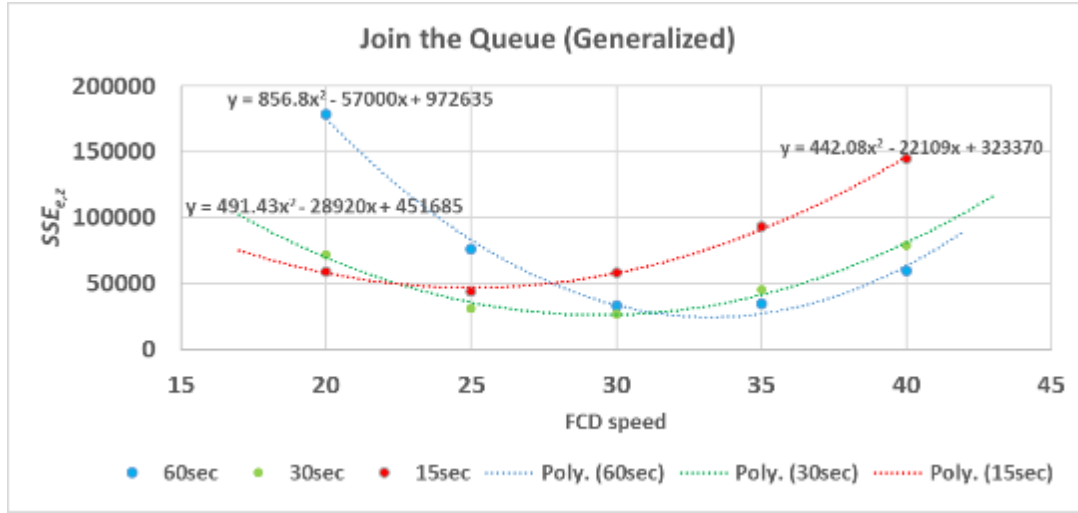


Figure 5.18. Derivation of $SSE_{e,z}$ and V_z function for V_{opt} determination for the test network.

Table 5.4. V_{opt} and corresponding $MAPE_Q$ and $RMSE_Q$ values for different λ values.

λ	V_{opt} (km/h)	C1		C2		C3	
		$MAPE_Q$ (%)	$RMSE_Q$ (m)	$MAPE_Q$ (%)	$RMSE_Q$ (m)	$MAPE_Q$ (%)	$RMSE_Q$ (m)
60 sec	33.3	30.6	15.7	27.8	16.9	9.9	13.7
30 sec	29.4	26.3	15.1	24.2	14.5	9.7	11.8
15 sec	25.0	24.4	13.4	24.3	19.5	9.8	12.4

5.3. Estimating Queue Length with Different Penetration Rates

To test the sensitivity of the model to FCD penetration rate (δ_{FCD}), same network has been rerun by choosing different FCD vehicle penetration in VISSIM simulation considering C2 input values. For this analysis, six different penetration rates were selected as $\delta_{FCD} = \{5\%, 10\%, 15\%, 25\%, 35\% \text{ and } 50\%\}$. However, especially, under low penetration rates, lack of enough probe vehicles over a segment within the selected epoch time caused lack of FCD speeds for some time intervals and segments, and thus, endangered the speed field estimation step. To overcome this problem, for missing FCD speeds, archival values were assigned as mostly done in commercial data processing.

Though it is not possible to know the use and preparation of archival information in commercial FCD speeds, for this study, two alternative archival data sets were prepared such that archival speed values come from either a) a simulation-based archive from 30 VISSIM simulation runs, or b) short term archival data which was average of the last 5 min values at a segment. For the former, VISSIM simulations were generated using the same total demand of 950 veh/h but with different random seeds as

- 6 simulation run with study demand
- 6 simulation run with 10% increase in demand
- 6 simulation run with 15% increase in demand
- 6 simulation run with 10% decrease in demand
- 6 simulation run with 15% decrease in demand

Taking the average of speeds of all simulation runs for every segment s , $s \in S$ provided archival FCD speed value.

5.3.1. Queue Length Estimation Results

Queue length estimation results for different penetration rates are provided in Table 5.5 for both archival data. It was observed that both archival data produced almost same estimation errors expect for $\delta_{FCD}=5\%$. This is mainly due to the effect of the archival data in which archive usage for this penetration was 43.9%. The model estimated the queue lengths with $MAPE_Q$ of 26.3% and $RMSE_Q$ of 17.3 m for $\delta_{FCD}=50\%$, which were slightly higher when compared to full penetration rate results. It means that even 50% penetration rate of FCD vehicles, the model produced promising estimation results.

While the $MAPE_Q$ and $RMSE_Q$ were found as 26.9% and 18.8 m, respectively for $\delta_{FCD} = 35\%$, these values were calculated as 36.5% and 22.2 m for $\delta_{FCD} = 25\%$. For $\delta_{FCD} = 15\%$, $MAPE_Q$ and $RMSE_Q$ values were around 40% and 30 m, respectively but sharp increase in $MAPE_Q$ was observed and reached to 60% when $\delta_{FCD} = 5\%$.

Calculated v_{opt} value was around 31.0 km/h for short term archival data and it did not substantially change with the penetration rate. It was dropped to 28.0 km/h when $\delta_{FCD} = 5\%$. On the other hand, based on the simulation-based archival data, calculated v_{opt} was almost same until $\delta_{FCD} = 15\%$, it was calculated as 24.3 for $\delta_{FCD} = 15\%$ and $\delta_{FCD} = 10\%$. With the lower penetration rate slightly lower v_{opt} was calculated as 23.2 km/h. In addition to the numerical results, Figure 5.19 and Figure 5.20 illustrate the thematic speed maps for different penetration rates with optimum iso-speed contours for simulation-based and short term archival data sets, respectively.

Table 5.5. Performance evaluation and v_{opt} values under different penetration rate of FCD.

δ_{FCD} (%)	Archive usage (%)	From simulation-based archival data			From short term archival data		
		v_{opt} (km/h)	$MAPE_Q$ (%)	$RMSE_Q$ (m)	v_{opt}	$MAPE_Q$ (%)	$RMSE_Q$ (m)
100	-	30.8	21.8	14.2	30.8	21.8	14.2
50	0.9	30.8	27.1	17.8	31.0	26.3	17.3
35	1.3	31.2	27.8	18.6	31.0	26.9	18.8
25	4.0	31.5	36.5	22.1	31.5	36.5	22.2
15	16.7	24.3	42.8	30.8	30.5	40.3	30.2
10	23.1	24.3	49.4	32.2	31.1	46.9	32.4
5	43.9	23.2	59.1	39.9	28.0	67.2	47.6

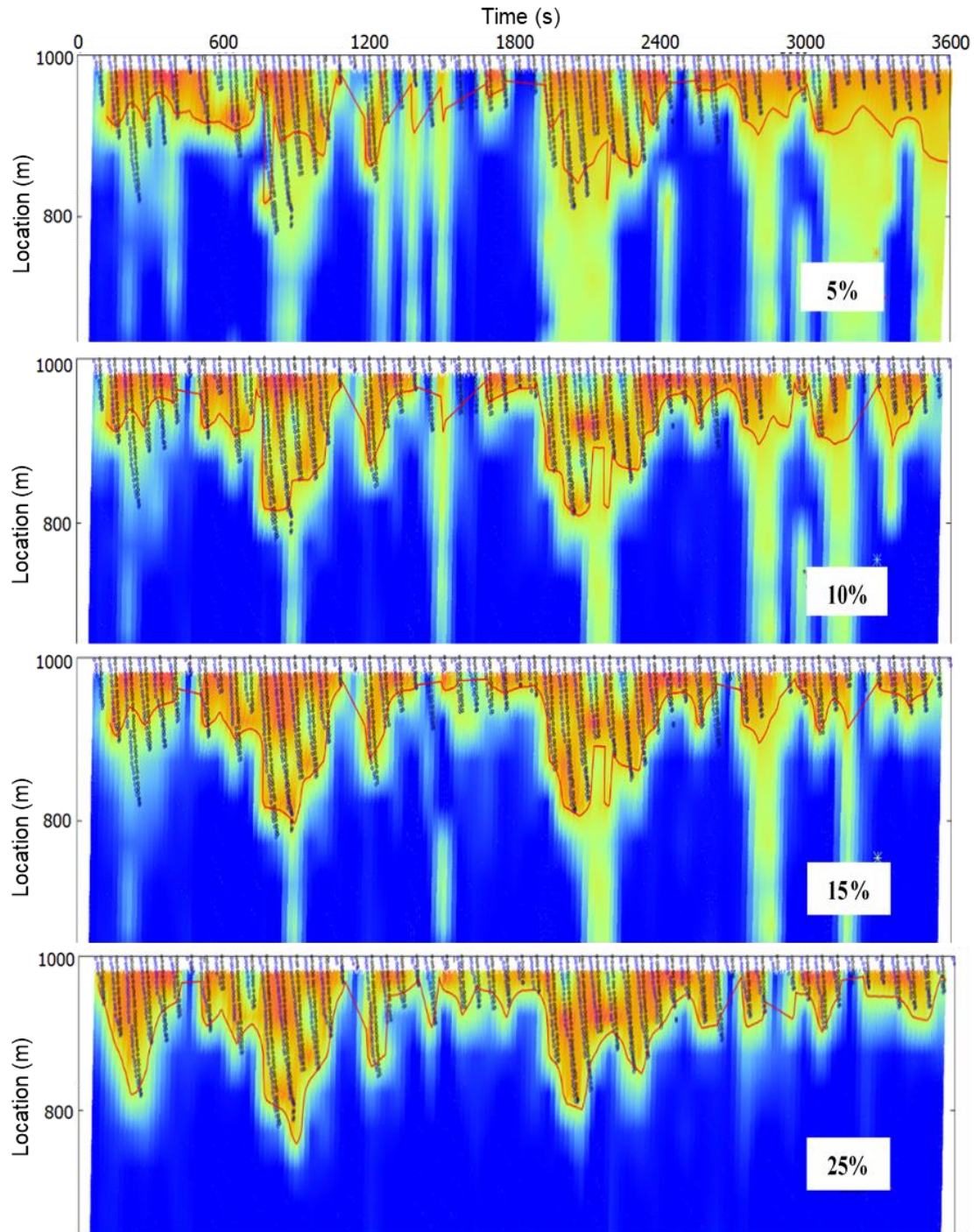


Figure 5.19. Queue length estimation result with different FCD vehicle penetration rate for simulation-based archival data.

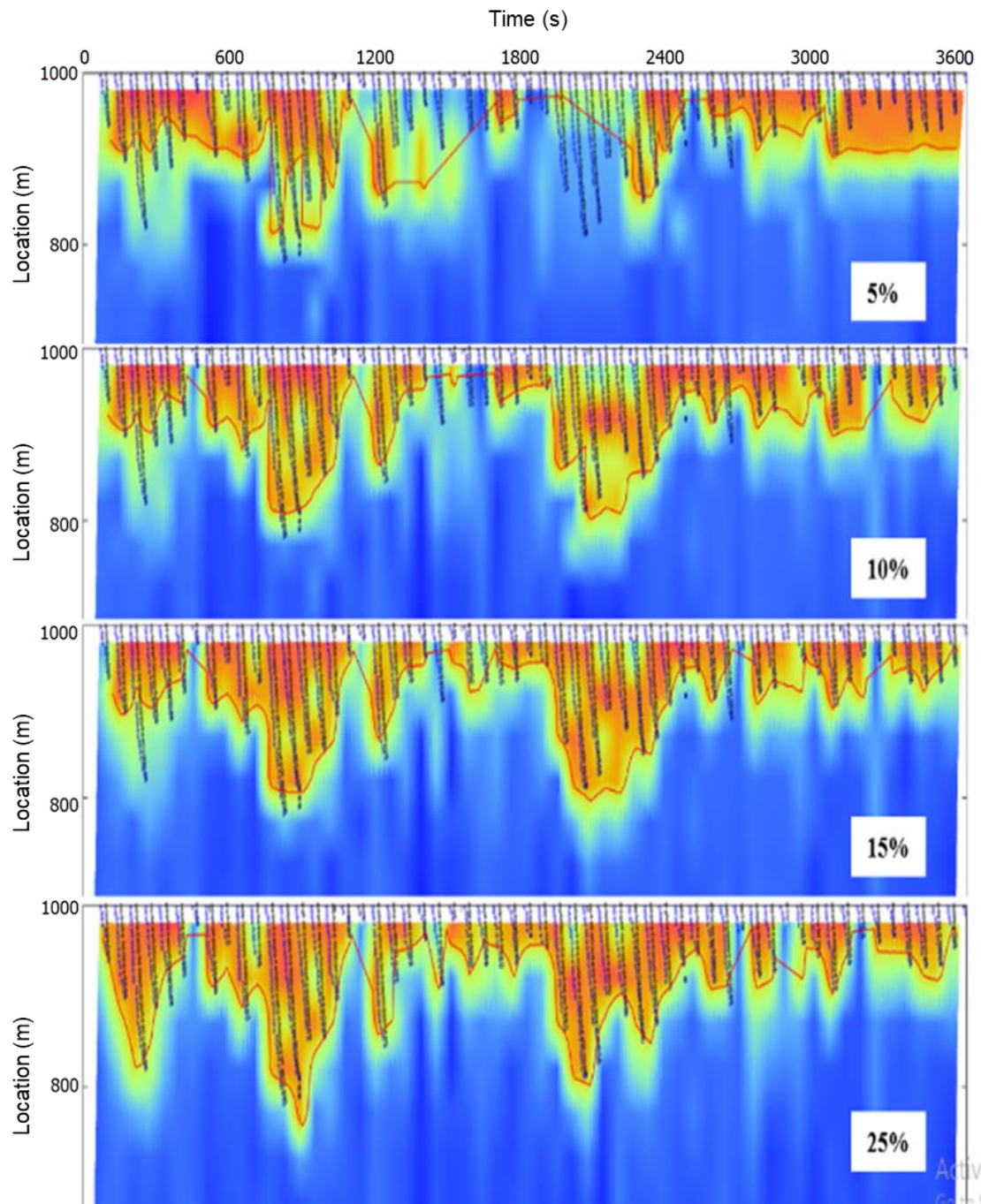


Figure 5.20. Queue length estimation result with different FCD vehicle penetration rate for short term archival data.

CHAPTER 6

QUEUE LENGTH ESTIMATION WITH COMMERCIAL FCD

In addition to the simulation-based study, the proposed model was also applied to commercial FCD speed data for two study corridors described in Chapter 3. In this section, current potential of commercial FCD for queue length estimation was discussed for signalized intersection and uninterrupted urban arterial.

6.1. Queue Length Estimation at Signalized Intersection

The model performance for queue length estimation in commercial FCD was tested in two approaches of the two consecutive intersections (see Figure 3.4) as described in Section 3.3. FCD speeds were provided for 8 segments with various segment lengths as shown in Table A.2. While considering the Approach 1 of the Int 1, 4-node quadratic interpolation method was implemented to FCD speed data which resulted in thematic speed map during 17:15 to 17:26 on November 30, 2017. Joint representation of lane-based actual queue lengths with thematic speed maps is illustrated in Figure 6.1a. During the analysis period, the intersection was oversaturated for all cycles in which the average queue lengths extended to almost 210 m far from the stop line location.

To determine the v_{QL} for queue length estimation, different speed thresholds were selected and iso-speed contours were trying to draw during the analysis period. Selected speed thresholds were 15 km/h, 20 km/h, 25 km/h and 30 km/h for this approach. However, it was difficult to draw iso-speed contours for some v_z values (see Figure 6.1b) since multiple queue front locations could be detected for the selected v_z for the same imaginary vehicles. For example, many iso-speed contour

can be drawn when v_z was 15 km/h. However, drawing all possible iso-speed contours for this v_z could not represent the maximum queue locations as shown in Figure 6.1b. When $v_z=30$ km/h, it was not appropriate to draw iso-speed contour because it did not clearly represent the maximum queue locations as well. On the other hand, iso-speed contour of 20 km/h and 25 km/h seemed to be best fit for the study case and provided to draw continuous iso-speed contour near the maximum queue locations. Even more deviations were observed for the second and third cycles, drawing 25 km/h iso-speed contour estimated the maximum queue location of the remaining cycles. Thus, v_{QL} for this approach can be selected either 20 km/h or 25 km/h in which queue length estimation errors are provided in Table 6.1. Estimated queue lengths for six cycles produced $MAPE_Q$ and $RMSE_Q$ of 7.68% and 23.21 m, respectively when v_{QL} was selected as 20 km/h. On the other hand, selection of v_{QL} as 25 km/h resulted in increase of $MAPE_Q$ to 16.41% and $RMSE_Q$ to 36.33 m.

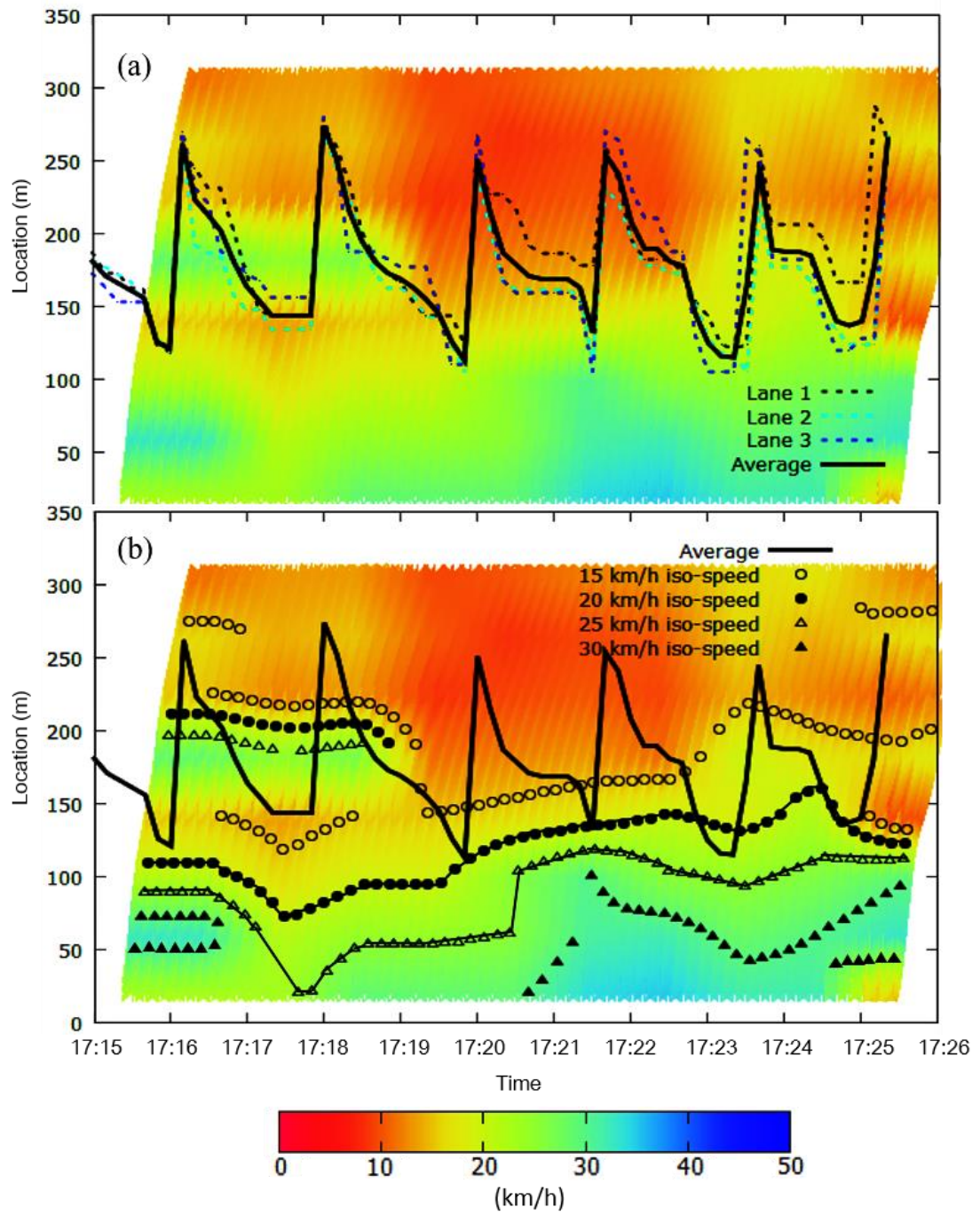


Figure 6.1. a) Observed queue lengths with thematic speed map, b) observed average queue lengths with iso-speed contours for Approach 1.

Table 6.1. $MAPE_Q$ and $RMSE_Q$ of estimated queue lengths for different v_{opt} values for Approach 1.

Cycle #	Observed Queue Length	Estimated Queue Length (m)	
		$v_{QL} = 20$ km/h	$v_{QL} = 25$ km/h
1	207.2	218.1	167.8
2	183.5	236.2	228.5
3	215.0	217.7	271.6
4	195.6	193.3	209.2
5	213.3	195.4	232.0
6	191.1	193.6	215.9
$MAPE_Q$		7.68%	16.41%
$RMSE_Q$		23.21 m	36.33 m

To gain further insights about v_{QL} , a longer duration beyond the control dataset can be selected at the full peak hour of 17:00-18:00 for the same day. The ground truth data collection time was also indicated in broken lines as shown in Figure 6.2. It can be clearly observed that selection of v_{QL} as 15 km/h could not provide the consistent queue length profile between 17:00 to 17:30 in which the approach was oversaturated in this time interval (see Figure 6.2a). However, after 17:30, it provided a consistent queue length profile until the end of the analysis period. The growing of the queues could be clearly captured from 17:05 to 17:17 by either selecting v_{QL} of 20 km/h or 25 km/h. At time 17:17 queue lengths were extended to 258 m far from the intersection stop line (70 m far from the initial segment in Figure 6.2b) when v_{QL} was 20 km/h. At time 17:11-17:19, v_{QL} of 20 km/h estimated two possible queue lengths in which some part of the this time interval was also fall into the ground truth data collection time interval as shown in Figure 6.1b. This situation may be due to the stop and move traffic in that time interval or the noises as well as the low penetration rate of FCD. It was also proved in Figure 6.1b that the possible queue length could be the farthestmost location from the stop line of the intersection. Similar situation was also observed at time interval 17:26-17:30 in Figure 6.2b. Queue lengths were gradually decreased after 17:30 remained almost constant at time 17:45 to 17:55.

Selection of v_{QL} as 25 km/h provided smooth queue length estimation profile in general (see Figure 6.3a). Multiple queue lengths was also observed at time interval 17:11-17:19. On the other hand, selection of v_{QL} as 30 km/h did not provide the queue length estimation profile. Instead, it provided the border between the low speed zones and higher speed zones as shown in Figure 6.3b.

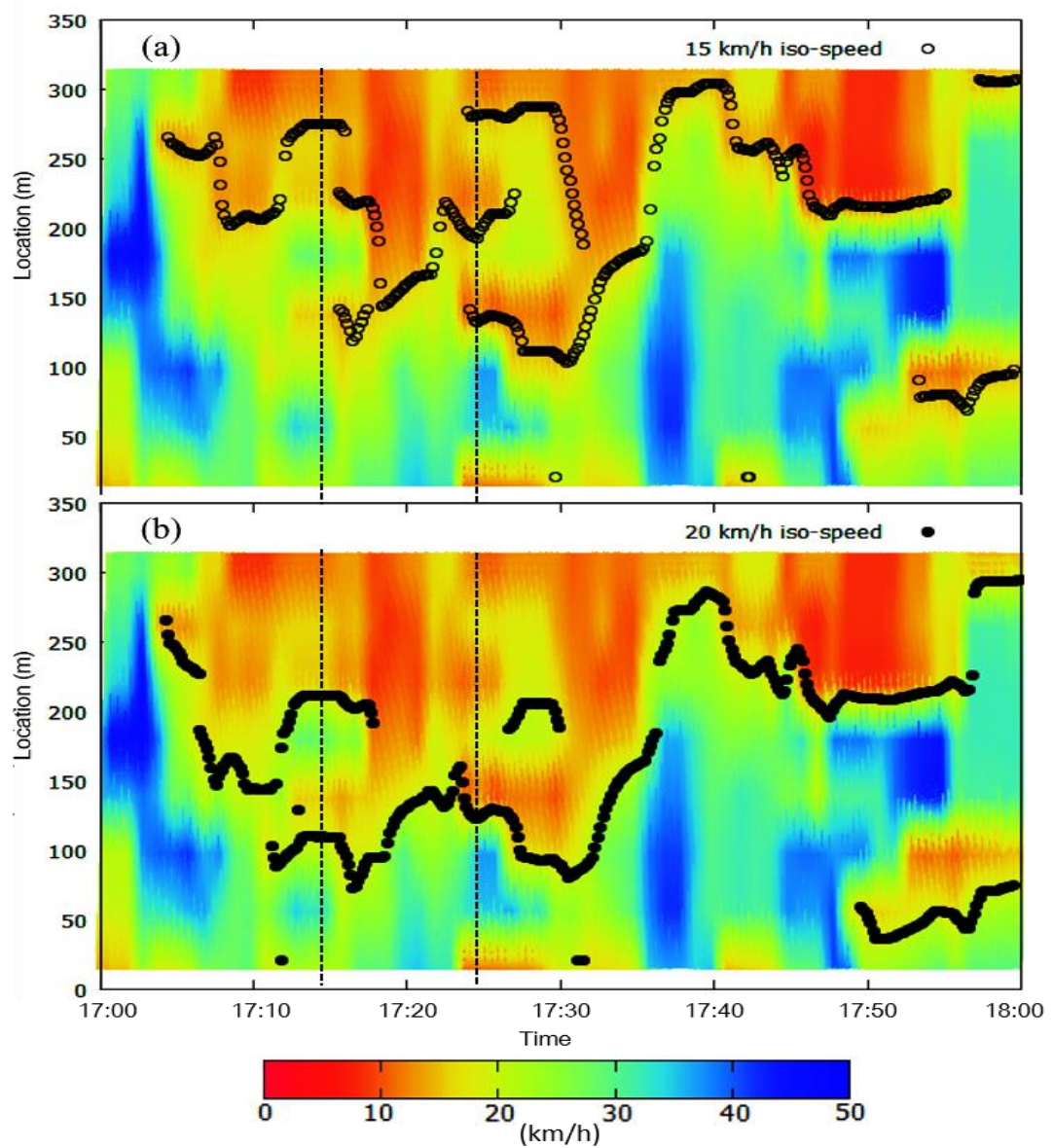


Figure 6.2. Thematic speed map of Approach 1 with a) $v_{QL} = 15$ km/h, b) $v_{QL} = 20$ km/h.

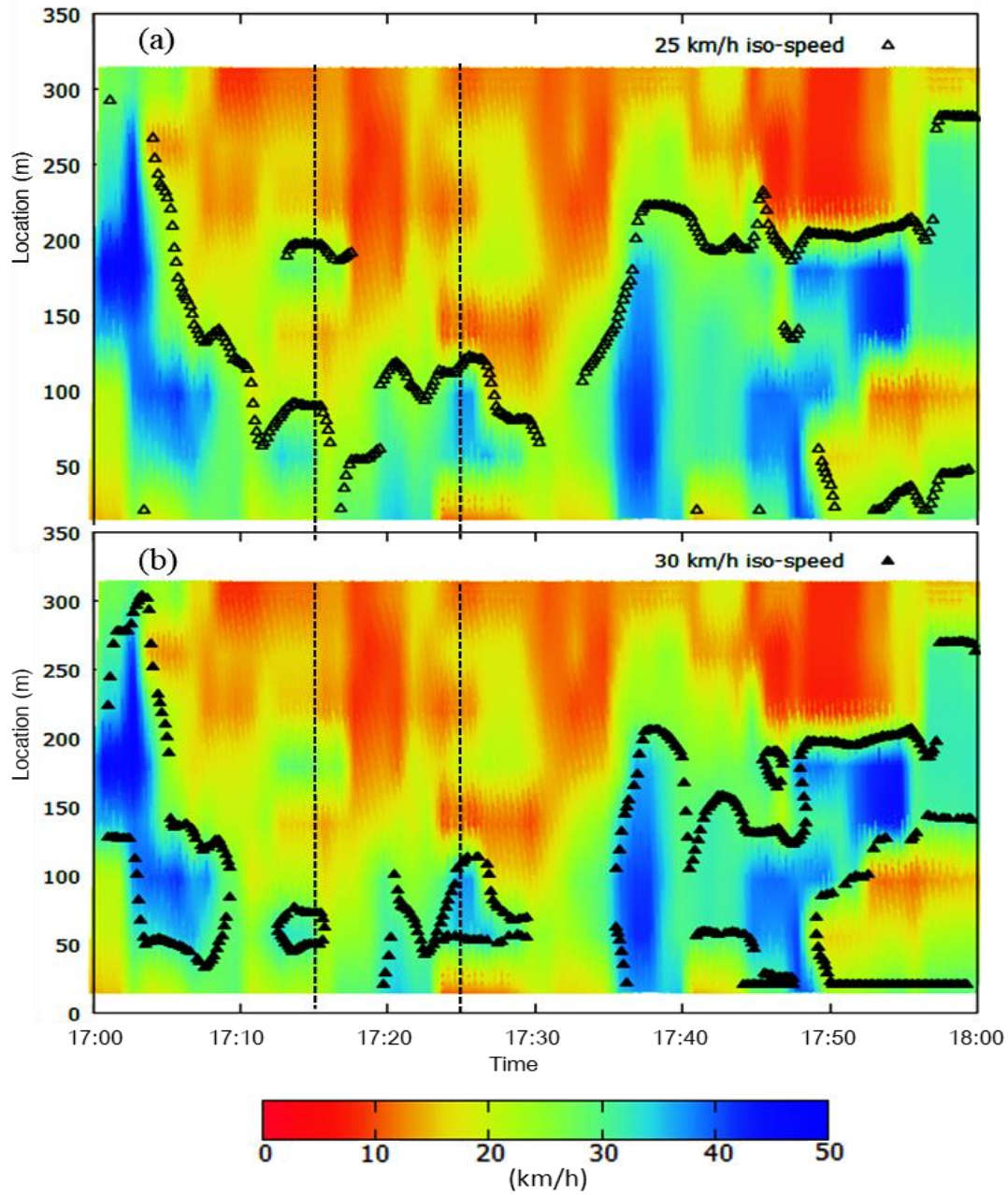


Figure 6.3. Thematic speed map of Approach 1 with a) $v_{QL} = 25$ km/h, b) $v_{QL} = 30$ km/h.

Approach 2

For Approach 2 of the Int 2 (see Figure 3.4), thematic speed map of the FCD speeds with the observed queue lengths is illustrated in Figure 6.4a. The effect of the low penetration rate in the dataset was clearly observed in this approach. For example,

while the observed queue lengths were extended to almost 110 m far from the stop line in cycles 2 and 3 at between 17:17 and 17:20, FCD speed could not reflect the real situation. This approach was not as oversaturated as the previous one in which the average queue lengths were ranging from 75 m to 125 m. (Note: There was a systematic error in the farthestmost segment from the stop line of the intersection, Segment ID “1212701”, FCD speed was not published for this segment, so the approach length was around 284 m.)

Due to the undersaturated traffic condition, multiple queue front location was not captured during the analysis period and it could be possible to draw only one continuous iso-speed contour for all selected v_z as shown in Figure 6.4b. In the light of the determined v_{QL} values for the previous approach, calculation of queue length estimation errors for the same v_{QL} values also produced promising results as tabulated in Table 6.2. When $v_{QL}=20$ km/h, $MAPE_Q$ and $RMSE_Q$ were found as 19.45% and 27.77 m, respectively. On the other hand, selection of v_{QL} as 25 km/h resulted in almost 3% decrease in $MAPE_Q$ and 6.58 m decrease in $RMSE_Q$ value (see Table 6.2).

Similar to Approach 1, queue length profiles were further examined for the peak hour of 17.00-18.00. For each v_{QL} value, queue length profiles were depicted over time as shown in Figure 6.5. While v_{QL} of 15 km/h provided inconsistent queue length profile at time 17:00-17:15, queue growing and dissipation profile can be observed for the remaining time intervals (see Figure 6.5a). This may be mainly due to the undersaturated condition of the approach in this time interval since it did not provide reliable queue length profile when the approach was oversaturated (see Figure 6.2a). When v_{QL} was selected as 20 km/h, it presented consistent queue length profile over time in general but multiple queue front locations were detected at time 17:34-17:36 (see Figure 6.5b). As discussed, this may be due to the queue growing and dissipation

process or the noises in FCD. Similar profile was also observed when v_{QL} was 25 km/h (see Figure 6.5c). Finally, Figure 6.5d represents the queue length profile of 30 km/h, but as it is discussed previously, this value was generally not represent the queue lengths, instead distinguished between the high regimes from slow ones.

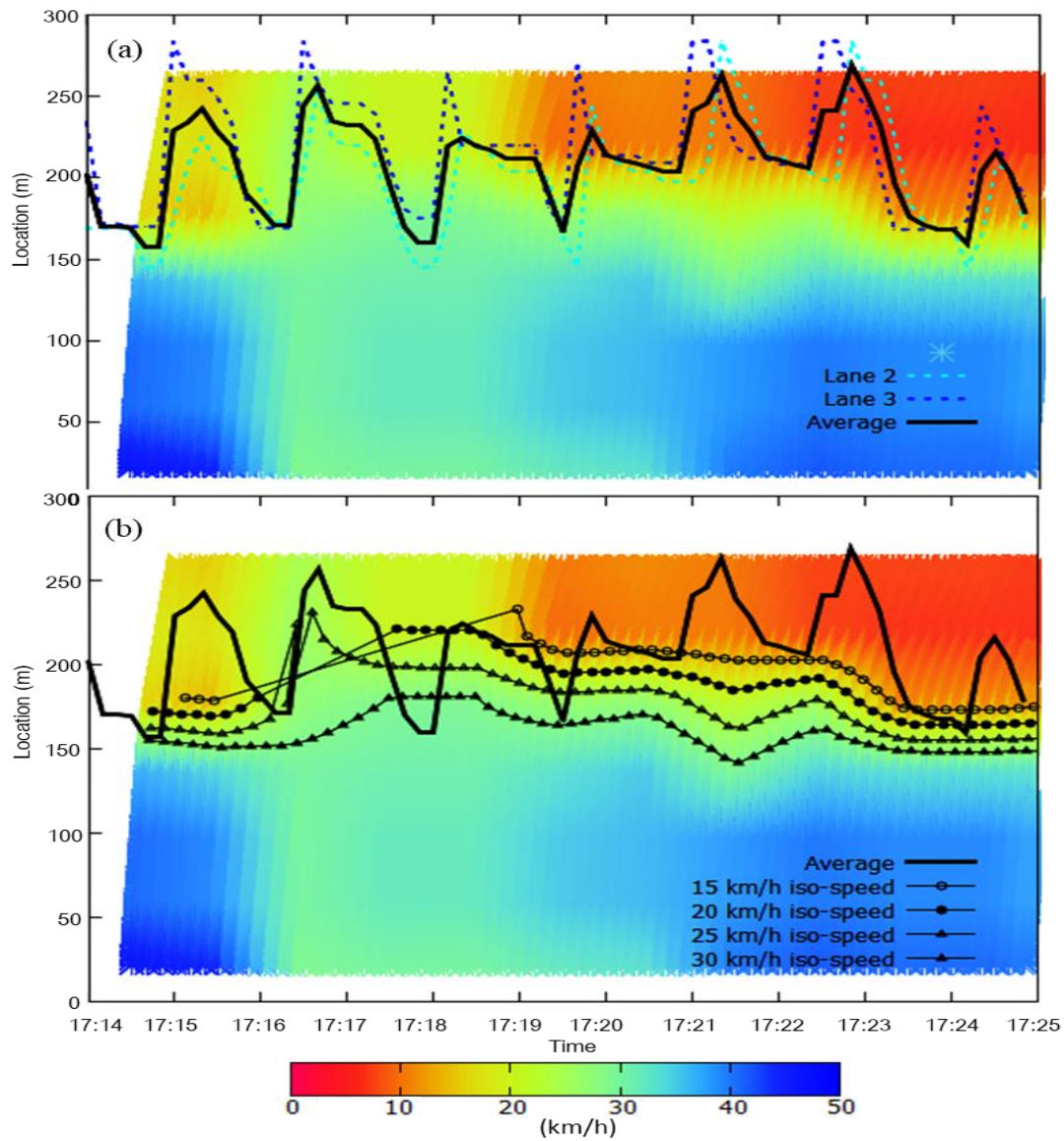


Figure 6.4. a) Observed queue lengths with thematic speed map, b) observed average queue lengths with iso-speed contours for Approach 2.

Table 6.2. $MAPE_Q$ and $RMSE_Q$ of estimated queue lengths for different v_{opt} values for Approach 2.

Cycle #	Observed	Estimated Queue Length (m)	
		$v_{QL}=20$ km/h	$v_{QL}=25$ km/h
1	126.5	112.1	121.6
2	113.0	94.0	113.1
3	124.0	63.2	85.4
4	117.5	89.2	100.3
5	80.5	89.9	103.3
6	78.0	92.9	106.2
7	124.5	119.5	128.7
$MAPE_Q$		19.45%	16.80%
$RMSE_Q$		27.77 m	21.19 m

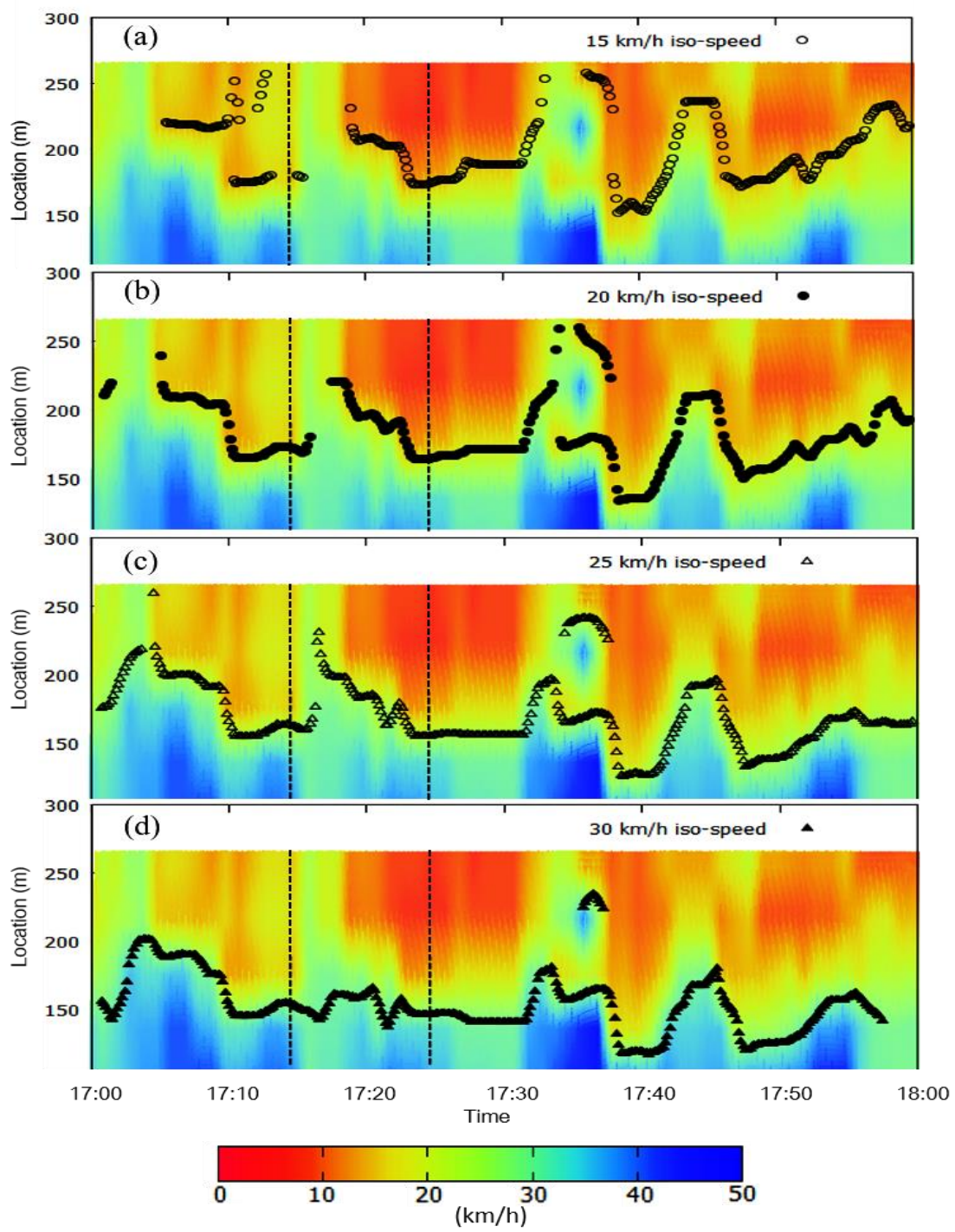


Figure 6.5. Thematic speed map of Approach 2 with a) $v_{QL} = 15$ km/h, b) $v_{QL} = 20$ km/h, c) $v_{QL} = 25$ km/h, and d) $v_{QL} = 30$ km/h.

6.2. Queue Length Estimation on Dumlupınar Boulevard

Queue length estimation of the study corridor was performed during two study days, October 21, 2016 and October 25, 2016 in which the GT data was also available as discussed in Section 3.2.1. Analysis period only includes the morning peak hours between 07:30-09:00 to examine the queue lengths around bottleneck locations.

4-node quadratic interpolation method was applied to FCD speed data for 82 segments (see Figure 3.2 for the study corridor and Table A.1 for the segment lengths) in which imaginary vehicles were sent from the first segment of the study corridor for every 10 sec. Speed field estimation provided the thematic speed map which gave insight about the potential bottleneck locations as shown in Figure 6.6 and Figure 6.7, respectively. Three bottleneck locations were detected in which major bottleneck location was around Segment 72 (in J2 with 3293 m far from the initial segment). Second bottleneck location was at Segment 48 (at 2200 m in Figure 6.6) and final bottleneck location was around J1. The speed field estimation of the corridor also produced similar results with the LOS-based urban traffic monitoring discussed in Section 3.4.4 (see Figure 3.11). Among these bottleneck locations, long queues from the upstream of the Segment 72 were observed for the both study days and queue length analysis only focused on only around this location.

Queue join locations were determined by selecting two v_{QL} values as 27.0 km/h and 42 km/h as discussed in Section 4.2. When v_{QL} was selected as 27.0 km/h, the border of the queue growing profile was observable at between 07:30 and 08:00 (see Figure 6.6a). After this time, multiple queue join locations were detected at some locations; representing stop and move traffic before reaching to bottleneck release location. Effect of the bottleneck location caused to extend the queue lengths up to 1600 m far from the bottleneck location at time 08:10 (see Figure 6.7a). Queue lengths were gradually decreased after 08:15 and almost dissipated at time 08:40. On the other hand,

selection of v_{QL} as 42 km/h provided more smooth queue growing and dissipation profile as shown in Figure 6.6b. Queue lengths started to increase at 07:30 and reached to 1800 m at time 08:15 (see Figure 6.7a). Queue lengths were almost constant between 08:15-08:30 and then gradually decreased.

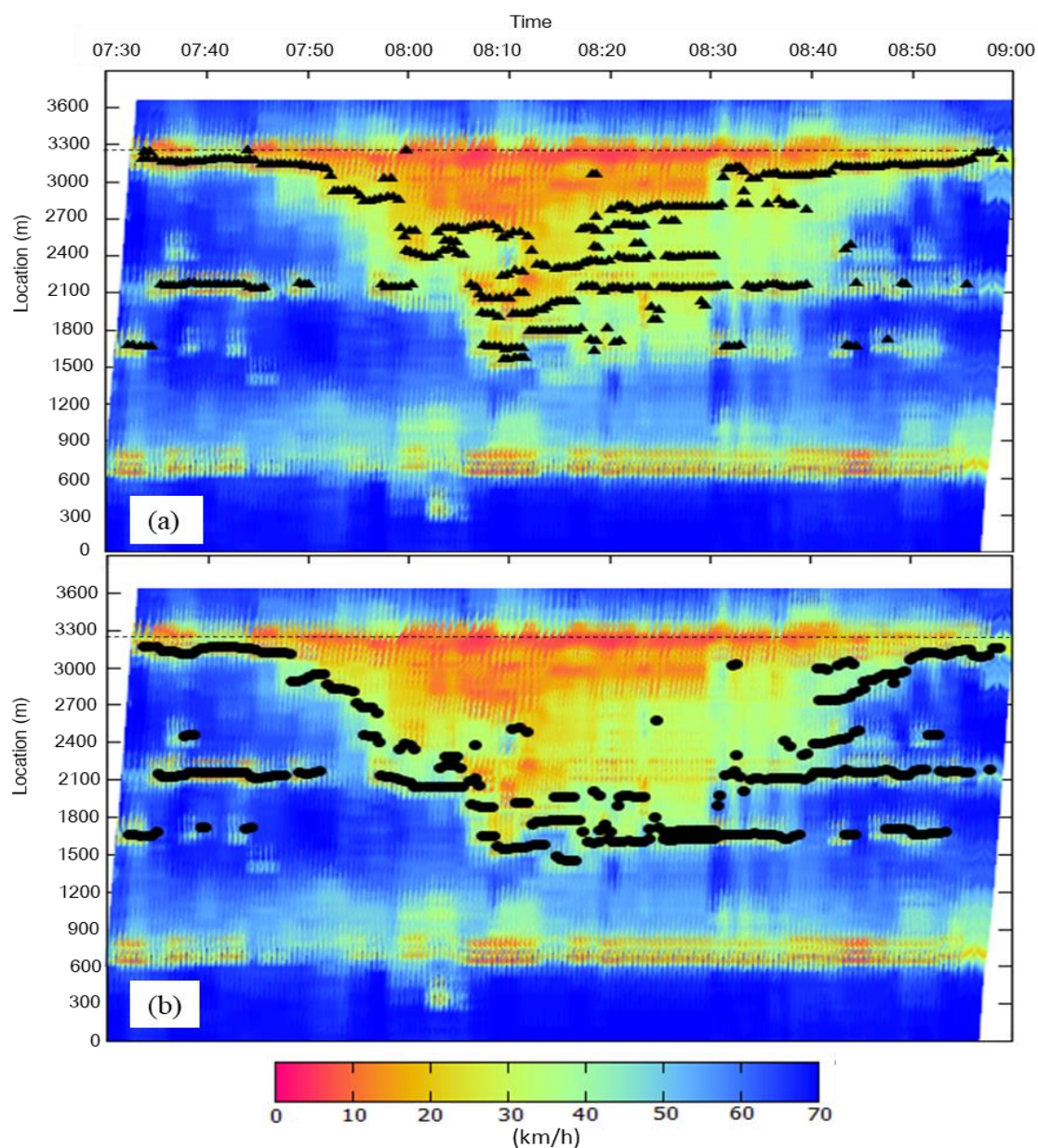


Figure 6.6. Thematic speed map obtained from commercial FCD speed data with a) $v_{QL} = 27$ km/h, b) $v_{QL} = 42$ km/h for queue length estimation on October 21, 2017.

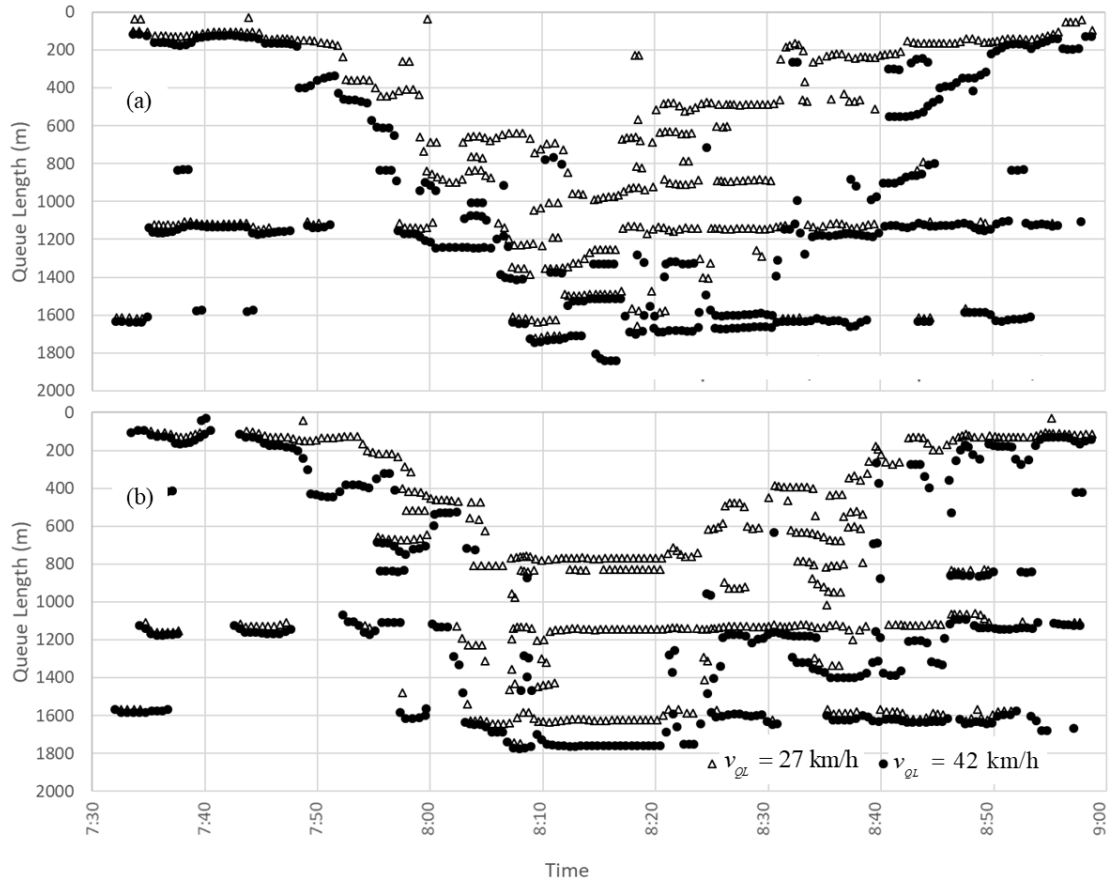


Figure 6.7. Estimated queue lengths for two different v_{QL} values for Dumlupınar Blvd. on a) October 21, 2017, b) October 25, 2017.

Queue length profile of the second day also provided the border of the queue growing and dissipation profile when v_{QL} was 27 km/h (see Figure 6.8a). Queue lengths were started to increase after 07:45 and reached to maximum queue location at 08:05 suggesting 800 m in length (see Figure 6.7b). Among 08:05-08:25, queue lengths remained constant and then gradually decreased. Stop and move traffic was also more observable during 08:00-08:25, but selection of v_{QL} as 42 km/h, eliminated many of them and suggesting maximum queue length of 1800 m from the upstream of the bottleneck location (see Figure 8.b). In overall, during the analysis period, queue length profile of the second day is illustrated in Figure 6.7b.

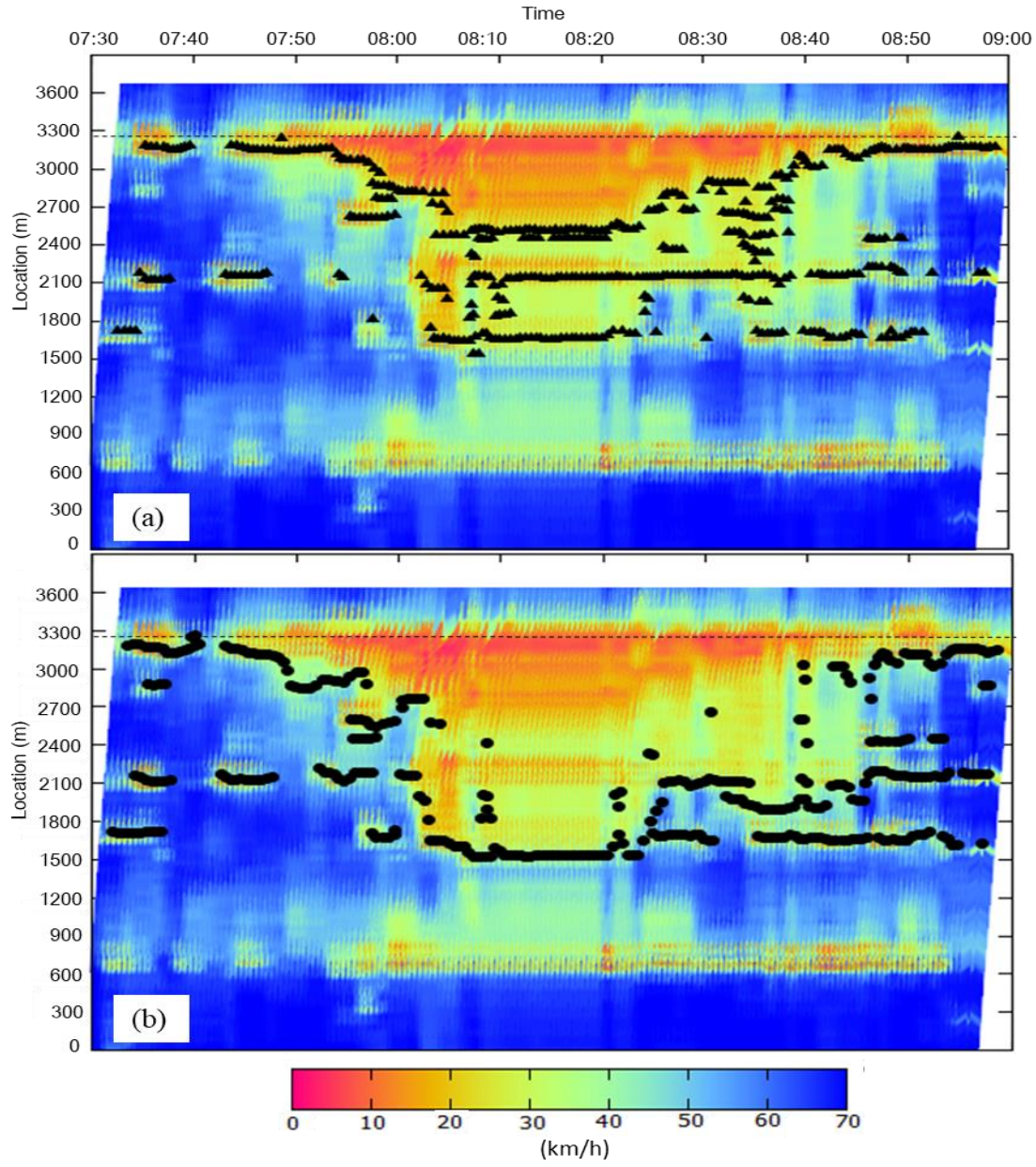


Figure 6.8. Thematic speed map obtained from commercial FCD speed data with a) $v_{QL} = 27$ km/h, b) $v_{QL} = 42$ km/h for queue length estimation on October 25, 2017.

To determine appropriate v_{QL} for FCD, lane-based individual vehicle travel speeds obtained for control Segment 57 were utilized. For GT data, queued vehicles were determined by 27 km/h speed threshold limit. In other words, a vehicle speed lower than that value assumed as in the queue. For the same segment, imaginary vehicle speeds generated from 4-node quadratic interpolation method was derived and imaginary queued vehicles were identified for the two v_{QL} values, separately and compared with the GT data. To provide a continuity, thematic speed map of the Segments 56, 57 and 58 were derived for October 25, 2016 during 07:45-08:45 as shown in Figure 6.9a. Lane-based vehicular speed maps for the same time interval are illustrated in Figures 6.9b, 6.9c and 6.9d for lane 1, lane 2 and lane 3, respectively. Joint representation of the queued vehicles for each lanes as well as the imaginary queued vehicles are illustrated in Figure 6.9e. The x-axis represents the time and y-axis includes dummy variable to clearly compare the queued vehicles with the imaginary ones. The results indicated that almost all observed vehicles were in the queue during 07:53-08:39, but selection of v_{opt} as 27 km/h estimated the queued vehicles only at some points and had limited success. However, selection of v_{opt} as 42 km/h provided better estimation results except the time interval of 07:50-07:54 as shown in Figure 6.9e. This is mainly due to the late response of FCD speed for the sudden speed change as discussed previously.

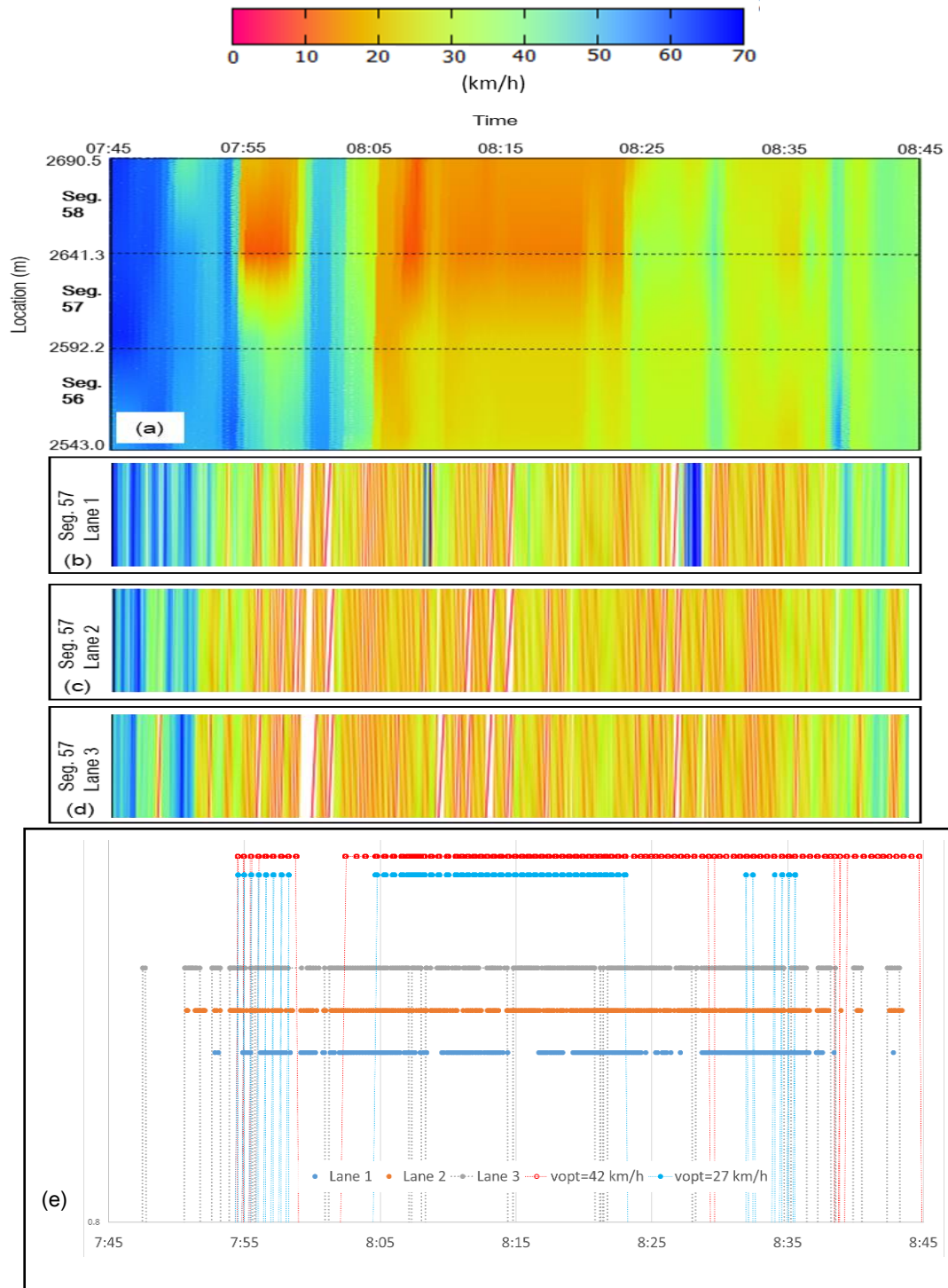


Figure 6.9. Thematic speed map of a) Segments 56, 57 and 58, b) lane 1, c) lane 2, d) lane 3, e) comparison of lane-based queued vehicles with imaginary queued vehicle for different v_{QL} .

6.3. Generalization of Queue Length Estimation for Study Corridor

For uninterrupted flow condition, selection of v_{QL} is based on the determination of the severely congested state defined in HCM (2010). Based on the target speed of the study corridor, one-third of it would provide the possible queue join threshold speed. However, it is very crucial to estimate the corresponding FCD speed since the current quality of commercial FCD indicated that it overestimated the speeds under congested period. For this purpose, the GT speed data were utilized to derive analytical relation between two. For this study, after implementation of the transformation function, v_{QL} value was determined as 42 km/h and provided promising queue length estimation result.

When considering v_{QL} for the signalized intersections, while v_{QL} of 20 km/h produced less estimation error for the Approach 1 of the study corridor, v_{QL} of 25 km/h generated lower estimation error for the other approach. However, all two v_{QL} values produced tolerable estimation errors. Thus, it could be possible to select only one v_{QL} for the study case either 20 km/h or 25 km/h. Alternatively, it could be possible to estimate queue length profile by drawing iso-speed contours starting from 20 km/h and increasing speed threshold value by 1 km/h up to speed threshold value of 25 km/h. Thus, for every 1 km/h, iso-speed contours can be drawn which provided possible queue length profile, indicating formation and dissipation of the queue lengths of the approaches during analysis period as shown in Figure 6.10. For Approach 1, while v_{QL} of 20 km/h estimated the queue length as 182 m at time 17:20, v_{QL} of 21 km/h, 22 km/h, 23 km/h, 24 km/h and 25 km/h estimated the queue length as 184 m, 187m, 191 m, 195 m and 199 m, respectively at the same time. Thus, taking the average of these provided average queue length, and implementing the same procedure during the analysis period provided the average queue length profile over time which was the generalized queue length profile as shown in Figure 6.10.

However, the results indicated that at some locations selected v_{QL} estimated the queue lengths at multiple locations. For example, during 17:12-17:18 all v_{QL} 's estimated the queue lengths at two locations that this can be due to the noises in the dataset or there was multiple queue formation and dissipation at this time interval. Without information of the GT data, it could not possible to decide in which queue length was the accurate one. Hence, the average queue length profile was much more deviated from the expected location as shown in Figure 6.10. Same situation was also observable for the Approach 2 during 17:35-17:38.

Average queue length profile of the analysis period revealed that:

- For Approach 1, queue lengths were gradually increased and reached to 175 m at time 17:10. The approach was oversaturated during 17:10-17:30 in which the queue lengths were generally in between 175 m to 250 m. After 17:30, queue lengths were gradually decreased, the approach becomes undersaturated traffic condition at time 17:40 in which the queue lengths were ranged in 50 m to 100 m.
- For Approach 2, queue lengths were generally in between 60 m to 120 m during 17:10 to 17:30, and the maximum value was achieved at time 17:40 with 150 m. During the analysis period, the approach was undersaturated in general.

It should be noted that at some locations, iso-speed contours were intersected each other which was drawn by broken lines in Figure 6.10. For example, at time 17:12, iso-speed contour of 22 km/h coincided with iso-speed contour of 24 km/h and 25 km/h for Approach 1. This is mainly due to the fact that, during 17:11-17:16, imaginary vehicle speeds were not dropped to 22 km/h at this time interval. Similar situation was also observed for 23 km/h iso-speed contour for the same time interval.

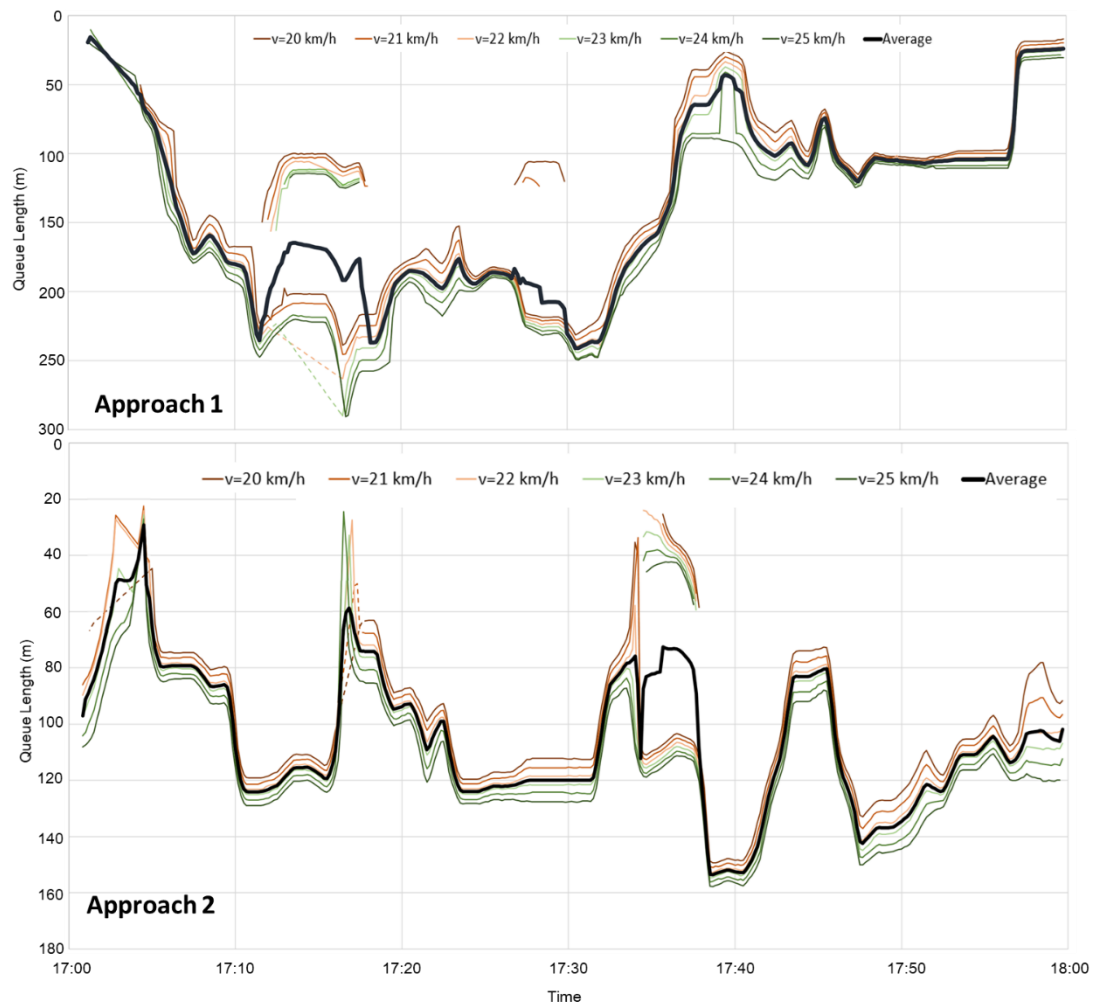


Figure 6.10. Generalized queue length profile obtained from different speed thresholds for Approach 1 and 2.

CHAPTER 7

CONCLUSIONS AND FURTHER RECOMMENDATIONS

In this chapter, general overview and conclusions of this thesis is summarized and followed by the further recommendations.

7.1. General Overview and Conclusions

Traditional methods to estimate the queue lengths are input-output models and LWR shock wave model which require perfect arrival traffic flow data. This data is commonly provided by the sensors such as loop detectors. Although loop detectors enable high quality traffic data, the vehicles are detected only at certain locations. Furthermore, cost of installation and operation of this sensor make it harder to locate everywhere for urban arterials with complex network and queue formation structures. On the other hand, since vehicle-to-vehicle and vehicle-to-infrastructure communication technologies are growing, the traffic data obtained from GPS equipped vehicles, namely FCD, provides new horizon to develop methods to estimate the queue lengths. When compared to other traffic data sources, FCD is a relatively cheap traffic data source with high coverage area, which can carry spatio-temporal speed information over long urban corridors in real-time. The increasing availability of GPS-equipped vehicles in traffic will keep FCD as an important traffic data source in the near future in which the current penetration rate of FCD was in between 1% to 5% in Ankara.

This thesis focuses on developing a new model to estimate queue length via commercial FCD speed. Without information of arrival traffic flow rate, signal timing data or queue related characteristics, the model only requires FCD speed as input. The methodology was mainly based on the determination of the speed threshold value providing the minimum queue length estimation error. Implementation of 4-node

quadratic interpolation provided the speed field estimation as well as the imaginary vehicle trajectory data in which these would later be used to identify the potential bottleneck locations. After identification of the bottleneck locations, selecting appropriate speed threshold and identifying queue join location of the imaginary vehicles based on this speed threshold value would give insight about the spatio-temporal formation and dissipation of the queue length over time.

The proposed model was tested in three different cases as

- VISSIM simulation environment by creating a hypothetical signalized intersection,
- two approaches of the two urban signalized intersections, and
- uninterrupted urban arterial located in Ankara.

In simulation-based analysis, model performance was evaluated for various traffic demands and signal cycle times considering undersaturated and oversaturated traffic condition. For all cases, the model produced tolerable queue length estimation errors for all scenarios that $RMSE_Q$ was in a range of 13 m-16 m. Furthermore, the overall analysis revealed that 5 km/h speed threshold assumption for joining the queue is not valid for FCD since it encompasses the average speeds of both moving and stopping vehicles for the selected epoch time. Thus, for the epoch time of 60 sec, a signalized intersection with 70 km/h design speed, optimum speed value depicting the queue length was around 30 km/h. Further evaluation of different epoch times (15 sec and 30 sec) of FCD speeds also enabled to give insight of the sensitivity of FCD precision in the future FCD formats. Smaller epoch time of FCD speed allowed prediction of the queue dynamics more precisely; however, estimation errors were not found to be significant. The only significant difference was in the optimum speed threshold value in which the lower epoch time produced lower optimum speed threshold value. Additionally, the model performance was tested under different FCD penetration rates, suggesting $RMSE_Q$ of 30 m at even 15% penetration rate seems to be acceptable.

Implementation of the proposed model to commercial FCD speed had also great success in estimating queue lengths when compared to observed ones for urban signalized intersection case. Even for the noises in the commercial FCD speed, v_{QL} of 20 km/h and 25 km/h provided reasonable queue length estimation errors ranging from 7.68% to 19.45% in $MAPE_Q$ values and 21.19 m to 36.33 m in $RMSE_Q$ values. Hence any of which can be selected as the v_{QL} of the signalized intersection. Alternatively, to generalize the methodology to signalized corridors, multiple v_{QL} 's can be selected, and taking the average of the queue lengths obtained from each v_{QL} at a given time, and repeat the same procedure during the analysis period provides the generalized average queue length profile of the study corridor.

Queue length profiles of some of the v_{QL} showed that multiple queues can be detected behind a bottleneck location at the same time. This can be explained by either due to the low penetration and noise in FCD speed or multiple queue growing and dissipation occurring simultaneously. In that case, without support of GT data, it is not easy to decide which one is the real queue length or whether there is unstable flow condition causing multiple queue formations. Another critical issue is that as commercial FCD is processed data, low penetration of FCD may generate bigger estimation errors. For this reason, GT data should be collected at certain intervals to evaluate FCD quality and to calibrate the v_{QL} value.

For the third case, implementation of the method to an uninterrupted urban arterial provided to detect potential bottleneck locations on the arterial. Queue formation and dissipation around the bottleneck location were detected by selecting two different v_{QL} values. Based on HCM (2010) procedure for identifying v_{QL} , one-third of the target speed was calculated and resulted in v_{QL} of 27.0 km/h. Queue length estimation

power was further improved by performing transformation function which resulted in v_{QL} of 42.0 km/h. Different than signalized intersection, multiple queue join locations were frequently observed suggesting stop and move traffic before reaching to bottleneck location. Selection v_{QL} as 42.0 km/h revealed that FCD had great success to estimate queued vehicles when compared to GT data for the control segment. Thus, for uninterrupted flows, the GT data should be collected to derive the transformation function between GT and FCD speed.

As a conclusion, FCD can be used as a traffic data source for determination of a queue length and is expected to be used extensively as its penetration rate increases.

7.2. Recommendations for Future Studies

In the light of the research findings for queue length estimation via commercial FCD, further recommendations for future studies are listed below:

- This thesis has not addressed the question of real-time queue estimation. Thus, the proposed model can be modified to estimate the queue length in real-time for all approaches of the intersection which will be used as an input for real-time traffic signal optimization. Signal timings can be optimized more accurately which resulted in minimum delay and travel time; thus, better management of the signalized intersection.
- Similarly, real-time estimation of the queue lengths for uninterrupted urban arterials may provide real-time traffic management of the urban arterial.
- Since the commercial FCD is a processed data, fusing other traffic data sources with commercial FCD may significantly improve the accuracy of the queue length estimation. For example, fusing loop detectors with commercial FCD at a signalized intersection may decrease the estimation errors and eliminate the effect of the low penetration rate of FCD. Data fusion algorithms can be utilized.

- Similarly, locating loop detectors at certain locations (generally preferred at every 250 m from the bottleneck location (FHWA, 2006)) for uninterrupted urban arterials and fusing with the FCD may significantly improve the queue length estimation.

REFERENCES

- Adu-Gyamfi, Y.O., and Sharma, A. 2015. Reliability of probe speed data for Detecting congestion trends. In IEEE 18th International Conference on Intelligent Transportation Systems, Las Palmas, Spain, 15-18 Sept. 2015.
- Akcelik, R. 1999. A queue model for HCM 2000. ARRB Transportation Research Ltd., Vermont South, Australia.
- Anuar, K., Habtemichael, F., and Cetin, M. 2015. Estimating traffic flow rate on freeways from probe vehicle data and fundamental diagram. In IEEE 18th International Conference on Intelligent Transportation Systems, Las Palmas, Spain, 15-18 Sept. 2015.
- Altintasi, O., Tuydes-Yaman, H., and Tuncay, K. 2017. Detection of urban traffic patterns from Floating Car Data (FCD). Transportation Research Procedia, Vol. 22, 381-391 (doi.org/10.1016/j.trpro.2017.03.057).
- Badillo, B. E., Rakha, H., Rioux, T. W. and Abrams, M. 2012. Queue length estimation using conventional vehicle detector and probe vehicle data. In 15th International Conference on Intelligent Transportation Systems (ITSC), pp. 1674-1681.
- Bagheri, E., Mehran B. and Hellinga B. 2015. Real-time estimation of saturation flow rates for dynamic traffic signal control using connected-vehicle data. Transportation Research Record: Journal of the Transportation Research Board. No:2487, pp. 69-77.
- Ban, X. J., Hao, P., Sun, Z. 2011. Real time queue length estimation for signalized intersections using travel times from mobile sensors. Transportation Research Part C, 2011. Vol: 19, pp. 1133-1156.

- Brockfeld, E., Passfeld, B., and Wagner, P. 2007. Validating travel times calculated on the basis of taxi floating car data with test drives, 14th ITS Conference, Beijing, China, October 9th-13th.
- Cai, Q., Wang, Z., Zheng, L., Wu, B. and Wang, Y. 2014. Shockwave approach for estimating queue length at signalized intersections by fusing data from point and mobile sensors. Transportation Research Record: Journal of the Transportation Research Board. No: 2422, pp. 17-22.
- Cambridge Systematics. 2012. Travel time data collection white paper, Florida Dept. of Transportation, Tallahassee, FL.
- Cetin, M. 2012. Estimating queue dynamics at signalized intersections from probe vehicle data: Methodology based on kinematic wave model. Transportation Research Record: Journal of the Transportation Research Board. No: 2315, pp. 164–172.
- Chase, R.T, Williams, B.M., Rouphail, N.M. and Kim, S. 2012. Comparative evaluation of reported speeds from corresponding fixed-point and probe-based detection systems. Journal of Transportation research record, pp. 110-119.
- Cheng, Y., Qin, X., Jin, J., Ran, B. and Anderson, J. 2011. Cycle-by-cycle queue length estimation for signalized intersections using sampled trajectory data. Transportation Research Record, 2257(1), 87-94.
- Cheu, R.L., Xie, C., Lee, D.H. 2002. Probe Vehicle Population and Sample Size for Arterial Speed Estimation, Computer Aided Civil Infrastructure Engineering. Vol: 17(1), pp. 53–60.

- Comert G., and M. Cetin. 2009. Queue length estimation from probe vehicle location and the impacts of sample size. *European Journal of Operational Research*. Vol: 197, pp. 196-202.
- Elefteriadou, L., Roess, R., and McShane, W. 1995. Probabilistic nature of breakdown at freeway merge junctions. *Transportation Research Record*, No 1484:80–89.
- Fabritiis, C., Ragona, R., and Valenti, G. 2008. Traffic estimation and prediction based on real time floating car data. *Proceeding of the 11th International Conference on Intelligent Transportation Systems*, Beijing, China.
- FHWA. 2016. *Traffic Control Systems Handbook: Chapter 6. Detectors*. https://ops.fhwa.dot.gov/publications/fhwahop06006/chapter_6.htm#ref1.
- Greenshields, B. (1935). A study of traffic capacity. *Proceeding of the Highway Research Board*, Vol. 14, pp. 448-477.
- Haghani, A., Hamed, M., Sadabadi, K.F., Young, S., and Tarnoff, P. 2010. Data Collection of Freeway Travel Time Ground Truth with Bluetooth Sensors. *Transportation Research Record: Journal of the Transportation Research Board* pp. 60-68.
- Hall, F. L., Hurdle, V.F. and Banks, J.H. 1992. Synthesis of recent work on the nature of speed-flow and flow occupancy relationships on freeways. *Transportation Research Record No:1365*, TRB, National Research Council, Washington D.C, pp. 12-18.
- HCM 2010. *Highway Capacity Manual*, Transportation Research Board of the National Academies, Washington, D.C., USA.

- Herrera, J.C., Work D.B, Herring, R., Ban, X.G., Jacobson, Q., Bayen A.M. 2010. Evaluation of Traffic Data Obtained via GPS-enabled Mobile Phones: The Mobile Century Field Experiment. Transportation Research Part C: Emerging Technology Vol: 18(4), pp. 568–583.
- Hong, J., Zhang, X., Wei Z., Li, L. and Ren Y. 2007. Spatial and temporal analysis of probe vehicle-based sampling for real-time traffic information system. Proc. 2007 IEEE Intelligent Vehicles Symposium. Istanbul, Turkey, pp. 1234–1239. [https://doi.org/10.1061/\(ASCE\)TE.1943-5436.0000815](https://doi.org/10.1061/(ASCE)TE.1943-5436.0000815).
- Hu, J., Fontaine, M.D., and Ma, J. 2016. Quality of private sector travel-time data on arterials. Journal of Transportation Engineering, 142(4). Available from: [https://doi.org/10.1061/\(ASCE\)TE.1943-5436.0000815](https://doi.org/10.1061/(ASCE)TE.1943-5436.0000815).
- Kerner, B.S., C. Demir, R.G. Herrtwich, S. L. Klenov, H. Rehborn, M., Aleksic, A. Haug. 2005. Traffic State Detection with Floating Car Data in Road Networks. Proceeding of the 8th International IEEE conference on Intelligent Transportation Systems, Vienna, Austria, September 13-16.
- Kim S., and Coifman, B. 2014. Comparing INRIX speed data against concurrent loop detector stations over several months. Transportation Research Part C 49:59-72.
- Klein, L., Mills, M.K. and Gibson, R.P. 2006. Traffic Detector Handbook: Third edition-Vol (1). Publication number: FHWA-HRT-06-108.
- Klunder, G.A., Taale, H., Kester, L. and Hoogendoorn, S. 2017. Improvement of Network Performance by In-Vehicle Routing Using Floating Car Data. Journal of Advanced Transportation, Volume 2017, <https://doi.org/10.1155/2017/8483750>

- Kondyli, A., George, B., and Elefteriadou, L. 2016. Comparison of travel time measurement methods along freeway and arterial facilities. *Transportation Letters, The International Journal of Transportation Research*. Doi: <http://dx.doi.org/10.1080/19427867.2016.1245259>.
- Latimer, C., and Glotzbach, G. 2012. Evaluation of third party travel time data. ITS America 22nd Annual Meeting and Exposition, 21-23 May 2012, National Harbor, MD. Available from: <http://itswc.confex.com/itswc/AM2012/webprogram/Paper10870.html>.
- Leduc, G. 2008. Road Traffic Data: Collection Methods and Applications (Technical report-- JRC 47967). Working Papers on Energy, Transport and Climate Change.
- Li, Q., Ge, Q., Miao, L. and Qi, M. 2012. Measuring variability of arterial road traffic condition using archived probe data. *Journal of Transportation Systems Engineering and Information Technology*. Vol. 12(2).
- Li, J.Q., Zhou, K., Shladover, S.E. and Skabardonis, A. 2013. Estimating queue length under connected vehicle technology using probe vehicle, loop detector, and fused data. *Transportation Research Record: Journal of the Transportation Research Board*, No: 2356, 17–22.
- Liu, D., Kitamura, Y., Zeng, X., Araki, S., Kakizaki, K. 2015. Analysis and visualization of traffic conditions o road network by route bus probe data. *IEEE 18th International Conference on Intelligent Transportation Systems*.
- Liu, H., Xinkai, W., Wenteng, M., Heng, H. 2009. Real-time queue length estimation for congested signalized intersections. *Transportation Research Part C*, Vol: 17, pp. 412-427.

- Mannering, F.L., Washburn, S.S. and Kilareski, W.P. 2009. Principles of highway engineering and traffic analysis. 4th edition, John Wiley&Sons, Inc.
- Muck, J. 2002. Using detectors near the stop-line to estimate traffic flows. Traffic Engineering and Control 43, 429–434.
- Neumann, T. 2010. Floating-Car Data for urban traffic monitoring: A new approach, its applications and future visions. The Young European Arena of Research.
- Pan, S., Jiang, B., Zou, N. and Jia, L. 2011. Average speed estimation using multi-type Floating Car Data. Proceeding of the IEEE, International Conference on Information and Automation, Shenzhen, China.
- Pascale, A., Mavroeidis, D., Thanh-Lam, H. 2015. Spatio-temporal clustering of urban networks: a real case scenario in London, CD-ROM. Transportation Research Board of the National Academies, Washington, D.C.
- Petrovska, N. and Stevanovic, A. 2015. Traffic Congestion Analysis Visualisation Tool, In: IEEE 18th International Conference on Intelligent Transportation Systems.
- Pipes, L. A. (1967). Car following models and the fundamental diagram of road traffic, Transportation Research, Vol. 1, pp. 21-29.
- Pongnumkul, S., Kamsiriphipan, N., Poolsawas, J. and Amornwat, W. 2013. Congestion Grid: A Temporal Visualization of Road Segment Congestion Level Data. In: 13th International Symposium on Communications and Information Technologies.
- Quayle, S.M, Koonce, P., DePencier, D. and Bullock D. M. 2010. Arterial performance measures with media access control readers Portland, Oregon,

- pilot study. *Transportation Research Record: Journal of the Transportation Research Board*. No. 2192, Washington, D.C., pp. 185–193.
- Reinthal, M., Weichenmeier, F., Nowotny, B. and Hildebrandt, R. 2010. Evaluation of Speed Estimation by Floating Car Data (within the research Project dmotion (research report).
- Schneider, W.H., Turner, S.M. Roth, J., and Wikander, J. 2010. Statistical validation of speeds and travel times provided by a data service. Technical report: FHWA/OH-2010/2, 2010.
- Sharma, A., Bullock, D.M., Bonneson, J. 2007. Input–output and hybrid techniques for real-time prediction of delay and maximum queue length at a signalized intersection. *Transportation Research Record*, No: 2035, TRB, National Research Council, Washington, DC, pp. 88–96.
- Shoufeng, L., Yanhui, M. and Ximin, L., 2013. The analysis of characterization of urban traffic congestion based on mixed speed distribution of taxi GPS data. *Applied Mechanics and Materials*, Vol. 241-244, 2076-2081.
- Strong, D.W., Nagui M.R, Ken C. 2006. New calculation method for existing and extended HCM delay estimation procedure. No:06-0106, Proceedings of the 85th annual meeting of the Transportation Research Board, Washington, DC.
- Skabardonis, A. and Geroliminis, N. 2008. Real-time Monitoring and Control on Signalized Arterials. *Journal of Intelligent Transportation Systems*. 12 (2), 64–74.
- Sunderrajan, A., Viswanathan, V., Cai, W. and Knoll. A. 2016. Traffic State Estimation Using Floating Car Data. *Procedia Computer Science*. Vol:80, pp. 2008-2018.

- Tiaprasert, K., Zhang, Y., Wang, X. B. and Zeng, X. 2015. Queue length estimation using connected vehicle technology for adaptive signal control. *IEEE Transactions on Intelligent Transportation Systems*. 16(4).
- Unal, O. and Cetin M. 2014. Estimating Queue Dynamics and Delays at Signalized Intersections from Probe Vehicle Data. Presented at 93th Annual Meeting of the Transportation Research Board, Washington, D.C.
- Underwood, R. T. (1961). Speed, volume, and density relationship: Quality and theory of traffic flow, Yale Bureau of Highway Traffic, pp. 141-188.
- Vandenberghe, W., Vanhauwaert, E., Verbrugge, S., Moerman, I. and Demeester P. 2012. Feasibility of Expanding Traffic Monitoring Systems with Floating Car Data Technology. *IET Intelligent Transportation systems*. Vol: 6(4), pp. 347-354.
- Van Aerde, M. and Rakha, H. 1995. Multivariate calibration of single regime speed-flow-density relationships. 6th International Vehicle Navigation and Information System. July 30-August 2, pp. 334-341.
- Van Aerde, M. (1995). Single regime speed-flow-density relationship for congested and congested highways, In 74th TRB Annual Conference, ed. Washington, D.C.
- Vasudevan, M., Negron, D., Feltz, M., Mallette, J., Wunderlich, K. 2015. Predicting Congestion States from Basic Safety Messages Using Big Data Analytics, CD-ROM. Transportation Research Board of the National Academies, Washington, D.C.

- Wang, X., Liu, H., Yu, R., Deng, B., Chen, X. and Wu, B. 2014. Exploring operating speeds on urban arterials using floating car data: case study in shanghai. *Journal of Transportation Engineering*, doi: 10.1061/(ASCE)TE.1943-5436.0000685.
- Wang, Z., Cai, Q., Wu, B., Zheng, L. and Wang, Y. 2017. Shockwave-Based Queue Estimation Approach for Undersaturated and Oversaturated Signalized Intersections Using Multi-Source Detection Data. *Journal of Intelligent Transportation Systems Technology, Planning, and Operations*. Vol: 21(3), pp. 167-178.
- Webster F. 1958. Traffic Signal Settings. Road Research Technical Paper 39. Road Research Laboratory, London.
- Xu, L., Yue, Y. and Li, Q. 2013. Identifying urban traffic congestion pattern from historical Floating Car Data. 13th COTA International conference of Transportation Professionals (CICTP 2013).
- Zhao, N., Yu, L., Zhao, H. and Wen G. 2009. Analysis of Traffic Flow Characteristics on Ring Road Expressways in Beijing: Using Floating Car Data and Remote Traffic Microwave Sensor Data. *Transportation Research Record: Journal of the Transportation Research*, pp. 178-185.

APPENDICES

A. STATIC INFORMATION TABLE OF FCD SEGMENTS

Table A.1. *Static information of the FCD road segments on Dumlupınar Blvd.*

Segment Id	Length (m)	Road Class	Start Coordinate	End Coordinate	Local Id
676555	48.24	1	32.725874;39.906164	32.726438;39.906186	1
676556	48.24	1	32.726438;39.906186	32.727001;39.906209	2
676557	48.24	1	32.727001;39.906209	32.727565;39.906229	3
676116	40.56	1	32.727565;39.906229	32.728038;39.90625	4
676117	40.56	1	32.728038;39.90625	32.728512;39.906271	5
676118	40.56	1	32.728512;39.906271	32.728985;39.906293	6
676119	40.56	1	32.728985;39.906293	32.729459;39.906314	7
902667	40.87	1	32.729459;39.906314	32.729936;39.906326	8
902668	40.87	1	32.729936;39.906326	32.730413;39.906349	9
902669	40.87	1	32.730413;39.906349	32.730891;39.906369	10
902670	40.87	1	32.730891;39.906369	32.731368;39.906393	11
902671	40.87	1	32.731368;39.906393	32.731845;39.906416	12
131016	40.87	1	32.731845;39.906416	32.732203;39.906426	13
1233325	46.49	1	32.732203;39.906426	32.732528;39.906438	14
184647	46.49	1	32.732528;39.906438	32.733071;39.906453	15
184648	46.49	1	32.733071;39.906453	32.733614;39.906469	16
184649	46.49	1	32.733614;39.906469	32.734157;39.906485	17
184650	46.49	1	32.734157;39.906485	32.734701;39.9065	18
676110	40.33	1	32.734701;39.9065	32.735171;39.906523	19
676111	40.33	1	32.735171;39.906523	32.735642;39.906545	20
676107	49.36	1	32.735642;39.906545	32.736104;39.906564	21
676108	49.36	1	32.736104;39.906564	32.736565;39.906594	22
676109	49.36	1	32.736565;39.906594	32.737025;39.906627	23
198299	49.36	1	32.737025;39.906627	32.737601;39.906657	24
198300	49.36	1	32.737601;39.906657	32.738177;39.906685	25
198301	49.36	1	32.738177;39.906685	32.738754;39.906705	26
198302	49.36	1	32.738754;39.906705	32.73933;39.906729	27
198303	49.36	1	32.73933;39.906729	32.739907;39.90675	28
6905751	26.91	1	32.739907;39.90675	32.740049;39.906756	29
6905750	26.91	1	32.740049;39.906756	32.740364;39.906768	30

Table A.1. *Static information of the FCD road segments on Dumlupınar Blvd (continued).*

Segment Id	Length (m)	Road Class	Start Coordinate	End Coordinate	Local Id
6810212	49.16	1	32.740364;39.906768	32.740938;39.906789	31
6810213	49.16	1	32.740938;39.906789	32.741512;39.90681	32
6810214	49.16	1	32.741512;39.90681	32.742086;39.906833	33
6810215	49.16	1	32.742086;39.906833	32.74266;39.906856	34
6810216	49.16	1	32.74266;39.906856	32.743234;39.906884	35
6810217	49.16	1	32.743234;39.906884	32.743808;39.906912	36
6810218	49.16	1	32.743808;39.906912	32.744382;39.906932	37
6810219	49.16	1	32.744382;39.906932	32.744956;39.906953	38
6810220	49.16	1	32.744956;39.906953	32.745531;39.90697	39
6810221	49.16	1	32.745531;39.90697	32.746105;39.906989	40
6810222	49.16	1	32.746105;39.906989	32.746679;39.907015	41
6810223	49.16	1	32.746679;39.907015	32.747253;39.907041	42
6810224	49.16	1	32.747253;39.907041	32.747827;39.907066	43
6810225	49.16	1	32.747827;39.907066	32.748401;39.907091	44
6810226	49.16	1	32.748401;39.907091	32.748975;39.907115	45
6810227	49.16	1	32.748975;39.907115	32.749549;39.907139	46
6810228	49.16	1	32.749549;39.907139	32.750122;39.907165	47
6810229	49.16	1	32.750122;39.907165	32.750696;39.907192	48
6810230	49.16	1	32.750696;39.907192	32.75127;39.907215	49
6810231	49.16	1	32.75127;39.907215	32.751845;39.907229	50
6810232	49.16	1	32.751845;39.907229	32.752419;39.90725	51
6810233	49.16	1	32.752419;39.90725	32.752993;39.90728	52
6810234	49.16	1	32.752993;39.90728	32.753567;39.907302	53
6810235	49.16	1	32.753567;39.907302	32.754141;39.90732	54
6810236	49.16	1	32.754141;39.90732	32.754716;39.907337	55
6810237	49.16	1	32.754716;39.907337	32.755289;39.907363	56
6810238	49.16	1	32.755289;39.907363	32.755863;39.90739	57
6810239	49.16	1	32.755863;39.90739	32.756438;39.90741	58
6810240	49.16	1	32.756438;39.90741	32.757012;39.907428	59
6810241	49.16	1	32.757012;39.907428	32.757586;39.907449	60
6810242	49.16	1	32.757586;39.907449	32.75816;39.907472	61
198322	39.45	1	32.75816;39.907472	32.758621;39.907491	62
198323	39.45	1	32.758621;39.907491	32.759082;39.90751	63
198324	39.45	1	32.759082;39.90751	32.759542;39.907529	64
198325	39.45	1	32.759542;39.907529	32.760003;39.907546	65
198326	48.25	1	32.760003;39.907546	32.760567;39.907565	66
198327	48.25	1	32.760567;39.907565	32.76113;39.907588	67

Table A.1. *Static information of the FCD road segments on Dumlupınar Blvd (continued).*

Segment Id	Length (m)	Road Class	Start Coordinate	End Coordinate	Local Id
198328	48.25	1	32.76113;39.907588	32.761694;39.907616	68
198329	48.25	1	32.761694;39.907616	32.762257;39.907644	69
198330	48.25	1	32.762257;39.907644	32.76282;39.907672	70
198320	28.29	1	32.76282;39.907672	32.76315;39.907687	71
198321	28.29	1	32.76315;39.907687	32.763481;39.907699	72
205309	39.48	1	32.763481;39.907699	32.763942;39.907712	73
1209316	39.18	1	32.763942;39.907712	32.764399;39.907724	74
1209317	39.18	1	32.764399;39.907724	32.764857;39.907741	75
1209318	13.03	1	32.764857;39.907741	32.765009;39.907745	76
835497	13.60	1	32.765009;39.907745	32.765167;39.907757	77
5565077	39.18	1	32.765167;39.907757	32.765649;39.907765	78
5565078	39.18	1	32.765649;39.907765	32.76613;39.907781	79
5565079	39.01	1	32.76613;39.907781	32.766611;39.907797	80
5565080	39.01	1	32.766611;39.907797	32.767093;39.907813	81
184687	39.01	1	32.767093;39.907813	32.767549;39.907822	82
Note: Average speed and speed limit of the road segments are 70 km/h.					

Table A.2. Static information of the FCD road segments on Muhsin Yazıcıoğlu Street.

Segment ID	Length (m)	Road Class	Average Speed	Speed Limit	Start Coordinate	End Coordinate
Int 1 - Approach 1						
2004037	40.90	6	46	50	32.809644; 39.903973	32.809424; 39.904302
2004038	40.90	6	46	50	32.809424; 39.904305	32.809178; 39.904616
2004039	40.90	6	46	50	32.809178; 39.904616	32.808912; 39.904922
2004049	40.90	6	46	50	32.808912; 39.904922	32.808646; 39.905242
2004050	40.90	6	46	50	32.808646; 39.905242	32.808379; 39.905557
2004051	40.90	6	46	50	32.808379; 39.905557	32.808111; 39.905874
2004052	40.90	6	46	50	32.808111; 39.905874	32.807843; 39.906191
2004053	40.90	6	46	50	32.807843; 39.906191	32.807575; 39.906508
Int 2-Approach 2						
1212701	41.43	6	46	50	32.807425; 39.906336	32.807658; 39.906015
1212702	41.43	6	46	50	32.807658; 39.906015	32.807934; 39.905709
1212703	41.43	6	46	50	32.807934; 39.905709	32.808210; 39.905402
1212704	41.43	6	46	50	32.808210; 39.905402	32.808484; 39.905094
1212705	41.43	6	46	50	32.808484; 39.905094	32.808773; 39.904795
2004040	38.85	6	46	50	32.808773; 39.904795	32.809025; 39.904504
2004041	38.85	6	46	50	32.809025; 39.904504	32.809283; 39.904216
2004042	38.85	6	46	50	32.809283; 39.904216	32.809538; 39.903926

B. METHODOLOGY FOR GT VERSUS FCD EVALUATION

Quality of the available FCD speed was evaluated by comparing the GT and FCD datasets via different analyses as described below:

Descriptive Evaluation: This step includes visual assessment of quality of FCD in describing speed profile and fundamental diagram. For the former, speed profiles by \bar{u}^t and \bar{u}_{FCD}^t were graphed together to reveal insights about the reliability of FCD speeds. GT-based maximum and minimum vehicle speeds, u_{\max}^t and u_{\min}^t , were also included to give an idea about the potential reasons behind deviations in FCD values, as well as level of outliers in the FCD. For the latter, a GT diagram was obtained by plotting (q^t versus \bar{u}^t), which was compared against a fused diagram plotted as (q^t versus \bar{u}_{FCD}^t). This fused diagram provides a visual check on whether the expected traditional distribution could be obtained or not, especially detecting any problems in portraying the congested and uncongested regimes. Note: In the fundamental diagram plots, a single regime traffic flow model was also fit to GT values using Van Aerde (1995) formulation as between flow, speed and density k^t as

$$q^t = \bar{u}^t * k^t \quad \text{and} \quad k^t = \frac{1}{c_1 + \frac{c_2}{u_f - \bar{u}^t} + c_3 \bar{u}^t} \quad [\text{B.1}]$$

where u_f represents the free flow speed, and c_1 , c_2 and c_3 are model parameters describing congested and uncongested part of the relation as discussed in Zhao et al. (2009) and Anuar et al. (2015).

Speed Estimation Performance Evaluation: The success of FCD speeds as a surrogate measure for real speeds was evaluated based on the following performance measures:

- i) MAPE was used in (Wang et al. 2014; Anuar et al. 2015; Hu et al. 2016) to measure error in speeds and calculated as

$$MAPE_u = \frac{1}{T} \sum_{t=1}^T \left| \frac{\bar{u}_{FCD}^t - \bar{u}^t}{\bar{u}^t} \right| * 100 \quad [B.2]$$

ii) RMSE was applied in (Anuar et al. 2015) for speed errors, and formulated as

$$RMSE_u = \sqrt{\frac{1}{T} \sum_{t=1}^T (\bar{u}_{FCD}^t - \bar{u}^t)^2} \quad [B.3]$$

where T shows the analysis period in terms of minutes.

iii) Furthermore, a regression analysis R^2 (correlation coefficient) was determined for the speed transformation function of

$$\hat{u}_{FCD}^t = f(\bar{u}_{FCD}^t) \quad [B.4]$$

to decide whether there was a strong relation between the FCD speeds and real values. However, the regression analysis was performed for the whole study period as well as only peak periods as FCD speed quality was expected to differ during congested regimes. Furthermore, it was repeated with filtered FCD speed datasets, to see the impact on data filtering the performance of speed transformation.

LOS Estimation Performance: Instead of estimating speeds directly, it is also very helpful to estimate LOS, a quantitative measure representing quality of service for traffic monitoring purposes. HCM (2010) defined LOS level for urban roads based on “the reductions in travel speed as a percentage of the free-flow speed of the corridor” as shown in Table A-1. With this definition, for an urban corridor with 90 km/h speed limit, speeds over 60 km/h correspond to uncongested regimes, while LOS C represents “stable flow” and speeds below 36 km/h (LOS E and F) designate “unstable/congested flow” conditions (Note: Due to the aforementioned truncation at 70 km/h, it was not possible to determine “LOS A” and “LOS B” separately, but, a joint state of “A/B” was defined, whereas the remaining 4 levels were exactly matched with LOS C to LOS F).

Table B.1 Average speed intervals and corresponding LOS values for urban roads based on HCM (2010).

LOS	HCM Flow Condition	Travel Speed as a Percentage of Base Free-flow Speed	Travel Speed Intervals for speed limit= 90 km/h	Traffic State
A	Free flow conditions	>85%	$\bar{u}' > 77\text{km/h}$	A/B
B	Unimpeded flow condition	67%-85%	$60\text{km/h} < \bar{u}' < 77\text{km/h}$	
C	Stable flow	50%-67%	$45\text{km/h} < \bar{u}' < 60\text{km/h}$	C
D	Approaching to unstable flow	40%-50%	$36\text{km/h} < \bar{u}' < 45\text{ km/h}$	D
E	Unstable flow	30%-40%	$27\text{km/h} < \bar{u}' < 36\text{km/h}$	E
F	Congested flow	<30%	$\bar{u}' < 27\text{km/h}$	F

To assess the power of FCD speed in estimating real-time LOS at control Segment 57, LOS for a time interval t , was estimated by GT (LOS^t) and FCD (LOS_{FCD}^t), which were later used to calculate performance measures again, MAPE and RMSE values as formulated

$$MAPE_{LOS} = \frac{1}{T} \sum_{t=1}^T \left| \frac{LOS^t - LOS_{FCD}^t}{LOS^t} \right| * 100 \quad [\text{B.5}]$$

$$RMSE_{LOS} = \sqrt{\frac{1}{T} \sum_{i=1}^T (LOS^t - LOS_{FCD}^t)^2} \quad [\text{B.6}]$$

Similar to speed estimation performance evaluation, a correlation coefficient between LOS^t and LOS_{FCD}^t was calculated for LOS performance evaluation, as well.

In addition to the evaluation of the LOS performance of FCD at a control location (Segment 57), the potential use of commercial FCD for urban corridor monitoring was evaluated for the entire study corridor.

Data Preprocessing: To minimize the impact of FCD speed related problems in the quality evaluation, two different set of data was formed. First, to compensate for the truncation in the FCD speeds, a truncated set from GT speeds, denoted as \bar{u}_{tr}' , was created and use as an alternative GT set. Secondly, extreme values in FCD were

filtered, and a cleaned-up data set were created. This set were denoted by \bar{u}'_{FCD*} , where “*” stands for the filtering process. Upper and lower limits for the FCD speed filter were determined by analyzing the distribution of Absolute Speed Error, ASE , which is $ASE^t = |\bar{u}'_{FCD} - \bar{u}^t|$ defined for each time, $t \in T$. A tolerance upper limit was chosen by simply assuming two folds of the interquartile (IQR) range for the ASE to create an upper limit for tolerance in the errors as

$$ASE_{tolerance} = Q3_{ASE} + 2IQR_{ASE} \quad [B.7]$$

where $Q3$ represents the 75-percentile value. FCD speeds with ASE larger than the tolerance were filtered out.

C. ESTIMATION OF QUALITY OF FCD UNDER VARYING PENETRATION RATES

The quality of FCD under varying penetration rates was evaluated by creating various FCD subsets from GT speed dataset, u_i^t , using Monte Carlo simulations (Figure C.1). In this process, assuming a selected penetration rate, δ , a randomly selected speed subset was created, first; the average of the selected speeds was used to obtain “simulated FCD average speed data”, $\tilde{u}_{FCD,k}^t$, for every minute t in the k^{th} Monte Carlo simulation. For each penetration rate, in every simulation scenario k , simulated FCD speed values were compared with the GT values, to calculate speed MAPE and RMSE measures denoted by, $MAPE_{u,k}^\delta$ and $RMSE_{u,k}^\delta$, respectively. Overall analysis of the scenarios provided average, minimum and maximum values for the MAPE, for each selected δ , denoted as \overline{MAPE}_u^δ , $MAPE_{u,\min}^\delta$ and $MAPE_{u,\max}^\delta$, respectively. In this study, six different penetration rates were selected as $\delta = \{5\%, 10\%, 15\%, 25\%, 35\% \text{ and } 50\%\}$, and $k=20$. Randomly generated Monte Carlo simulations were created for each penetration rate, δ . Increasing the number of Monte Carlo simulations yielded only minor changes in the results. Plotting the change of these performance measures against penetration rate produced characteristic functions for these errors. As MAPE and RMSE values against a flow-based penetration rate, δ_q , would be more useful in analyzing the current FCD penetration rate, δ_q for each penetration rate, δ , was determined based on the ratios of the GT flow and speed dataset (Table C.1). The function between the MAPE and RMSE values against δ_q was later used to draw insights about the current FCD penetration rate in the study area.

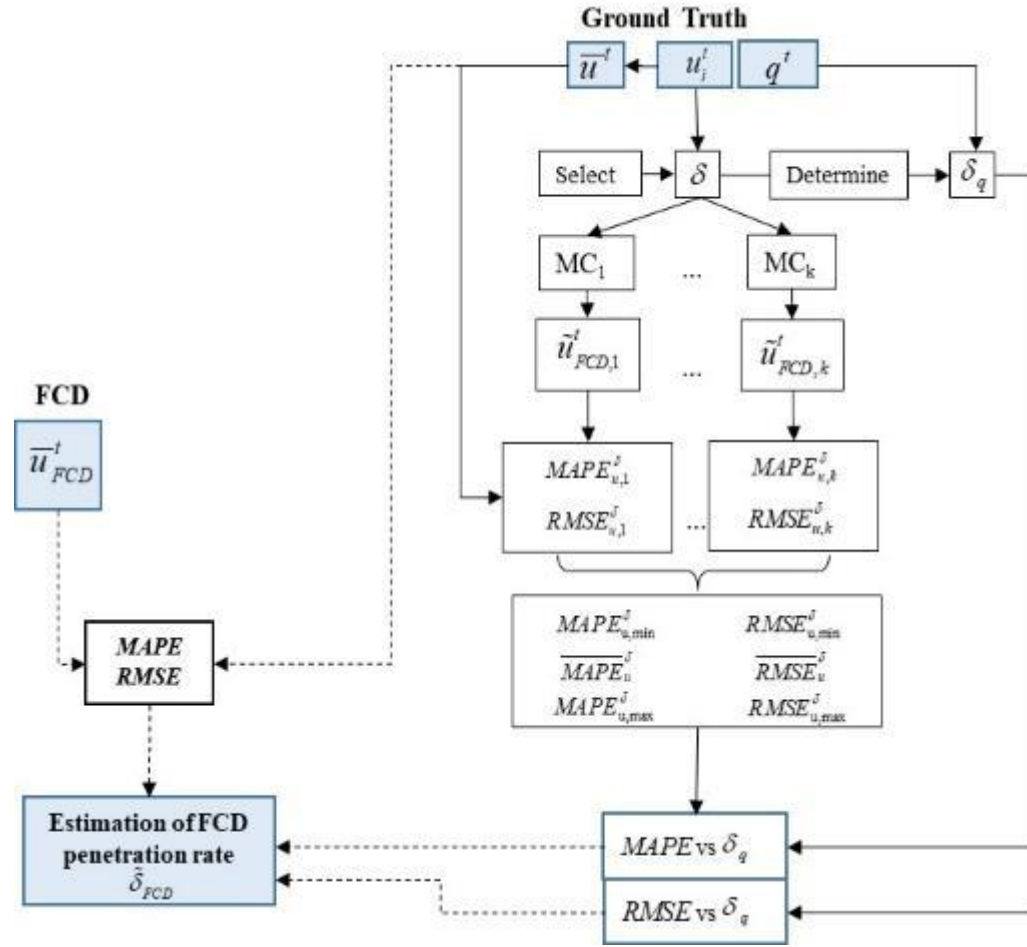


Figure C.1. Monte Carlo simulation approach to derive quality-penetration rate relation for FCD speed.

Table C.1. δ and corresponding δ_q values for different time periods of the day of October 25, 2016.

δ (%)	δ_q (%)		
	All day	Peak period	Off-peak
5	3.49	2.21	3.77
10	6.38	4.06	6.88
15	9.27	5.93	10.00
25	15.10	9.59	16.30
35	20.91	13.27	22.57
50	29.59	18.73	31.96

Compiling the results of 20 Monte Carlo simulations (randomly created using the GT speed data from October 25, 2016) for each of six selected FCD penetration rates, δ , the change of performance measures of Speed R^2 (Figure C.2), $MAPE_u$ and $RMSE_u$ values (Figure C.3) were depicted. Despite fluctuations among random scenarios, there was a visible reduction in both error measures, when δ was increased, as expected. When 5% of the GT speed data was used to simulate FCD speeds, \tilde{u}'_{FCD} , ($\delta = 5\%$ which corresponded to $\delta_q = 3.49\%$ for the whole study period in Table C.1), speed R^2 values were in between 0.70 to 0.80, which is promising result. Even for 10% penetration rate, R^2 values were raised to 0.85. After 25% penetration rate, this value was very closed to 1.00. According to the Figure 3.17a, the $MAPE_u$ values were in the range of 9%-11% and $RMSE_u$ changed within the range of 9-11 km/h for $\delta = 5\%$. Error measures decreased 50%, when δ was increased to 15%. Availability of much higher FCD penetration rates brought the error measures $MAPE_u$ and $RMSE_u$ down (as low as 2% and 2 km/h).

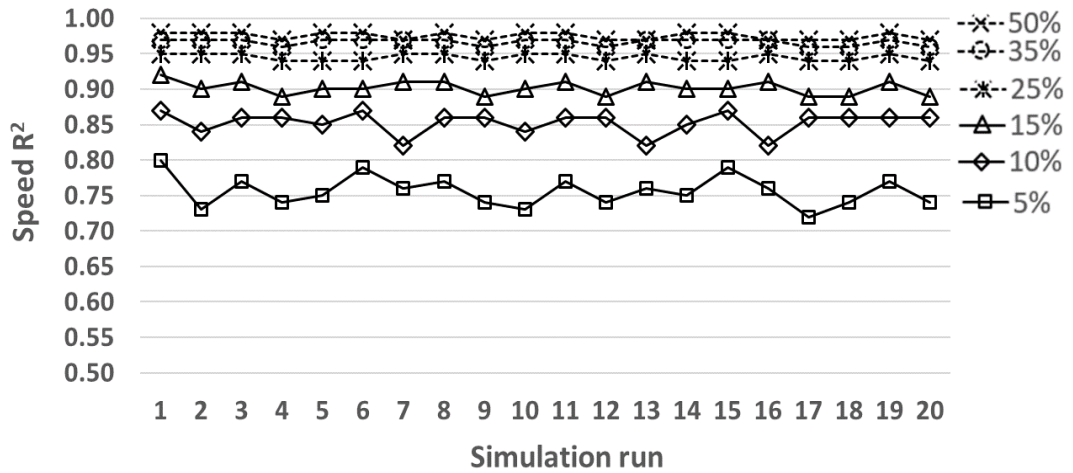


Figure C.2. Variation of Speed R^2 performance of Monte Carlo simulation by penetration rate.

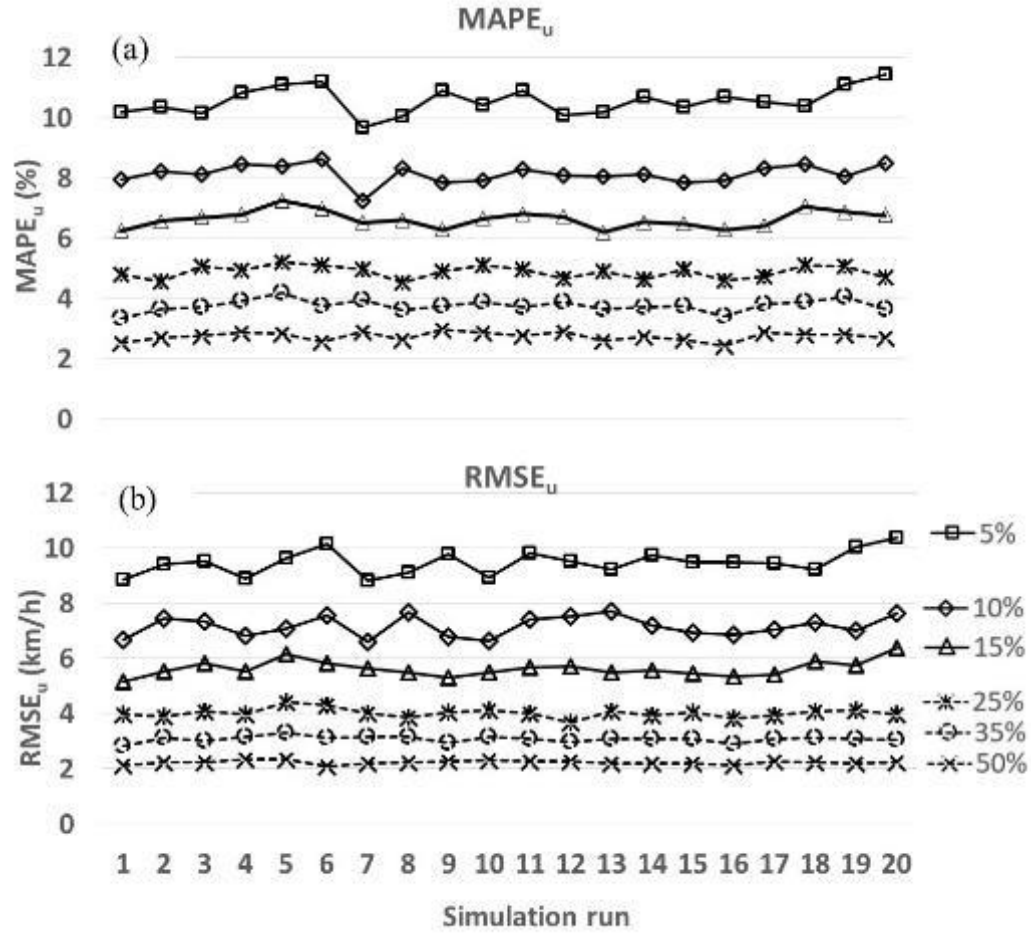


Figure C.3. Variation of $MAPE_u$ and $RMSE_u$ performance for Monte Carlo Simulations.

Average, maximum and minimum values of $MAPE_u$ and $RMSE_u$ among 20 MC runs were plotted against the flow-based FCD penetration rates, δ_q , to obtain a relationship between the two. Due to variations in the $MAPE_u$ and $RMSE_u$ values in the peak and off-peak periods, plots were created for these periods as well in Figures C.4, C.5 and C.6, respectively. For both plots indicated a strong logarithmic decay between FCD penetration rates and error measures.

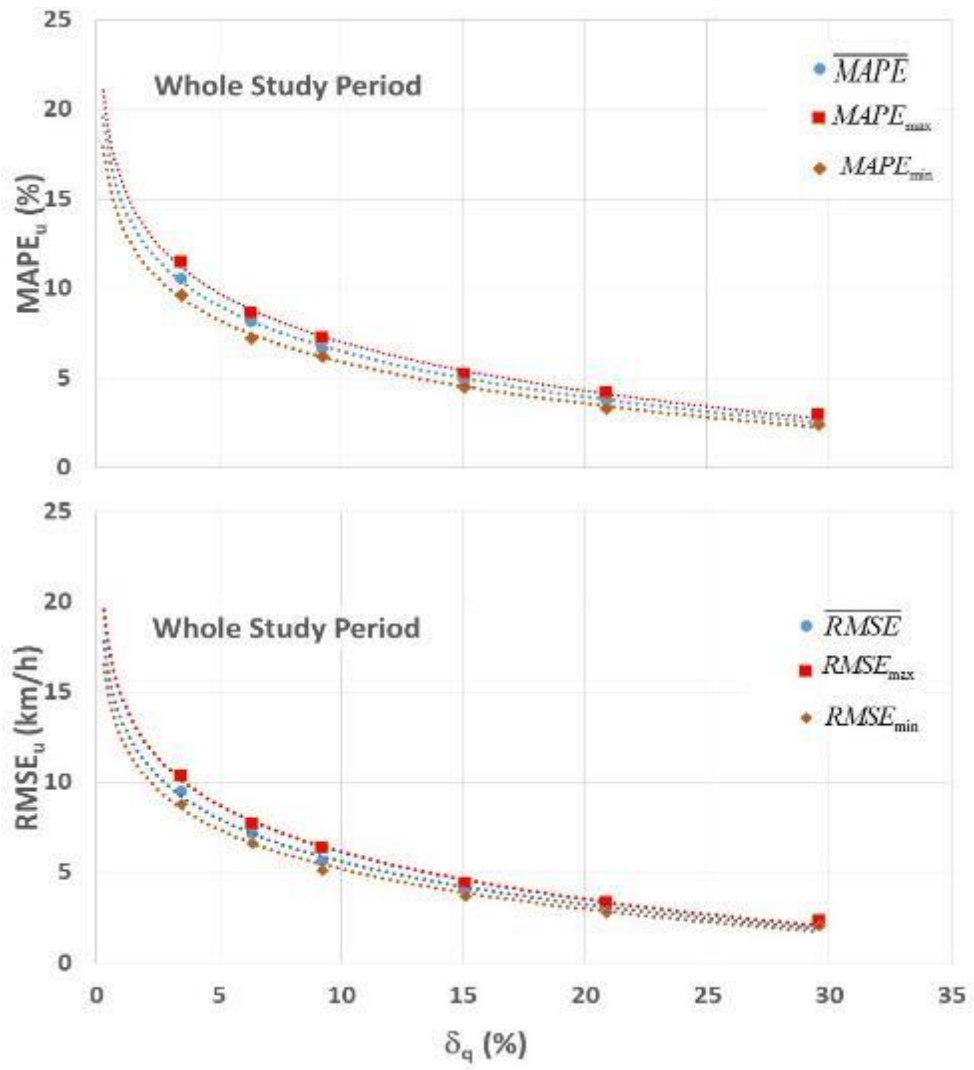


Figure C.4. Variations of $MAPE_u$ and $RMSE_u$ measures as a function of penetration rates for whole analysis period.

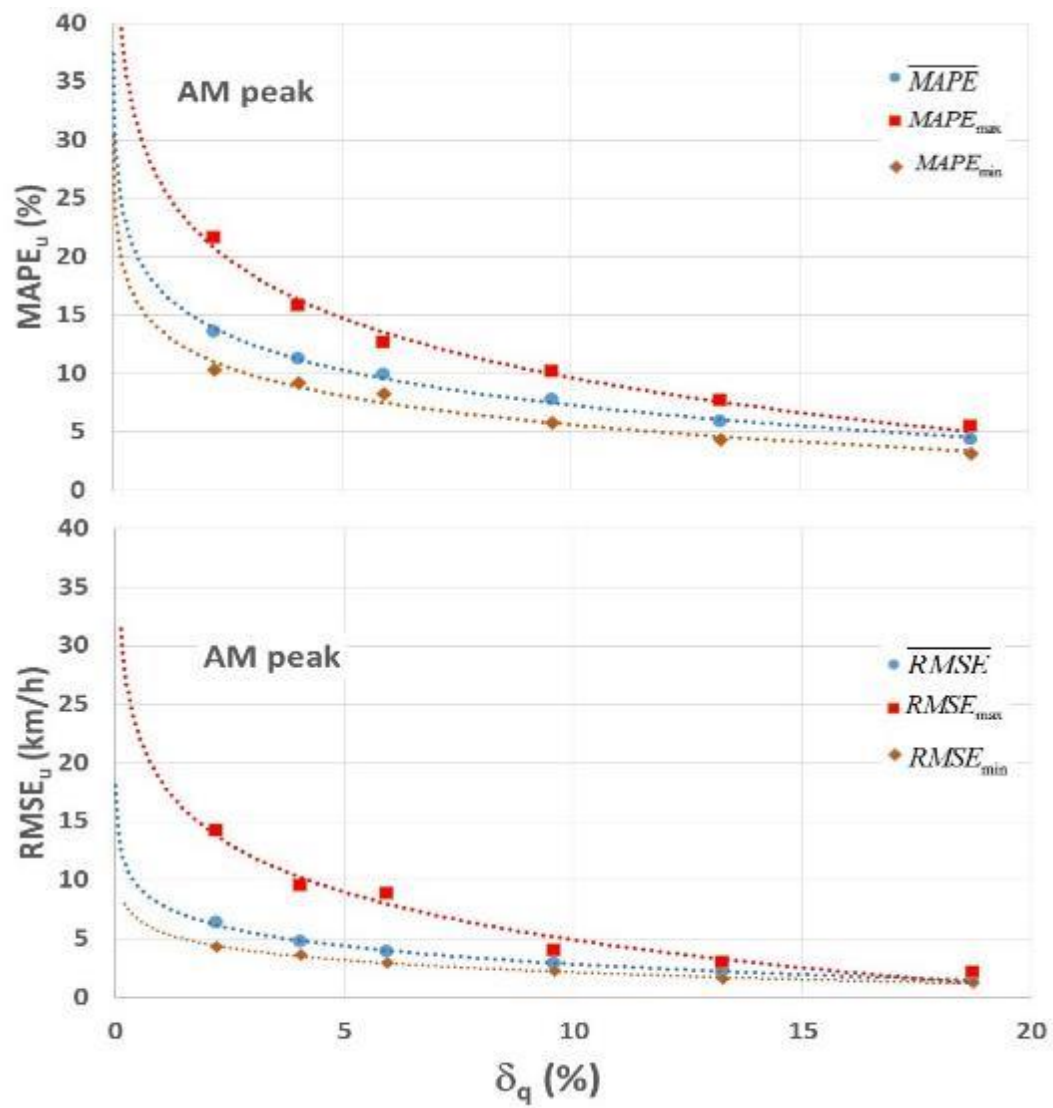


Figure C.5. Variations of $MAPE_u$ and $RMSE_u$ measures as a function of penetration rates for AM peak.

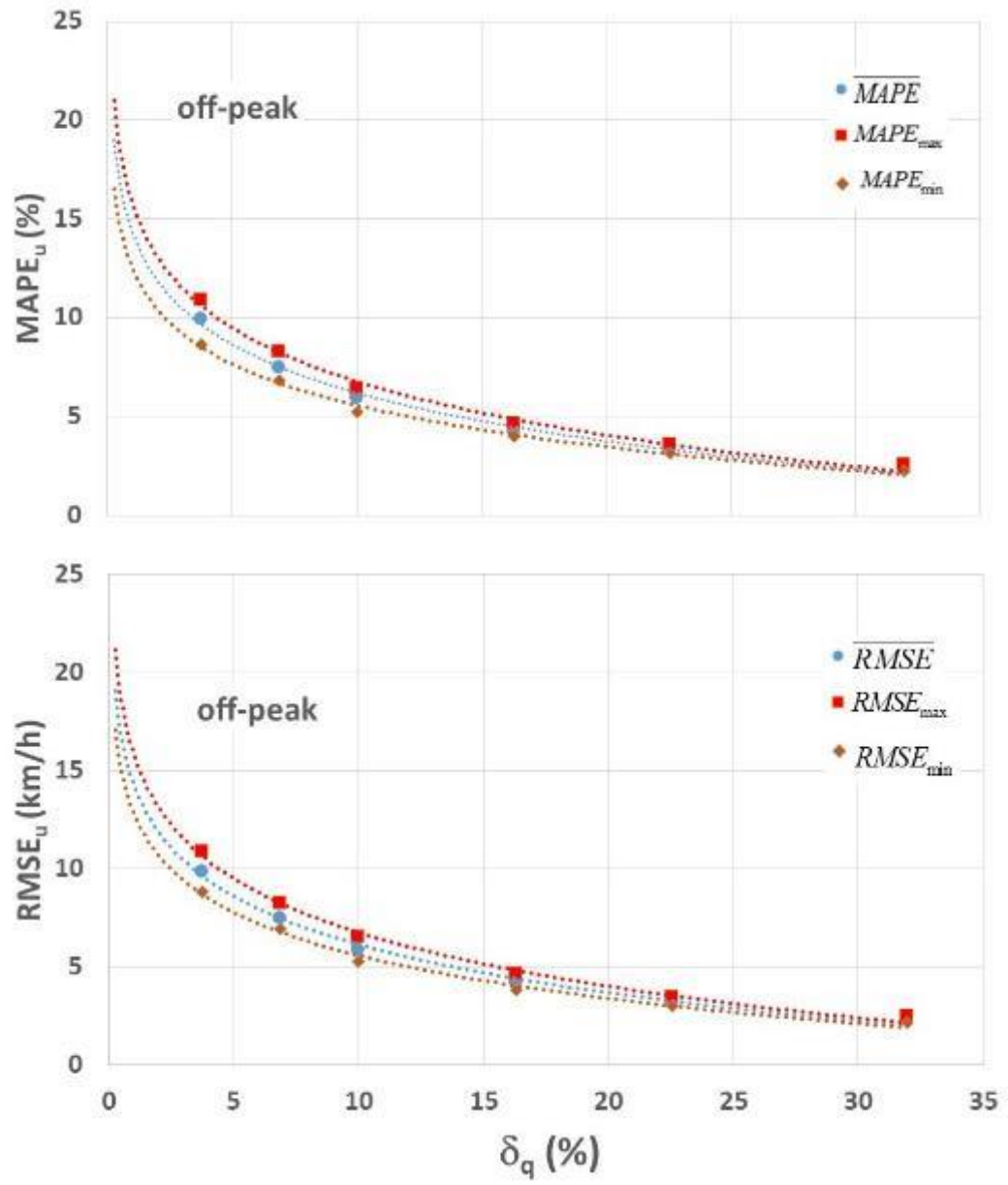


Figure C.6. Variations of $MAPE_u$ and $RMSE_u$ measures as a function of penetration rates for off-peak period.

CURRICULUM VITAE

PERSONAL INFORMATION

Altıntaşı, Oruç
Nationality: Turkish (TC)
Date and Place of Birth: 05 May 1986, Erzurum
Marital Status: Married
Phone: +90 312 210 24 65
Fax: +90 312 210 54 01
email: aoruc@metu.edu.tr

EDUCATION

Degree	Institution	Year of Graduation
MS	METU Civil Engineering	2013
BS	Anadolu Univ. Civil Engineering	2009
High School	Eskişehir Anadolu High School, Eskişehir	2004

WORK EXPERIENCE

Year	Place	Enrollment
2010-Present	Middle East Technical University Civil Engineering	Research Assistant

FOREIGN LANGUAGES

Advanced English

PUBLICATIONS

Journal Articles

1. Altıntasi Oruc, Hediye Tuydes-Yaman, and Kagan Tuncay (2019) “Monitoring Urban Traffic from Floating Car Data (FCD): Using Speed or a Los-Based State Measure” In: Macioszek E., Sierpiński G. (eds) Directions of Development of Transport Networks and Traffic Engineering. TSTP 2018. Lecture Notes in Networks and Systems, Vol. 51, pp. 163-173, Springer, Cham (doi.org/10.1007/978-3-319-98615-9_15)
2. Altıntasi, Oruc, Hediye Tuydes-Yaman, and Kagan Tuncay (2017). “Detection of Urban Traffic Patterns from Floating Car Data (FCD)”. Transportation Research Procedia, Vol. 22, 381-391 (doi.org/10.1016/j.trpro.2017.03.057).

3. Altintasi, Oruc and Hediye Tuydes-Yaman (2016) “Best Option For Reducing On-Campus Private Car-Based CO2 Emissions: Reducing VKT or Congestion?”, METU Journal of Faculty of Architecture, Vol.33 (1); pp.87-105; (doi: 10.4305/METU.JFA.2016.1.4).
4. Altintasi, Oruc and Hediye Tuydes-Yaman (2016). “Utilization of RFID Data to Evaluate Campus Commute Characteristics”. Pamukkale Üniversitesi Mühendislik Fakültesi Dergisi Vol. 22(3), 171-177 (doi: 10.5505/pajes.2015.68725).
5. Tuydes-Yaman, Hediye, Oruc Altintasi and Nuri Sendil (2015) “Better Estimation of Origin-Destination Matrix Using Automated Intersection Movement Count Data”. Canadian Journal of Civil Engineering. Vol. 42 (7), pp. 490-502; (doi: 10.1139/cjce-2014-0555

Conferences

1. Altintasi Oruc, Hediye Tuydes-Yaman and Kagan Tuncay (2018). “Traffic Flow Characteristics of an Urban Arterial Based on Different Traffic Flow Models”. 13th International Congress on Advances in Civil Engineering, October 12-14, Çeşme-İzmir, Turkey.
2. Altintasi Oruc, Hediye Tuydes-Yaman and Kagan Tuncay (2016). “Identification of Localities in Speed Patterns for Urban Arterials using Floating Car Data (FCD)”. 12th International Congress on Advances in Civil Engineering, October 21-23, Istanbul, Turkey.
3. Özgür-Cevher, Ö., Oruc Altintasi, Hediye Tuydes-Yaman and Ela Babalık-Sutcliffe, (2016) “Assessing the Link between Rail Transit Usage and Multimodal Integration”. Accepted for poster presentation at 95th Annual Meeting of the Transportation Research Board, January 8-12, Washington D.C, USA.
4. Tuydes-Yaman, Hediye, Pinar Karatas and Oruc Altintasi, (2015) “Lessons Learnt From METU Campus Walkability Evaluations”, Proceedings of 94th Transportation Research Board Annual Meeting, Washington DC, USA, January.
5. Karatas, Pinar, Hediye Tuydes-Yaman and Oruc Altintasi, (2014) “Evaluating Pedestrian Level of Service at Middle East Technical University (METU) Campus”, Proceedings of the 11th International Congress on Advances in Civil Engineering, İstanbul Technical University, İstanbul, Turkey, 21-25 October.

6. Altintasi, Oruc and Hediye Tuydes-Yaman (2014). "Determination of Origin-Destination Matrix of METU Campus Travelers Using RFID Data". Proceedings of the 11th international Congress on Advances in Civil Engineering, October 21-25, Istanbul, Turkey.
7. Altintasi, Oruc and Hediye Tuydes-Yaman, (2013) "Commute Behavior of METU Campus Travelers" The 18th International Conference of Hong Kong Society for Transportation Studies, December 14-16, Hong Kong, China.
8. Yucel, Sule, Hediye Tuydes-Yaman , Oruc Altintasi and Murat Ozen, (2013) Determination of Vehicular Travel Patterns in an Urban Location Using Bluetooth Technology" Accepted to be presented at ITS America 23rd Annual Meeting and Expo, Nashville, Tennessee, USA, April 22-24.
9. Altintasi, Oruc and Hediye Tuydes-Yaman, (2012) "Assessing Sustainable Campus Transportation Policies for METU: Policies for In-campus Mobility", Proceedings of the 10th International Congress on Advances on Civil Engineering, Ankara, Turkey, 17-19 October.